METAL ION COMPLEXING PROPERTIES OF THE TWO-DIMENSIONAL, HIGHLY PREORGANIZED LIGAND 1,10-PHENANTHROLINE-2,9-DICARBOXYLIC ACID

Darren Landon Melton

A Thesis Submitted to the
University of North Carolina Wilmington in Partial Fulfillment
Of the Requirements for the Degree of
Master of Science

Department of Chemistry

University of North Carolina Wilmington

2005

Approved by

Advisory Committee

_____ _____

_____
Chair

Accepted by

_____
Dean, Graduate School

TABLE OF CONTENTS

ABSTRACT iii

ACKNOWLEDGMENTS iv

DEDICATION v

LIST OF TABLES vi

LIST OF FIGURES vii

INTRODUCTION 1

METHODS 4

Synthesis of PDA 5

Titrations Involving PDA 8

Preparation of Crystals Submitted for X-ray Crystallography 16

^{153}Gd Radiolabeling of PDA 17

RESULTS AND DISCUSSION 18

Synthesis of PDA 18

Titrations Involving PDA 22

Titrations Involving Metals with PDA 25

Crystal Structure Results 67

^{153}Gd(III) Radiolabeling of PDA 86

CONCLUSIONS 89

LITERATURE CITED 92

ABSTRACT

Preorganized ligands have proven to be important to inorganic chemistry, yielding higher stability constants and sharper metal ion selectivity than their more flexible analogs. These ligands may have important applications in the biomedical, environmental, and industrial fields, to name a few. The ligand, 1,10-phenanthroline-2,9-dicarboxylate (PDA), was chosen for research and crystals of 1,10-phenanthroline-2,9-dicarboxylic acid were synthesized and then characterized by NMR and IR to determine their purity. Titration experiments were performed on aqueous solutions of the metal and PDA. A competing ligand, EDTA, was also introduced to the titration experiments and aided in the determination of formation constants, log K_1, for metal ions with PDA. UV/Vis spectrophotometry was used as a detection method for the formation of metal-PDA complexes. The log K_1 values for metal-PDA complexes were determined from UV absorbance data as a function of pH. Formation constants for metal ions such as Ca(II), Cd(II), Zn(II), Gd(III), and Pb(II) are reported, as well as the crystal structure of $[Ca(PDA)(H_2O)_2]$. ^{153}Gd(III)-radiolabeling experiments were also performed to indicate the stability of the Gd(III)-PDA complex. Overall, these experiments were used to obtain an understanding of the metal ion complexes of PDA.

ACKNOWLEDGMENTS

I would like to thank my advisor, Dr. Robert Hancock, for this research opportunity and all of the knowledge that he has given to me over the past few years. My committee members, Dr. John Tyrell and Dr. Sridhar Varadarajan, have been more than willing to answer any of the questions about my research and have helped me through many difficult syntheses.

A special thank you goes to my parents, Jeanne Melton and J. Edward Melton, for giving me their love and support throughout my career. I am forever indebted to you. I would also like to thank my brother, Ryan Melton, and my sister, Ginger Pate. They have both been a great influence and have always been there for me.

I would like to thank the faculty and my friends at UNCW, especially Michael Inscore and Beth Burnette. You have made my time at UNCW both memorable and enjoyable.

DEDICATION

I would like to dedicate this thesis to my grandmother, Mary Bost Taylor, whose who helped raise me and showed me her love and support. She was always there for me and she will forever hold a special place in my heart.

LIST OF TABLES

Table Page

1. The comparison of log K_1 data for metal ions with PDA and EDDA 32

2. The crystal data and structure refinement for the [Ca(PDA)(H_2O)$_2$] complex.....77

3. The atomic coordinates ($\times 10^4$) and equivalent isotropic displacement parameters (Å$^2\times 10^3$) for [Ca(PDA)(H_2O)$_2$]. U(eq) is defined as one third of the trace of the orthoganalized Uij tensor.....78

4. The hydrogen coordinates ($\times 10^4$) and isotropic displacement parameters (Å$^2\times 10^3$) for the [Ca(PDA)(H_2O)$_2$] complex.....79

5. The bond lengths (Å) for the [Ca(PDA)(H_2O)$_2$] complex.....80

6. The bond angles (deg) for the [Ca(PDA)(H_2O)$_2$] complex 81

7. The anisotropic displacement parameters (Å$^2\times 10^3$) for the [Ca(PDA)(H_2O)$_2$] complex. The anisotropic displacement factor exponent takes the form: $-2\pi^2$ [$h^2a^{*2}U11 + ... + 2hka^*b^*U12$]. 82

LIST OF FIGURES

Figure Page

1. A diagram of some common uses of metal ions in medicinal chemistry 2

2. A schematic of the flow cell apparatus used in the titration experiments 6

3. A schematic of the synthesis of PDA as reported by Chandler *et. al.* 7

4. The ^{1}H-NMR spectrum of impure 1,10-phenanthroline-2,9-dicarboxaldehyde in DMSO-d_6. 19

5. The IR spectrum of 1,10-phenanthroline-2,9-dicarboxaldehyde. 20

6. The ^{1}H-NMR spectrum of 1,10-phenanthroline-2,9-dicarboxylic acid in DMSO-d_6.....21

7. The IR spectrum of 1,10-phenanthroline-2,9-dicarboxylic acid monohydrate.....23

8. The absorbance versus wavelength (nm) spectra from the titration experiment conducted at 25.0 ± 0.1 °C for PDA in 0.10 *M* $NaClO_4$ for ionic strength. 24

9. The protonated species distribution diagram for PDA with respect to pH. 26

10. A diagram showing the three protonation events of PDA 27

11. The calculated strain energy (kcal·mol^{-1}) versus metal-oxygen bond length (Å) for M^{n+}-PDA complexes using Hyperchem embedded MM+ calculations. 31

12. The UV absorbance spectra for the titration of (a) 1:1 Ba(II) and PDA and (b) 1:1:1 Ba(II), PDA, and EDTA 33

13. The combined 246 nm corrected absorbance data versus pH from titration experiments involving Ba(II). The titration of PDA at this wavelength is also shown for reference. 34

14. The comparison of $\bar{n}$ observed versus $\bar{n}$ calculated with respect to pH at wavelengths of a.) 226 nm, b.) 235 nm, and c.) 280 nm for the competition of PDA and EDTA for Ba(II).....35

15. The UV absorbance spectra for the titration of (a) 1:1 Cd(II) and PDA and (b) 1:1:1 Cd(II), PDA, and EDTA 37

16. The combined 235 nm corrected absorbance data versus pH from titration experiments involving Cd(II). The titration of PDA at this wavelength is also shown for reference. 38

17. The comparison of $\bar{n}$ observed versus $\bar{n}$ calculated with respect to pH at wavelengths of a.) 235 nm, b.) 246 nm, and c.) 286 nm for the competition of PDA and EDTA for Cd(II). 39

18. The UV absorbance spectra for the titration of (a) 1:1 Ca(II) and PDA and (b) 1:1:1 Ca(II), PDA, and EDTA 40

19. The combined 235 nm corrected absorbance data versus pH from titration experiments involving Ca(II). The titration of PDA at this wavelength is also shown for reference. 41

20. The comparison of $\bar{n}$ observed versus $\bar{n}$ calculated with respect to pH at wavelengths of a.) 246 nm and b.) 280 nm for the competition of PDA and EDTA for Ca(II). 42

21. The UV absorbance spectra for the titration of (a) 1:1 Cu(II) and PDA and (b) 1:1:1 Cu(II), PDA, and EDTA 44

22. The combined 246 nm corrected absorbance data versus pH from titration experiments involving Cu(II). The titration of PDA at this wavelength is also shown for reference. 45

23. The comparison of $\bar{n}$ observed versus $\bar{n}$ calculated with respect to pH at wavelengths of a.) 235 nm, b.) 246 nm, and c.) 280 nm for the competition of PDA and EDTA for Cu(II). 46

24. The UV absorbance spectra for the titration of (a) 1:1 Gd(III) and PDA and (b) 1:1:1 Gd(III), PDA, and EDTA....47

25. The combined 280 nm corrected absorbance data versus pH from titration experiments involving Gd(III). The titration of PDA at this wavelength is also shown for reference. 48

26. The comparison of $\bar{n}$ observed versus $\bar{n}$ calculated with respect to pH at wavelengths of a.) 226 nm, b.) 235 nm, and c.) 280 nm for the competition of PDA and EDTA for Gd(III). 49

27. The UV absorbance spectra for the titration of (a) 1:1 La(III) and PDA and (b) 1:1:1 La(III), PDA, and DTPA 51

28. The combined 235 nm corrected absorbance data versus pH from titration experiments involving La(III). The titration of PDA at this wavelength is also shown for reference. 52

29. The comparison of $\bar{n}$ observed versus $\bar{n}$ calculated with respect to pH at wavelengths of a.) 235 nm, b.) 246 nm, and c.) 280 nm for the competition of PDA and DTPA for La(III). 53

30. The UV absorbance spectra for the titration of (a) 1:1 Pb(II) and PDA and (b) 1:1:1 Pb(II), PDA, and EDTA 54

31. The combined 246 nm corrected absorbance data versus pH from titration experiments involving Pb(II). The titration of PDA at this wavelength is also shown for reference. 55

32. The comparison of $\bar{n}$ observed versus $\bar{n}$ calculated with respect to pH at wavelengths of a.) 235 nm, b.) 246 nm, and c.) 280 nm for the competition of PDA and EDTA for Pb(II). 56

33. The UV absorbance spectra for the titration of (a) 1:1 Mg(II) and PDA and (b) 1:1:1 Mg(II), PDA, and EDTA 58

34. The combined 226 nm corrected absorbance data versus pH from titration experiments involving Mg(II). The sample solution used for the titration of Mg(II) and PDA contained 0.0333 *M* Mg(II). The titration of PDA at this wavelength is also shown for reference 59

35. The UV absorbance spectra for the titration of (a) 1:1 Ni(II) and PDA and (b) 1:1:1 Ni(II), PDA, and EDTA 61

36. The combined 246 nm corrected absorbance data versus pH from titration experiments involving Ni(II). The titration of PDA at this wavelength is also shown for reference. 62

37. The comparison of $\bar{n}$ observed versus $\bar{n}$ calculated with respect to pH at wavelengths of a.) 235 nm, b.) 246 nm, and c.) 280 nm for the competition of PDA and EDTA for Ni(II). 63

38. The UV absorbance spectra for the titration of (a) 1:1 Sr(II) and PDA and (b) 1:1:1 Sr(II), PDA, and EDTA 64

39. The combined 235 nm corrected absorbance data versus pH from titration experiments involving Sr(II). The titration of PDA at this wavelength is also shown for reference. 65

40. The comparison of $\bar{n}$ observed versus $\bar{n}$ calculated with respect to pH at wavelengths of a.) 235 nm, b.) 246 nm, and c.) 286 nm for the competition of PDA and EDTA for Sr(II) 66

41. The UV absorbance spectra for the titration of (a) 1:1 Zn(II) and PDA and (b) 1:1:1 Zn(II), PDA, and EDTA 68

42. The combined 280 nm corrected absorbance data versus pH from titration experiments involving Zn(II). The titration of PDA at this wavelength is also shown for reference. 69

43. The comparison of $\bar{n}$ observed versus $\bar{n}$ calculated with respect to pH at wavelengths of a.) 235 nm, b.) 246 nm, and c.) 280 nm for the competition of PDA and EDTA for Zn(II). 70

44. The crystal structure of the $[Co(PDA)_2]^{2-}$ complex. 71

45. The crystal structure of the $[Mg(PDA)(H_2O)_3]$ complex.....72

46. The crystal structure of the $[Ni(PDA)(H_2O)_3]$ complex 73

47. The IR spectrum of $[Ca(PDA)(H_2O)_2]$ crystals with the IR spectrum of PDA as a reference. 75

48. The crystal structure and atom assignments for the $[Ca(PDA)(H_2O)_2)]$ complex. 76

49. The IR spectrum of 2,9-bis(carbomethoxy)-1,10-phenanthroline. 84

50. The crystal structure and atom assignments for 2,9-bis(carbomethoxy)-1,10-phenanthroline monohydrate (DMOPA·H_2O). 85

51. The radio-TLC diagram of the ^{153}Gd(III)-PDA complex. 87

52. The radio-TLC diagram for the competition experiment of PDA and DTPA for ^{153}Gd(III). 88

53. The radio-TLC diagrams of the ^{153}Gd(III)-PDA complex before and after rat serum was added to the sample. 90

INTRODUCTION

Metals have been known to facilitate vital processes in the human body, so it is no surprise that a great deal of medicinal chemistry focuses on the study of metal-ligand design and interactions. Over time, the focus has broadened from approximately 24 essential elements in the body to find applications for nonessential elements. Figure 1 shows a periodic table and some uses for nonessential elements. Common inorganic applications to medicinal practices today range from chelation therapy, for the removal of metal ions such as Pb(II) from the body, to magnetic resonance imaging (MRI) and radiopharmacology.[1] A prime example of a nonessential element with applications in medicinal chemistry is Gd(III), which is used extensively in MRI contrast agents. Ligand design plays an important role in selectively chelating Gd(III) to prevent its toxic effects in the body by displacement with Zn(II). The rare-earth element, Gd(III), has 7 unpaired electrons that allow it to coordinate H_2O molecules to its inner sphere, which produces a contrast between the ^{1}H-signal of H_2O coordinated to Gd(III) and the ^{1}H-signal of H_2O found naturally in biological fluids. Since Gd(III) is highly toxic, Gd(III) is typically bound to a metal ion selective chelating agent, such as diethylenetriamine pentaacetic acid (DTPA), before being introduced to the body. As a result of this example and many others, ligand design efforts have focused mainly on forming complexes of high thermodynamic stability, which are selective for a desired metal ion. The selective binding of a metal ion to a ligand is enhanced by the degree of preorganization of the chelate structure. Donald J. Cram was the first to define the concept of preorganization.[2] A ligand is more preorganized when it is more constrained to be in the conformation required to complex a metal ion.

Crown ethers[3,4] and cryptands[5,6] are of the most common and widely studied macrocycles that form complexes, typically with alkali metals, of high thermodynamic stability due to their

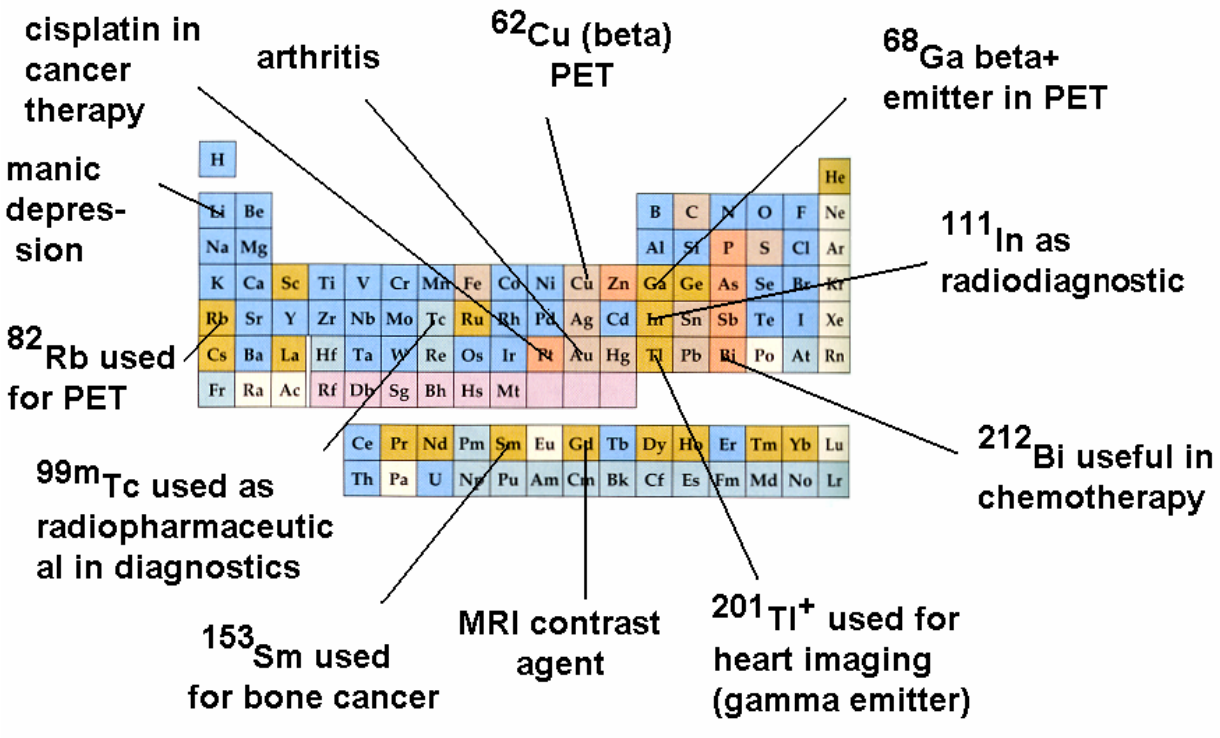

Figure 1: A diagram of some common uses of metal ions in medicinal chemistry.

preorganized conformations. Macrocycles with extended delocalized systems, such as porphyrins, display the highest thermodynamic stability. The enhanced complex stability of these ligands, macrocyclic[7] and cryptate[8] effects, has been a gateway to the discovery of chelating agents with similar binding properties. The inherent structural rigidity of these macrocycles allows them to selectively complex a particular metal ion over others.

To further enhance metal ion selectivity, coordination number of the desired metal ion to be complexed and the types of donor atoms contained within the binding site of the macrocycle should be taken into consideration. In the example of Gd(III) used in contrast agents for NMR, the chelating agent should bind Gd(III) effectively and not be displaced by Zn(II) found in the body. Both ethylenediamine tetraacetic acid (EDTA) and DTPA have similar donor atoms arranged in much the same way, but only DTPA[9] is

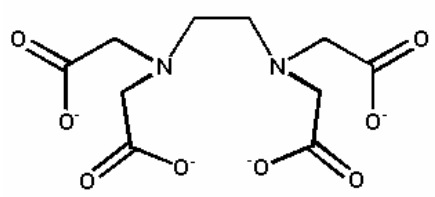

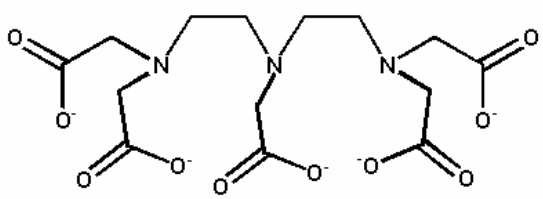

used in MRI contrast agents with Gd(III). The reason lies in that EDTA cannot effectively bind Gd(III) over Zn(II) although it has a high formation constant, log K_1, of 17.35 for Gd(III) because the formation constants are too similar.[10] The coordination number for Gd(III) is 9, therefore adequate selectivity for Gd(III) is seen for DTPA since there are 8 donor atoms versus 6 donor atoms for EDTA.

The ligand, 1,10-phenanthroline-2,9-dicarboxylate (PDA), was investigated to determine the binding constants for a variety of metal ions, presented in this thesis. PDA has a highly

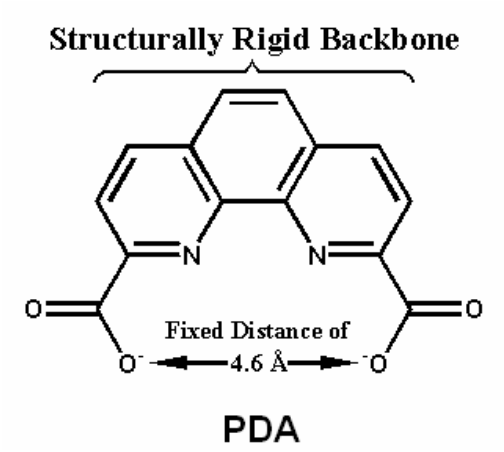

preorganized binding site with a fixed radius and is part of a class of ligands called hemicycles. Hemicycles bear the same structural rigidity and fixed conformation that most macrocycles do; however, unlike macrocycles, the structures contain terminal donor atoms that make them acyclic. Hemicycles also have several advantages such as increased thermodynamic stability, given by the macrocyclic effects, and possibly increased kinetic rates that allow for rapid metallation and demetallation. Another important advantage is that hemicycles are typically easier to synthesize and less expensive than their macrocyclic counterparts.

METHODS

All chemicals and reagents used were of analytical grade and purchased commercially. Aqueous metal-ligand solutions were made using deionized (DI) H_2O.

Characterization of ligands and metal-ligand complexes was performed using ^{1}H-NMR and FT-IR analysis. ^{1}H-NMR spectra were performed for organic synthesis products using a Bruker 400 MHz NMR spectrometer. All samples for ^{1}H-NMR analysis were prepared and referenced in DMSO-d_6. Infrared absorption spectra were taken of all synthesized organic products and crystallized metal-ligand complexes using a Polaris IR-10410 FT-IR instrument

(Mattson, Inc.) with WinFIRST software. Samples for FT-IR analysis were prepared as KBr pellets.

UV/Vis absorbance spectra were carried out for aqueous metal-ligand titration experiments using a double beam Cary 1E UV/Vis spectrophotometer (Varian, Inc.) and WinUV Version 2.00(25) software. A 1.0 cm quartz flow cell, fitted with a variable flow peristaltic pump, was used to refresh the metal-ligand aqueous solution after each titrant addition was made to the sample. A schematic of the flow cell apparatus is shown in Figure 2. Suitable equilibration times after each titrant addition were determined to be between 5 and 8 minutes, depending on the metal ion being studied. Absorbance scan ranges were from 190 to 350 nm at a rate of 600.00 nm/min. All absorbance spectra were referenced using DI H_2O and a 1.0 cm quartz cell filled with DI H_2O was placed in the path of the reference beam.

All pH values for the titration experiments were recorded using a SympHony SR60IC pH meter (VWR Scientific, Inc.), which was calibrated prior to each titration experiment using pH 4.01, 7.00, and 10.00 buffer solutions. Aqueous metal-ligand samples used in the titration experiments were of 0.10 *M* $NaClO_4$ for ionic strength and maintained at a constant 25.0 ± 0.1 °C throughout the experiment.

Synthesis of PDA

The synthesis of PDA was carried out as described in the literature[11] with a few modifications. A schematic of the synthesis is shown in Figure 3. Characterization of the products was performed using both ^{1}H-NMR and FT-IR analysis.

A mixture of 6.008 g of 2,9-dimethyl-1,10-phenanthroline monohydrate (26.55 mmol, Alfa Aesar, 99%) and 15.004 g of selenium dioxide (135.22 mmol, Alfa Aesar, 99+%) was placed in 400 mL of 4% DI H_2O/p-dioxane (Alfa Aesar, 99+%) in a 500 mL round bottom flask.

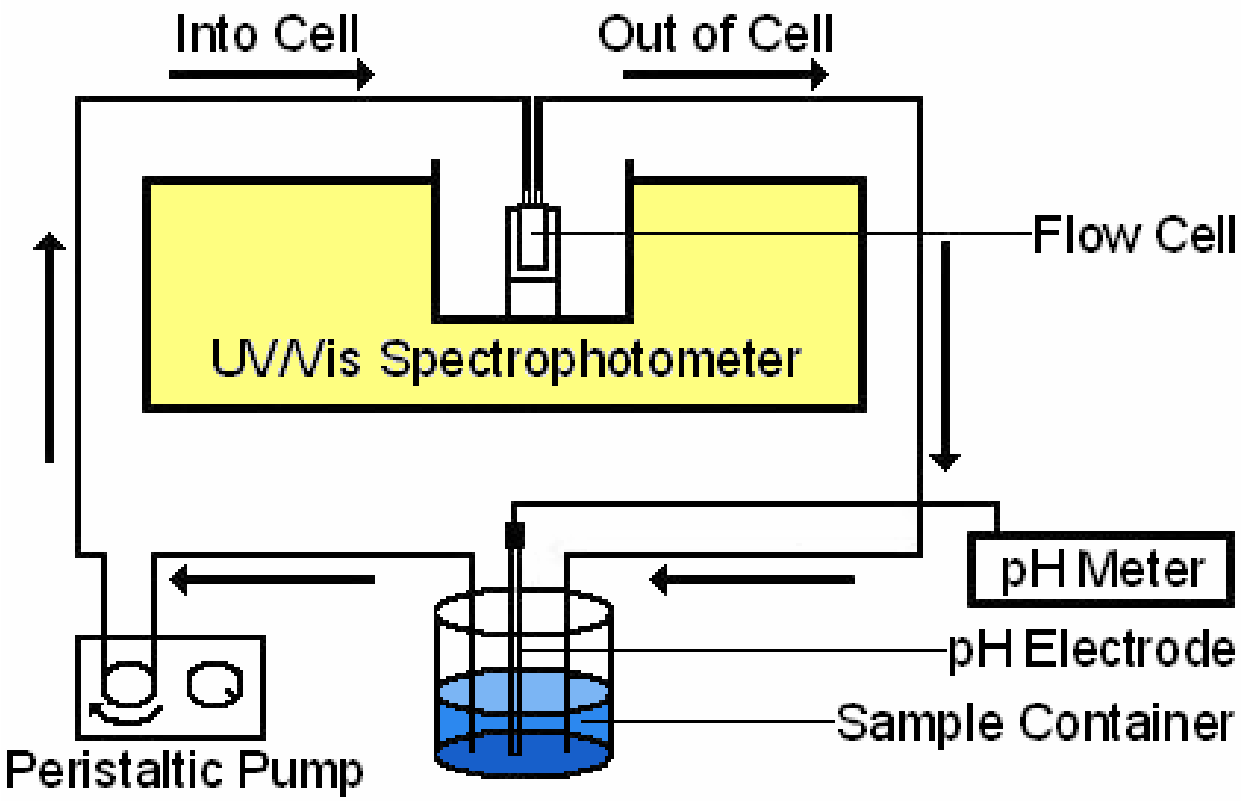

Figure 2: A schematic of the flow cell apparatus used in the titration experiments.

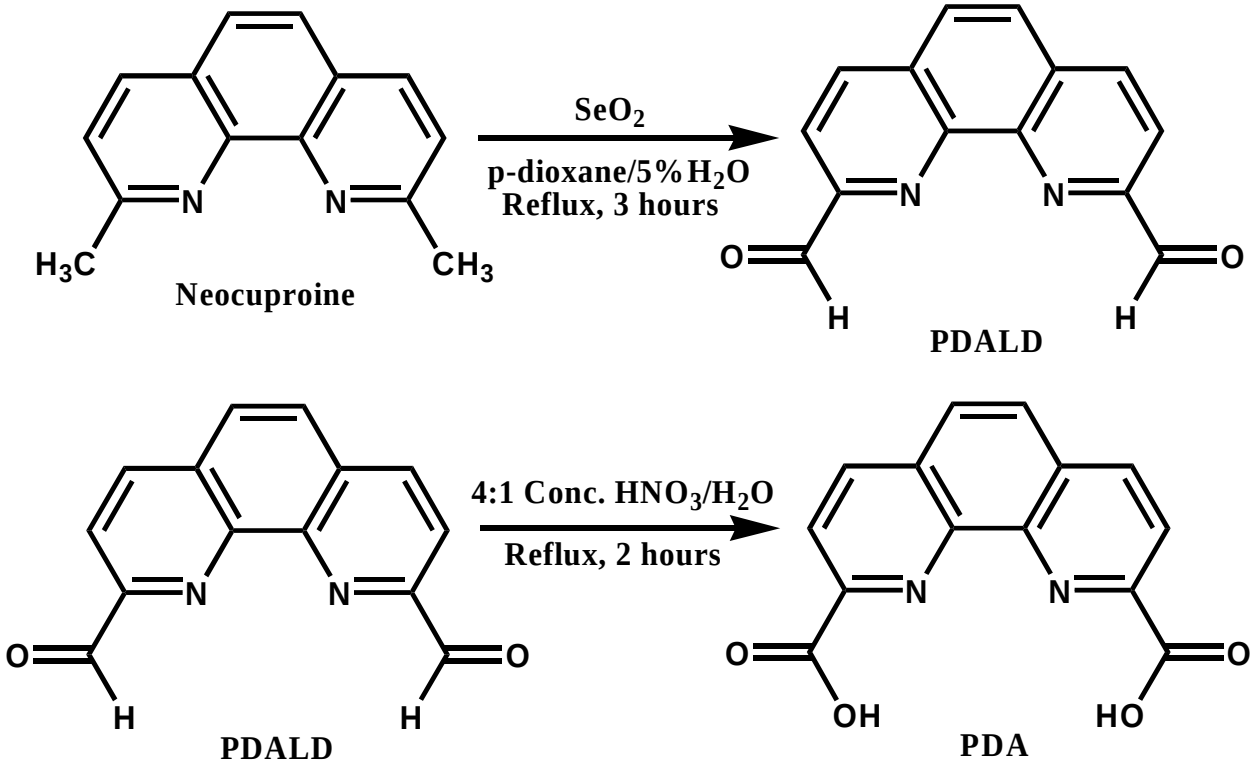

Figure 3: A schematic of the synthesis of PDA as reported by Chandler *et. al.*

The mixture was stirred and allowed to reflux at 101 °C in a wax bath for 3 hours. The hot solution was immediately filtered through a layer of celite (Fisher Scientific) and a yellow-orange product precipitated from the cold filtrate. The synthesis yielded 3.460 g of impure 1,10-phenanthroline-2,9-dicarboxaldehyde (14.65 mmol, 45.5%), which was separated from the filtrate by vacuum filtration and allowed to dry. The dialdehyde product was not taken through further purification steps since the next step of the synthesis involved further oxidation.

A solution of 3.000 g of non-purified 1,10-phenanthroline-2,9-dicarboxaldehyde (12.70 mmol) and 60 mL of 4:1 HNO_3 (15.8 N, Fisher Scientific)/H_2O was placed in a 150 mL round bottom flask. The mixture was stirred while refluxing at 122 °C for 2 hours. The solution was cooled to room temperature and poured over approximately 50 cc of crushed ice. The precipitated 1,10-phenanthroline-2,9-dicarboxylic acid was filtered out by vacuum filtration and allowed to dry. For further purification, the product was recrystallized from methanol and 2.157 g of 1,10-phenanthroline-2,9-dicarboxylic acid monohydrate (7.535 mmol, 59.3%) was obtained as fine, yellow needles.

Titrations Involving PDA

Acid-base titrations of aqueous metal-PDA solutions were monitored using UV/Vis spectrophotometry. At least two sets of experiments were performed for each metal ion with PDA. The first titration experiment involved the metal with PDA and the second experiment used a competing ligand, EDTA or DTPA, with the metal and PDA. Stock solutions of 1.00×10^{-3} *M* PDA (0.0286 g into 100 mL of 0.0100 *M* NaOH), 1.00×10^{-2} *M* Na_2EDTA (0.3722 g in 100 mL H_2O), and 1.00×10^{-2} *M* DTPA (0.3934 g into 100 mL H_2O) were used in the titration experiments. Titrant solutions of 0.0100 *M* $HClO_4$ (10.00 mL of 0.100 *M* $HClO_4$ in 100 mL DI

H_2O) in 0.0900 *M* $NaClO_4$ (1.1020 g in 100 mL DI H_2O, Aldrich, 99%) and 0.100 *M* $HClO_4$ (6.00 mL of 69-72% $HClO_4$ in 1.00 L H_2O, Fisher Scientific) were used to adjust the pH of the sample solutions used in the titrations. The ionic strength of each sample solution was held constant with 0.10 *M* $NaClO_4$ (1.2244 g into 100 mL H_2O).

Solution for titration of PDA

In order to determine the protonation constants for PDA, 100 mL of 2.00×10^{-5} *M* PDA (2.00 mL of 1.00×10^{-3} *M*) in 0.10 *M* $NaClO_4$ was prepared. A 50.00 ± 0.05 mL aliquot of this solution was placed in the flow cell setup described above and titrated with $HClO_4$. Absorbance spectra and pH values were recorded for each titrant addition.

Solutions for titrations of PDA with Barium(II)

A stock solution of 1.00×10^{-2} *M* $Ba(ClO_4)_2$ (0.3363 g, Aldrich, 97%, $Ba(ClO_4)_2$ in 100 mL of H_2O) was prepared for use in both sets of titration experiments. For the 1:1 Ba(II) and PDA titration experiment, the concentrations for each were 2.00×10^{-5} *M*. A 100 mL solution containing 200 μL of 1.00×10^{-2} *M* $Ba(ClO_4)_2$ and 2.00 mL of 1.00×10^{-3} *M* PDA was prepared. A 50.00 ± 0.05 mL portion of this solution was placed in the flow cell apparatus described above and titrated with $HClO_4$. For the ligand competition experiment of 1:1:1 Ba(II), PDA, and EDTA, the concentrations for each were 2.00×10^{-5} *M*. Additions of 200 μL of 1.00×10^{-2} *M* $Ba(ClO_4)_2$, 2.00 mL of 1.00×10^{-3} *M* PDA, and 200 μL of 1.00×10^{-2} *M* Na_2EDTA were made to a 100 mL volumetric flask, which was then filled to the mark with H_2O. A 50.00 ± 0.05 mL sample of the solution was placed in the flow cell apparatus described above and titrated with $HClO_4$.

Solutions for titrations of PDA with Cadmium(II)

A stock solution of 1.00×10^{-2} *M* $Cd(ClO_4)_2\cdot H_2O$ (0.3293 g, Aldrich, in 100 mL of H_2O) was prepared for use in both sets of titration experiments. For the 1:1 Cd(II) and PDA titration experiment, the concentrations for each were 2.00×10^{-5} *M*. A 100 mL solution containing 200 μL of 1.00×10^{-2} *M* $Cd(ClO_4)_2\cdot H_2O$ and 2.00 mL of 1.00×10^{-3} *M* PDA was prepared. A 50.00 ± 0.05 mL portion of this solution was placed in the flow cell apparatus described above and titrated with $HClO_4$. For the ligand competition experiment of 1:1:1 Cd(II), PDA, and EDTA, the concentrations for each were 2.00×10^{-5} *M*. Additions of 200 μL of 1.00×10^{-2} *M* $Cd(ClO_4)_2\cdot H_2O$, 2.00 mL of 1.00×10^{-3} *M* PDA, and 200 μL of 1.00×10^{-2} *M* Na_2EDTA were made to a 100 mL volumetric flask, which was then filled to the mark with H_2O. A 50.00 ± 0.05 mL sample of the solution was placed in the flow cell apparatus described above and titrated with $HClO_4$.

Solutions for titrations of PDA with Calcium(II)

A total of three titration experiments were performed to determine the log K_1 for Ca(II) with PDA. A stock solution of 1.00×10^{-2} *M* $Ca(ClO_4)_2\cdot 4H_2O$ (0.3110 g, Aldrich, 99%, in 100 mL of H_2O) was prepared for use in all of the titration experiments. For the 1:1 Ca(II) and PDA titration experiment, the concentrations for each were 2.00×10^{-5} *M*. A 100 mL solution containing 200 μL of 1.00×10^{-2} *M* $Ca(ClO_4)_2\cdot 4H_2O$ and 2.00 mL of 1.00×10^{-3} *M* PDA was prepared. A 50.00 ± 0.05 mL portion of this solution was placed in the flow cell apparatus described above and titrated with $HClO_4$. For the ligand competition experiment of 1:1:1 Ca(II), PDA, and EDTA, the concentrations for each were 2.00×10^{-5} *M*. Additions of 200 μL of

1.00×10^{-2} *M* $Ca(ClO_4)_2\cdot4H_2O$, 2.00 mL of 1.00×10^{-3} *M* PDA, and 200 μL of 1.00×10^{-2} *M* Na_2EDTA were made to a 100 mL volumetric flask, which was then filled to the mark with H_2O. A 50.00 ± 0.05 mL sample of the solution was placed in the flow cell apparatus described above and titrated with $HClO_4$. An additional PDA and EDTA competition experiment for Ca(II) was performed for 1:1:10 Ca(II), PDA, and EDTA. Additions of 200 μL of 1.00×10^{-2} *M* $Ca(ClO_4)_2\cdot4H_2O$, 2.00 mL of 1.00×10^{-3} *M* PDA, and 2.00 mL of 1.00×10^{-2} *M* Na_2EDTA were made to a 100 mL volumetric flask, which was then filled to the mark. A 50.00 ± 0.05 mL sample of the solution was placed in the flow cell apparatus described above and titrated with $HClO_4$.

Solutions for titrations of PDA with Copper(II)

A stock solution of 1.00×10^{-2} *M* $Cu(ClO_4)_2\cdot6H_2O$ (0.3705 g, Aldrich, in 100 mL of H_2O) was prepared for use in both sets of titration experiments. For the 1:1 Cu(II) and PDA titration experiment, the concentrations for each were 2.00×10^{-5} *M*. A 100 mL solution containing 200 μL of 1.00×10^{-2} *M* $Cu(ClO_4)_2\cdot6H_2O$ and 2.00 mL of 1.00×10^{-3} *M* PDA was prepared. A 50.00 ± 0.05 mL portion of this solution was placed in the flow cell apparatus described above and titrated with $HClO_4$. For the ligand competition experiment of 1:1:1 Cu(II), PDA, and EDTA, the concentrations for each were 2.00×10^{-5} *M*. Additions of 200 μL of 1.00×10^{-2} *M* $Cu(ClO_4)_2\cdot6H_2O$, 2.00 mL of 1.00×10^{-3} *M* PDA, and 200 μL of 1.00×10^{-2} *M* Na_2EDTA were made to a 100 mL volumetric flask, which was then filled to the mark with H_2O. A 50.00 ± 0.05 mL sample of the solution was placed in the flow cell apparatus described above and titrated with $HClO_4$.

Solutions for titrations of PDA with Gadolinium(III)

A stock solution of 1.00×10^{-2} *M* $Gd(NO_3)_3\cdot6H_2O$ (0.4513 g, Aldrich, 99.9%, in 100 mL of H_2O) was prepared for use in both sets of titration experiments. The 1.00×10^{-2} *M* $Gd(NO_3)_3\cdot6H_2O$ stock solution was adjusted to a pH of 3 using $HClO_4$. For the 1:1 Gd(III) and PDA titration experiment, the concentrations for each were 2.00×10^{-5} *M*. A 100 mL solution containing 200 μL of 1.00×10^{-2} *M* $Gd(NO_3)_3\cdot6H_2O$ and 2.00 mL of 1.00×10^{-3} *M* PDA was prepared. A 50.00 ± 0.05 mL portion of this solution was placed in the flow cell apparatus described above and titrated with $HClO_4$. For the ligand competition experiment of 1:1:1 Gd(III), PDA, and EDTA, the concentrations for each were 2.00×10^{-5} *M*. Additions of 200 μL of 1.00×10^{-2} *M* $Gd(NO_3)_3\cdot6H_2O$, 2.00 mL of 1.00×10^{-3} *M* PDA, and 200 μL of 1.00×10^{-2} *M* Na_2EDTA were made to a 100 mL volumetric flask, which was then filled to the mark with H_2O. A 50.00 ± 0.05 mL sample of the solution was placed in the flow cell apparatus described above and titrated with $HClO_4$.

Solutions for titrations of PDA with Lanthanum(III)

A total of three titration experiments were performed to determine the log K_1 for La(III) with PDA. A stock solution of 1.00×10^{-2} *M* $La(ClO_4)_3\cdot6H_2O$ (0.5454 g in 100 mL of H_2O) was prepared for use in all of the titration experiments. The 1.00×10^{-2} *M* $La(ClO_4)_3\cdot6H_2O$ stock solution was adjusted to a pH of 3 using $HClO_4$. For the 1:1 La(III) and PDA titration experiment, the concentrations for each were 2.00×10^{-5} *M*. A 100 mL solution containing 200 μL of 1.00×10^{-2} *M* $La(ClO_4)_3\cdot6H_2O$ and 2.00 mL of 1.00×10^{-3} *M* PDA was prepared. A 50.00 ± 0.05 mL portion of this solution was placed in the flow cell apparatus described above and titrated with $HClO_4$. For the ligand competition experiment of 1:1:1 La(III), PDA, and EDTA,

the concentrations for each were 2.00×10^{-5} *M*. Additions of 200 μL of 1.00×10^{-2} *M* $La(ClO_4)_3\cdot6H_2O$, 2.00 mL of 1.00×10^{-3} *M* PDA, and 200 μL of 1.00×10^{-2} *M* Na_2EDTA were made to a 100 mL volumetric flask, which was then filled to the mark with H_2O. A 50.00 ± 0.05 mL sample of the solution was placed in the flow cell apparatus described above and titrated with $HClO_4$. An additional experiment using 1:1:1 La(III), PDA, and DTPA was carried out. Additions of 200 μL of 1.00×10^{-2} *M* $La(ClO_4)_3\cdot6H_2O$, 2.00 mL of 1.00×10^{-3} *M* PDA, and 200 μL of 1.00×10^{-2} *M* DTPA were made to a 100 mL volumetric flask, which was then filled to the mark with H_2O. A 50.00 ± 0.05 mL portion of this solution was placed in the flow cell apparatus described above and titrated with $HClO_4$.

Solutions for titrations of PDA with Lead(II)

A stock solution of 1.00×10^{-2} *M* $Pb(ClO_4)_2\cdot3H_2O$ (0.4603 g, Alfa Aesar, 97%, in 100 mL of H_2O) was prepared for use in both sets of titration experiments. For the 1:1 Pb(II) and PDA titration experiment, the concentrations for each were 2.00×10^{-5} *M*. A 100 mL solution containing 200 μL of 1.00×10^{-2} *M* $Pb(ClO_4)_2\cdot3H_2O$ and 2.00 mL of 1.00×10^{-3} *M* PDA was prepared. A 50.00 ± 0.05 mL portion of this solution was placed in the flow cell apparatus described above and titrated with $HClO_4$. For the ligand competition experiment of 1:1:1 Pb(II), PDA, and EDTA, the concentrations for each were 2.00×10^{-5} *M*. Additions of 200 μL of 1.00×10^{-2} *M* $Pb(ClO_4)_2\cdot3H_2O$, 2.00 mL of 1.00×10^{-3} *M* PDA, and 200 μL of 1.00×10^{-2} *M* Na_2EDTA were made to a 100 mL volumetric flask, which was then filled to the mark with H_2O. A 50.00 ± 0.05 mL sample of the solution was placed in the flow cell setup described above and titrated with $HClO_4$.

Solutions for titrations of PDA with Magnesium(II)

For the Mg(II) and PDA titration experiment, the concentrations for were 0.0333 and 2.00×10^{-5} *M*, respectively. A 100 mL solution containing 0.0333 *M* $Mg(ClO_4)_2\cdot6H_2O$ (1.0932 g) and 2.00 mL of 1.00×10^{-3} *M* PDA was prepared. A 50.00 ± 0.05 mL portion of this solution was placed in the flow cell apparatus described above and titrated with $HClO_4$. For the ligand competition experiment of 1:1:1 Mg(II), PDA, and EDTA, the concentrations for each were 2.00×10^{-5} *M*. Additions of 200 μL of 1.00×10^{-2} *M* $Mg(ClO_4)_2\cdot6H_2O$ (0.3315 g into 100 mL H_2O), 2.00 mL of 1.00×10^{-3} *M* PDA, and 200 μL of 1.00×10^{-2} *M* Na_2EDTA were made to a 100 mL volumetric flask, which was then filled to the mark with H_2O. A 50.00 ± 0.05 mL sample of the solution was placed in the flow cell apparatus described above and titrated with $HClO_4$.

Solutions for titrations of PDA with Nickel(II)

A stock solution of 1.00×10^{-2} *M* $Ni(ClO_4)_2\cdot6H_2O$ (0.3616 g, Alfa Aesar, in 100 mL of H_2O) was prepared and used in both sets of titration experiments. For the 1:1 Ni(II) and PDA titration experiment, the concentrations for each were 2.00×10^{-5} *M*. A 100 mL solution containing 200 μL of 1.00×10^{-2} *M* $Ni(ClO_4)_2\cdot6H_2O$ and 2.00 mL of 1.00×10^{-3} *M* PDA was prepared. A 50.00 ± 0.05 mL portion of this solution was placed in the flow cell apparatus described above and titrated with $HClO_4$. For the ligand competition experiment of 1:1:1 Ni(II), PDA, and EDTA, the concentrations for each were 2.00×10^{-5} *M*. Additions of 200 μL of 1.00×10^{-2} *M* $Ni(ClO_4)_2\cdot6H_2O$, 2.00 mL of 1.00×10^{-3} *M* PDA, and 200 μL of 1.00×10^{-2} *M* Na_2EDTA were made to a 100 mL volumetric flask, which was then filled to the mark with H_2O. A 50.00 ± 0.05 mL sample of the solution was placed in the flow cell apparatus described above and titrated with $HClO_4$.

Solutions for titrations of PDA with Strontium(II)

A stock solution of 1.00×10^{-2} *M* $Sr(ClO_4)_2$ (0.4603 g, Aldrich, in 100 mL of H_2O) was prepared for use in both sets of titration experiments. For the 1:1 Sr(II) and PDA titration experiment, the concentrations for each were 2.00×10^{-5} *M*. A 100 mL solution containing 200 μL of 1.00×10^{-2} *M* $Sr(ClO_4)_2$ and 2.00 mL of 1.00×10^{-3} *M* PDA was prepared. A 50.00 ± 0.05 mL portion of this solution was placed in the flow cell apparatus described above and titrated with $HClO_4$. For the ligand competition experiment of 1:1:1 Sr(II), PDA, and EDTA, the concentrations for each were 2.00×10^{-5} *M*. Additions of 200 μL of 1.00×10^{-2} *M* $Sr(ClO_4)_2$, 2.00 mL of 1.00×10^{-3} *M* PDA, and 200 μL of 1.00×10^{-2} *M* Na_2EDTA were made to a 100 mL volumetric flask, which was then filled to the mark with H_2O. A 50.00 ± 0.05 mL sample of the solution was placed in the flow cell apparatus described above and titrated with $HClO_4$.

Solutions for titrations of PDA with Zinc(II)

A stock solution of 1.00×10^{-2} *M* $Zn(ClO_4)_2\cdot6H_2O$ (0.3293 g, Aldrich, in 100 mL of H_2O) was prepared for use in both sets of titration experiments. For the 1:1 Zn(II) and PDA titration experiment, the concentrations for each were 2.00×10^{-5} *M*. A 100 mL solution containing 200 μL of 1.00×10^{-2} *M* $Zn(ClO_4)_2\cdot6H_2O$ and 2.00 mL of 1.00×10^{-3} *M* PDA was prepared. A 50.00 ± 0.05 mL portion of this solution was placed in the flow cell apparatus described above and titrated with $HClO_4$. For the ligand competition experiment of 1:1:1 Zn(II), PDA, and EDTA, the concentrations for each were 2.00×10^{-5} *M*. Additions of 200 μL of 1.00×10^{-2} *M* $Zn(ClO_4)_2\cdot6H_2O$, 2.00 mL of 1.00×10^{-3} *M* PDA, and 200 μL of 1.00×10^{-2} *M* Na_2EDTA were made to a 100 mL volumetric flask, which was then filled to the mark with H_2O. A 50.00 ± 0.05

mL sample of the solution was placed in the flow cell apparatus described above and titrated with $HClO_4$.

Preparation of Crystals Submitted for X-ray Crystallography

[Ca(PDA)(H_2O)$_2$] crystal preparation

The synthesis of [Ca(PDA)(H_2O)$_2$] crystals was carried out by dissolving the 0.0709 g PDA (0.248 mmol) in *n*-butanol and 0.0765 g $Ca(ClO_4)_2 \cdot 4H_2O$ (0.246 mmol) in H_2O. The $Ca(ClO_4)_2 \cdot 4H_2O$ solution was placed into a 30 mm×150 mm test tube in a hot water bath at approximately 80 °C. A layer of *n*-butanol was then added to the aqueous solution of $Ca(ClO_4)_2 \cdot 4H_2O$ to allow an initial interface between *n*-butanol and H_2O to form. The *n*-butanol solution of PDA was added carefully to the test tube while hot. An effort was made to avoid disturbing the interface between the two solvents. After combining the layers, the contents of the test tube were left to cool with the hot water bath. This technique leads to slow diffusion of the Ca(II) salt and the ligand together at the interface of the two solvents. This results in a slow crystallization of the otherwise highly insoluble complex, which would otherwise precipitate too rapidly and form microcrystals unsuitable for X-ray crystallography. Crystals of [Ca(PDA)(H_2O)$_2$] accumulated on the interface of the *n*-butanol/H_2O layers and were collected by vacuum filtration. IR analysis and X-ray crystallography experiments were performed on the [Ca(PDA)(H_2O)$_2$] crystals.

DMOPA·H_2O crystal preparation

An impurity of PDA, 2,9-bis(carbomethoxy)-1,10-phenanthroline (DMOPA), was determined to be a byproduct of PDA when recrystallized from methanol. Crystals of DMOPA

were recrystallized from *n*-butanol and collected by vacuum filtration. IR analysis and X-ray crystallography experiments were performed on the DMOPA crystals.

^{153}Gd Radiolabeling of PDA

Lihui Wei, David Reichert, and Michael J. Welch at Washington University in St. Louis performed the radiolabeling and serum stability studies of ^{153}Gd(III) with PDA. A ^{153}Gd(III) and PDA radiolabeling experiment was performed to ensure that the ^{153}Gd(III)-PDA complex would form. A 4.5×10^{-3} *M* solution of PDA was prepared in ethanol. A mixture of 1.5 μL of $^{153}GdCl_3$ in 0.1 *M* HCl (no-carrier-added, 5.5 μCi) and 8.3 μL of the PDA solution were added to 90 μL of 0.1 *M* ammonium acetate for a pH of 7. The reaction mixture was incubated at 25 °C for 15 minutes to ensure complexation of ^{153}Gd(III) with PDA. The formation of a ^{153}Gd(III)-PDA complex was confirmed by radio-TLC using ITLC-SG for the stationary phase and ethanol as the mobile phase.

A competition experiment between PDA and DTPA for ^{153}Gd(III) was conducted to test the strength of the ^{153}Gd(III)-PDA complex. An equimolar concentration of DTPA was added to the solution of ^{153}Gd(III)-PDA in ammonium acetate at a pH of 7. The mixture was allowed to equilibrate for 2 days at 25 °C. The competition experiment was monitored by radio-TLC analysis using a mobile phase of 50:50 methanol/10% ammonium acetate on silica gel.

A serum stability study of the ^{153}Gd(III)-PDA complex was performed to determine if PDA interacts with proteins. A 10 μL portion of ^{153}Gd(III)-PDA in ammonium acetate with 90 μL of rat serum was incubated at 37 °C. The reaction mixture was monitored by radio-TLC using a stationary phase of ITLC-SG and a mobile phase of ethanol.

RESULTS AND DISCUSSION

Synthesis of PDA

The synthesis of 1,10-phenanthroline-2,9-dicarboxaldehyde (PDALD) resulted in an impure mixture. A yield of approximately 45.5% of PDALD was obtained from the synthesis. Selenium dioxide was effective for oxidizing 2,9-dimethyl-1,10-phenanthroline monohydrate to PDALD, although other oxidation states were also formed. PDALD was the major product, shown by the ^{1}H-NMR spectrum in Figure 4. The ^{1}H-NMR spectrum showed a peak for the aldehyde proton at 10.36 ppm, as well as the aromatic hydrogens on the phenanthroline ring at 8.30 (H5,6, singlet), 8.32 (H 3,8), and 8.81 (H4,7) ppm. Chandler, et. al. reports values of 10.45 ppm for the aldehyde proton and 8.25, 8.30, and 8.75 ppm, respectively, for the aromatic hydrogens. The IR spectrum of PDALD, shown in Figure 5, yielded a C=O stretch for the aldehyde at 1704 cm^{-1}. There was also a peak at 1734 cm^{-1} that closely matched the C=O stretch for 1,10-phenanthroline-2,9-dicarboxylic acid. A C=O stretch of 1720 cm^{-1} for PDALD was reported by Chandler, *et. al.*, which is not in agreement for the IR data obtained for this synthesis. Since the final product required full oxidation, further purification by recrystallization was not performed.

The objective for the syntheses was to obtain 1,10-phenanthroline-2,9-dicarboxylic acid. $[PDA]H_2$ was obtained from the oxidation of PDALD by 4:1 HNO_3/H_2O, with the impure $[PDA]H_2$ being purified by recrystallization from methanol. A yield of 59.3% was achieved for the final product, PDA. The melting point of the fine, yellow needles was 219.3 °C, compared to the literature value[11] of 231-232 °C. Despite the lowered melting point, ^{1}H-NMR and IR analysis produced clean spectra for the $[PDA]H_2$ crystals. The ^{1}H-NMR spectrum, shown in Figure 6, produced two sets of doublets at 8.42 ppm (H-3,8) and 8.74 ppm (H-4,7) and one

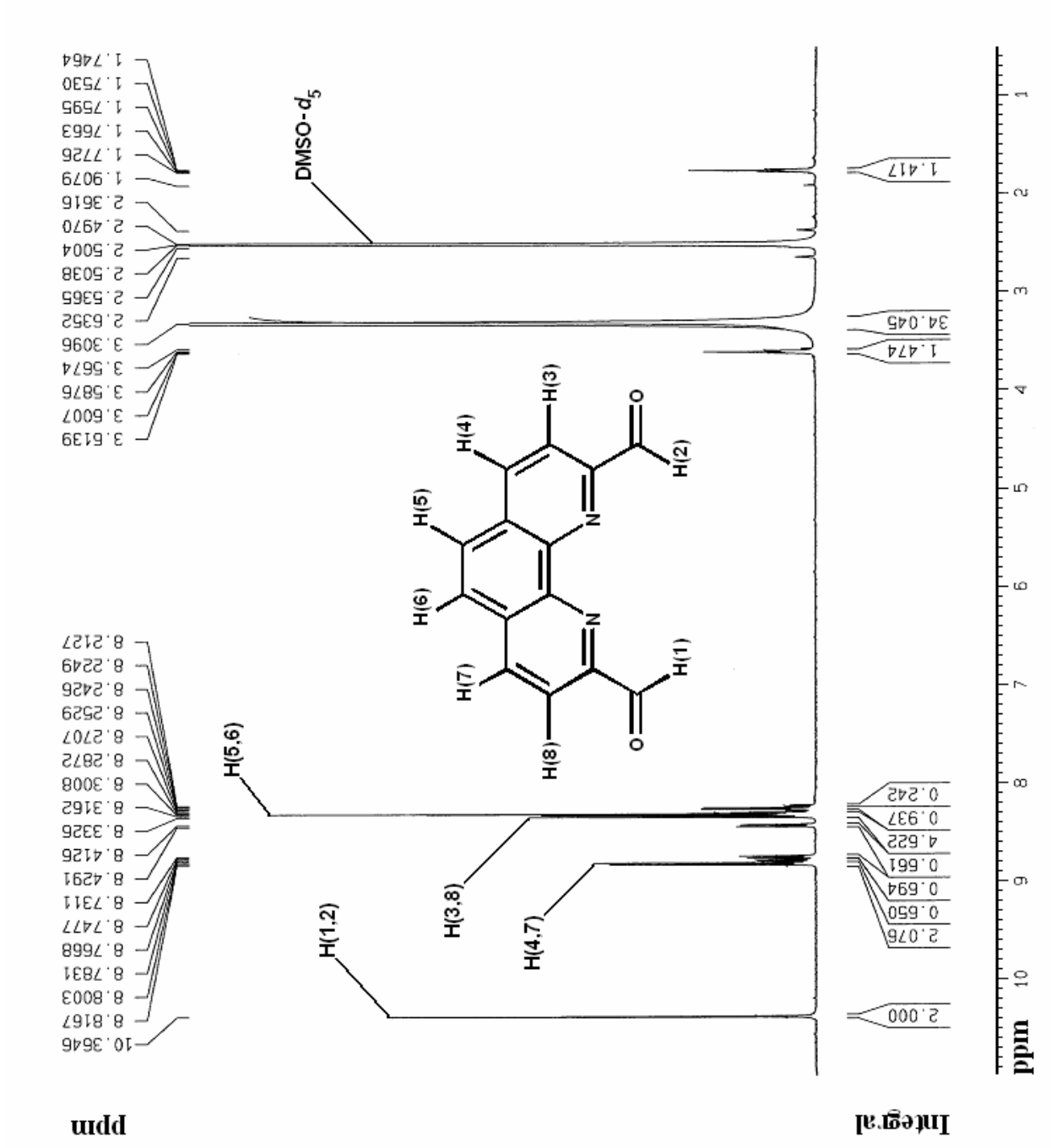

Figure 4: The ^{1}H-NMR spectrum of impure 1,10-phenanthroline-2,9-dicarboxaldehyde in DMSO-d_6.

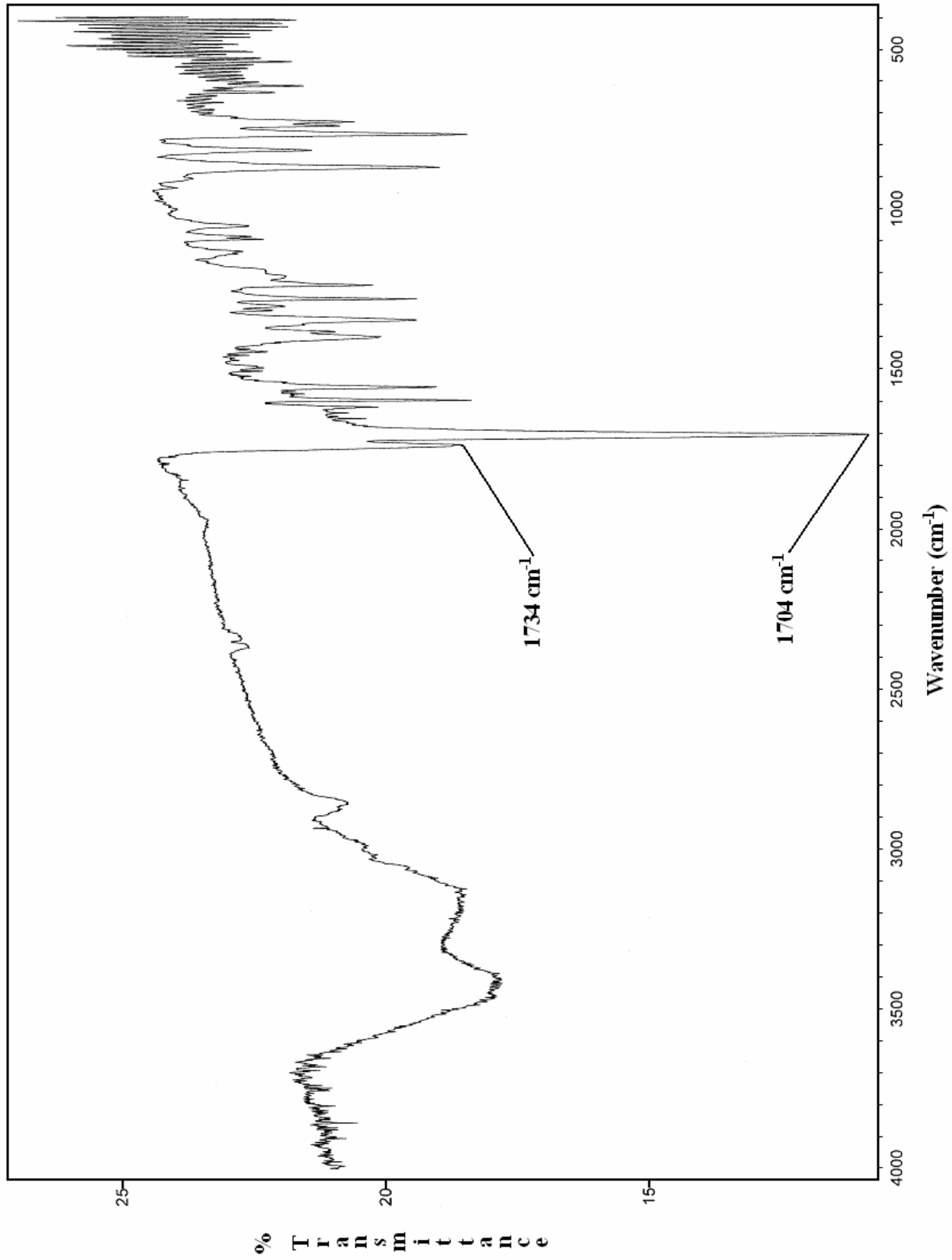

Figure 5: The IR spectrum of 1,10-phenanthroline-2,9-dicarboxaldehyde.

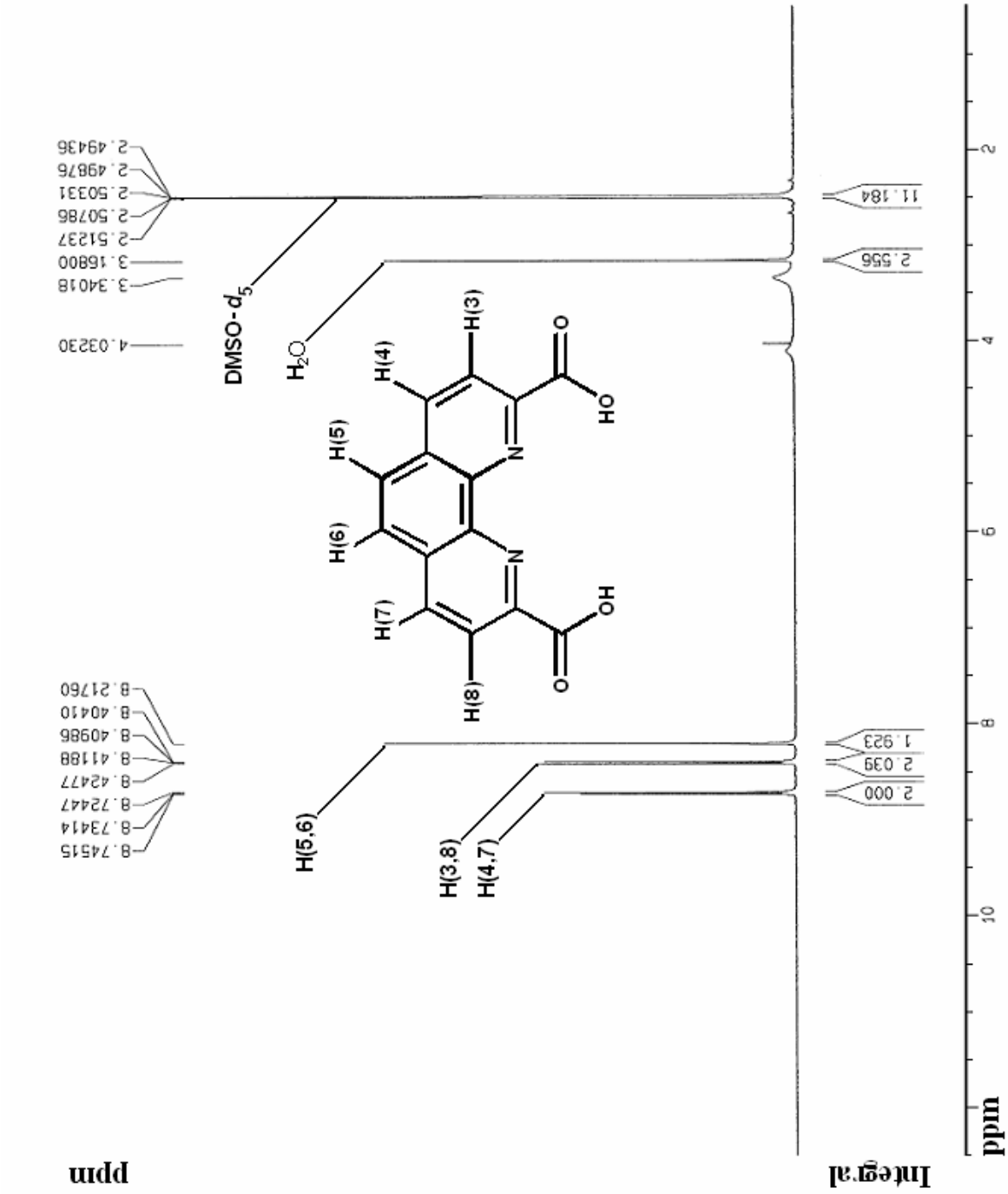

Figure 6: The ^{1}H-NMR spectrum of 1,10-phenanthroline-2,9-dicarboxylic acid in DMSO-d_6.

singlet at 8.22 ppm (H-5,6). Chandler, *et. al*. reported peak positions of 8.45, 8.75, and 8.20 ppm for $[PDA]H_2$, respectively, which are in close agreement with the values obtained for this experiment. The $[PDA]H_2$ was a monohydrate, so a peak for H_2O at 3.17 ppm was also seen. This was confirmed by the IR spectrum, where a peak for water was seen at 3384 cm^{-1}. Figure 7 shows the IR spectrum of $[PDA]H_2$ with peaks of 1739 cm^{-1} for the C=O stretch and 3079 cm^{-1} for the O-H of the carboxylic acid. The ^{1}H-NMR and IR spectra confirmed that PDALD had been successfully converted to $[PDA]H_2$. All of the solutions used in the titration experiments and the synthesis of $[Ca(PDA)(H_2O)_2]$ crystals were prepared from these crystals of $[PDA]H_2$.

Titrations Involving PDA

The titration experiments were performed utilizing UV/Vis spectroscopy as an analytical tool to detect metal complex formation involving PDA. Absorbance scans were performed from 190 to 350 nm for each titrant addition of $HClO_4$. Absorbance data were taken at selected wavelengths of 226, 235, 246, 280, and 286 nm. Absorbance maxima were shown at 235 and 280 nm for the free PDA. Upon complexation of PDA with a metal ion, a new peak at 246 nm was observed, as well as a peak shift from 280 to 286 nm. The presence of the 246 nm peak came to be regarded as diagnostic of the metal-ligand complex formation.

In order to determine the protonation constants for the ligand, PDA, a titration experiment was performed at 25.0 ± 0.1 °C in 0.10 *M* $NaClO_4$ for ionic strength. Figure 8 shows absorbance versus wavelength (nm) for the titration of PDA. Absorbance data from 226 nm was used to generate the plot of absorbance versus pH. The best plot was seen from the data taken at 226 nm for the absorbance spectra. The protonation constants for PDA were calculated using the absorbance data and pH values from this plot. Although sodium is typically an inert metal ion when introduced to a ligand, a log K_1 of 1.84 for sodium with EDTA was estimated from other

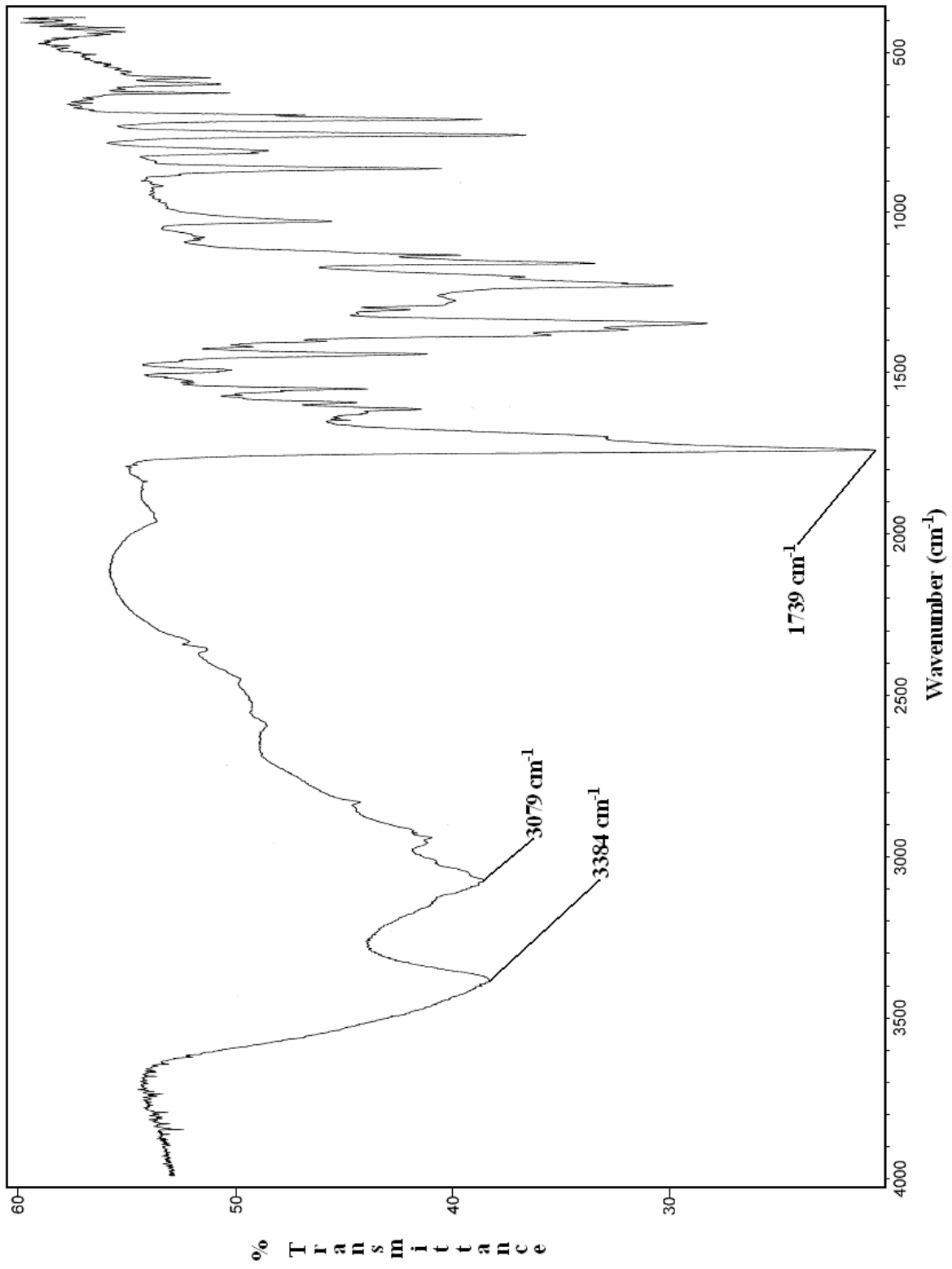

Figure 7: The IR spectrum of 1,10-phenanthroline-2,9-dicarboxylic acid monohydrate.

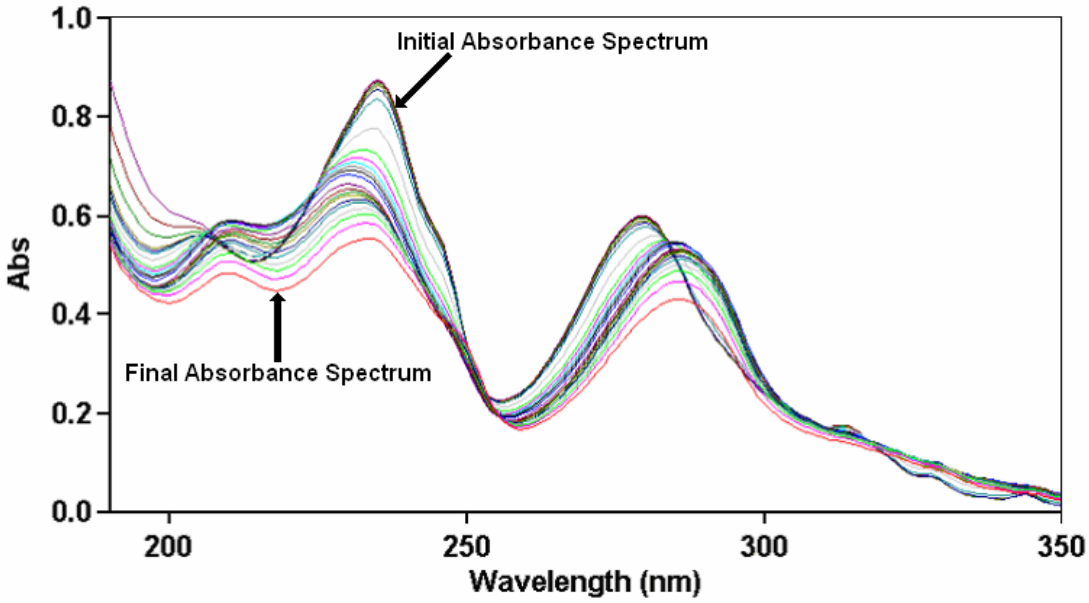

Figure 8: The absorbance versus wavelength (nm) spectra from the titration experiment conducted at 25.0 ± 0.1 °C for PDA in 0.10 *M* $NaClO_4$ for ionic strength.

reported pK backgrounds.[10] The corrected protonation constants of pK_1, pK_2, and pK_3 for PDA were 4.75, 3.71, and 2.09, respectively. The species distribution diagram of PDA, shown in Figure 9, gives the fraction of LH_3, LH_2, LH, and L relative to pH, where L is the dicarboxylate form of PDA. An illustration of the protonation events for PDA is shown in Figure 10. The third protonation event, pK_3, for PDA was difficult to see in most of the plots for absorbance versus pH due to the limits of the pH electrode. However, the absorbance data at 226 nm was the most useful for determining pK_3.

Titrations Involving Metals with PDA

At least two sets of titration experiments were performed for the determination of log K_1 for each metal ion. The first titration experiment yielded absorbance values as a function of pH for the metal ion with PDA. The protonation constants for PDA were determined to be fairly low, and it is therefore difficult to drive the metal from a PDA complex by conducting a direct titration experiment with acid, considering the high log K_1 values that metal ions exhibit with PDA. In order to solve this dilemma, a second titration experiment was implemented to drive a metal ion from the EDTA complex into the PDA complex. EDTA is a hexadentate ligand that has log K_1 values that are only slightly higher than the tetradentate ligand, PDA. The equilibrium being studied is given by Equation (1).

$$M^{n+}(EDTA)^{4-} + PDA^{2-} + H^{+} \leftrightarrows M^{n+}(PDA)^{2-} + [(EDTA)H]^{3-} \qquad (1)$$

This equation shows the exchange equilibrium of the metal ion between PDA and EDTA as a function of pH. The equilibrium was easily studied by monitoring absorbance since EDTA does not have a strong absorption band in the UV region. The titration experiment provided absorbance values as a function of pH for the competition of EDTA and PDA for the metal ion.

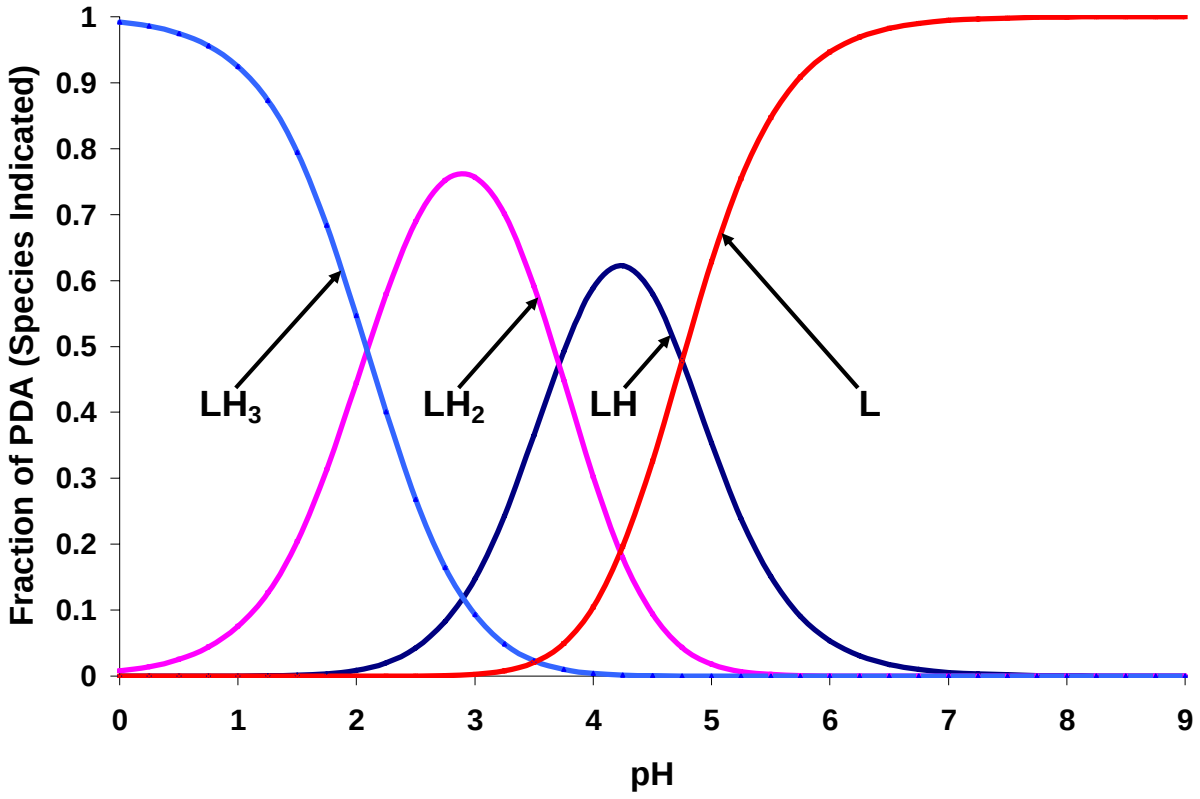

Figure 9: The protonated species distribution diagram for PDA with respect to pH.

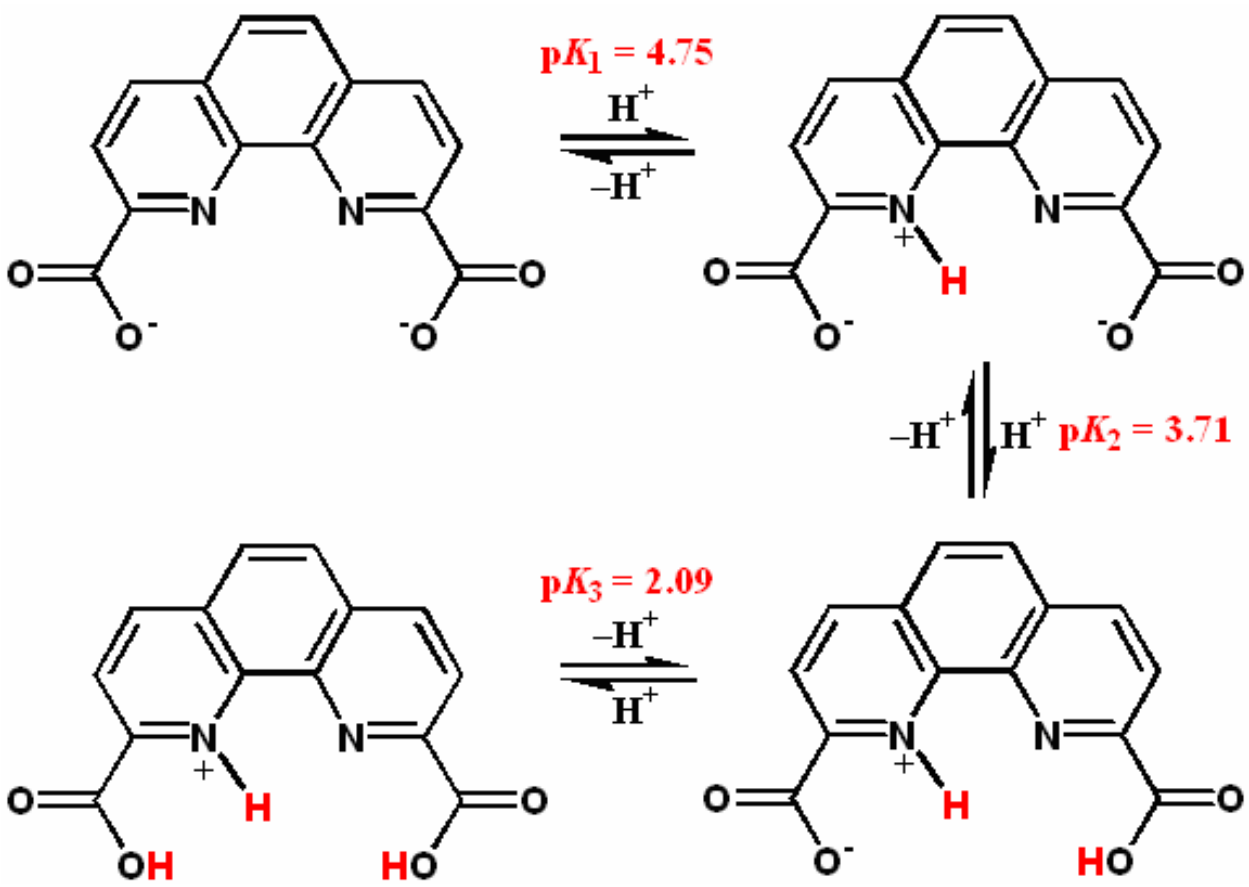

Figure 10: A diagram showing the three protonation events of PDA

As the pH of the solution is lowered, a transition was observed where Equation (1) shifts from left to right. The pK_1, first protonation constant, for EDTA is 9.52 at an ionic strength of 0.10 *M* $NaClO_4$.[10] PDA is a weaker proton base and has a much lower pK_1 at 4.75 for an ionic strength of 0.10 *M* $NaClO_4$. These large differences in pK_1 values allow PDA to complex the metal ion strongly at lower pH values relative to EDTA. The direct titration experiment of PDA with the metal ion was used only as a reference for competition reactions involving PDA and EDTA with a metal ion.

For each titration experiment, absorbance values were monitored as a function of pH. At every absorbance scan, pH values were also recorded and plotted as corrected absorbance versus pH using EXCEL. Using Equation (2), recorded absorbance values were corrected for dilution after each addition of titrant.

$$\text{Corrected Absorbance} = \frac{\text{Absorbance} \cdot \text{V}_{\text{total}}}{\text{V}_{\text{initial}}} \qquad (2)$$

Both plots of the PDA with the metal ion and the PDA and EDTA competition experiment with the metal ion were overlaid in EXCEL. The absorbances of the two plots were similar at lower pH values, where only the PDA complex existed. For the PDA and EDTA competition experiment with the metal ion, a crossover from the EDTA complex at higher pH values to the PDA complex at lower pH values was observed. This crossover produced a slope for which a pH_{50} value was calculated. The pH_{50} value is an inflection point in the slope where an equal distribution of the metal ion exists between the PDA and EDTA. In order to obtain the pH_{50}, pH and absorbance values were selected for the slope found from the plot of the competition experiment between PDA and EDTA for the metal ion. An $\bar{n}$ observed calculation was performed for the slope using Equation (3).

$$\bar{n}_{observed} = \frac{\text{Abs} - \text{Abs}_{\text{ini}}}{\text{Abs}_{\text{inf}} - \text{Abs}_{\text{ini}}} \quad (3)$$

The total ligand concentration, $[L]_{total}$, in the sample solution was also calculated using Equation (4).

$$[\text{L}]_{\text{total}} = \frac{[\text{L}]_{\text{ini}} \cdot \text{V}_{\text{ini}}}{\text{V}_{\text{total}}} \quad (4)$$

After the $\bar{n}$ values and the total ligand concentrations were known, the distribution between the complexed ligand, [ML] and the free ligand, [L], was calculated using Equations (5) and (6).

$$[\text{ML}] = \bar{n}_{observed} \cdot [\text{L}]_{\text{total}} \quad (5)$$

$$[\text{L}] = [\text{L}]_{\text{total}} - [\text{ML}] \quad (6)$$

The total hydrogen ion concentration, $[H^+]$, in the sample solution was calculated using Equation (7).

$$[\text{H}^+] = 10^{-\text{pH}} \quad (7)$$

The values obtained from Equations (5), (6), and (7) were used to calculate pH_{50} in Equation (8), where L_1 is PDA and L_2 is EDTA or DTPA.

$$\text{pH}_{50} = \frac{[\text{ML}_1][\text{L}_2\text{H}]}{[\text{ML}_2][\text{L}_1][\text{H}^+]} \quad (8)$$

Finally, the stability constant, log K_1, for each metal ion with PDA was calculated using Equation (9).

$$\log K_1\,(\text{PDA}) = \log K_1\,(\text{EDTA}) - \text{p}K_1\,(\text{EDTA}) + \text{pH}_{50} \quad (9)$$

Molecular modeling of metal ions with ionic radii of approximately 1.0 Å were shown to reduce the steric strain on PDA, and thus reduce the overall energy of the complex. The opposite effect occurs with smaller metal ions, such as Mg(II), and larger metal ions, such as Ba(II),

which distort the rigid structure of PDA. Molecular mechanics (MM+) calculations were performed for metal ions with PDA and a plot of energy (kcal·mol^{-1}) versus metal-oxygen bond length (Å) was generated, which is illustrated in Figure 11. The stability constants, log K_1, for metals with PDA from the titration experiments complemented the results obtained from the MM+ calculations. This shows an enhanced complex stability with metals of an ionic radius of approximately 1.0 Å.

The log K_1 results for metal ions with PDA were determined from absorbance data and corresponding pH values taken from the EDTA and PDA competition experiments with metal ions using Equations (1-9) shown above. Ethylenediamine dicarboxylic acid (EDDA) is the unpreorganized precursor to PDA, so the log K_1 results for PDA with the metal ions were compared to EDDA. The log K_1 values for PDA with the metal ions used in the titrations are displayed in Table 1, as well as the log K_1 values for EDDA with metal ions.[10] Also, Δ log K_1 between PDA and EDDA was calculated for each metal ion used and displayed in Table 1.

Barium(II)-PDA results

Ba(II) has an ionic radius of 1.36, which is slightly larger than the target radius of 1.0 Å for PDA. The UV absorbance spectra are shown in Figure 12 for the titration of Ba(II) with PDA. A example plot of corrected absorbance versus pH for Ba(II) is shown in Figure 13. Also, the observed and calculated $\bar{n}$ versus pH plots are shown in Figure 14. From the selected wavelengths described above, a log K_1 of 5.50 was calculated from the absorbance data using Equations (1-9). The reported formation constant for EDDA with Ba(II) was 3.3, which was weaker when compared to the log K_1 for that of PDA with Ba(II). A Δ log K_1 of 2.20 between the log K_1 values of PDA and EDDA with Ba(II) was calculated and showed a slight increase in

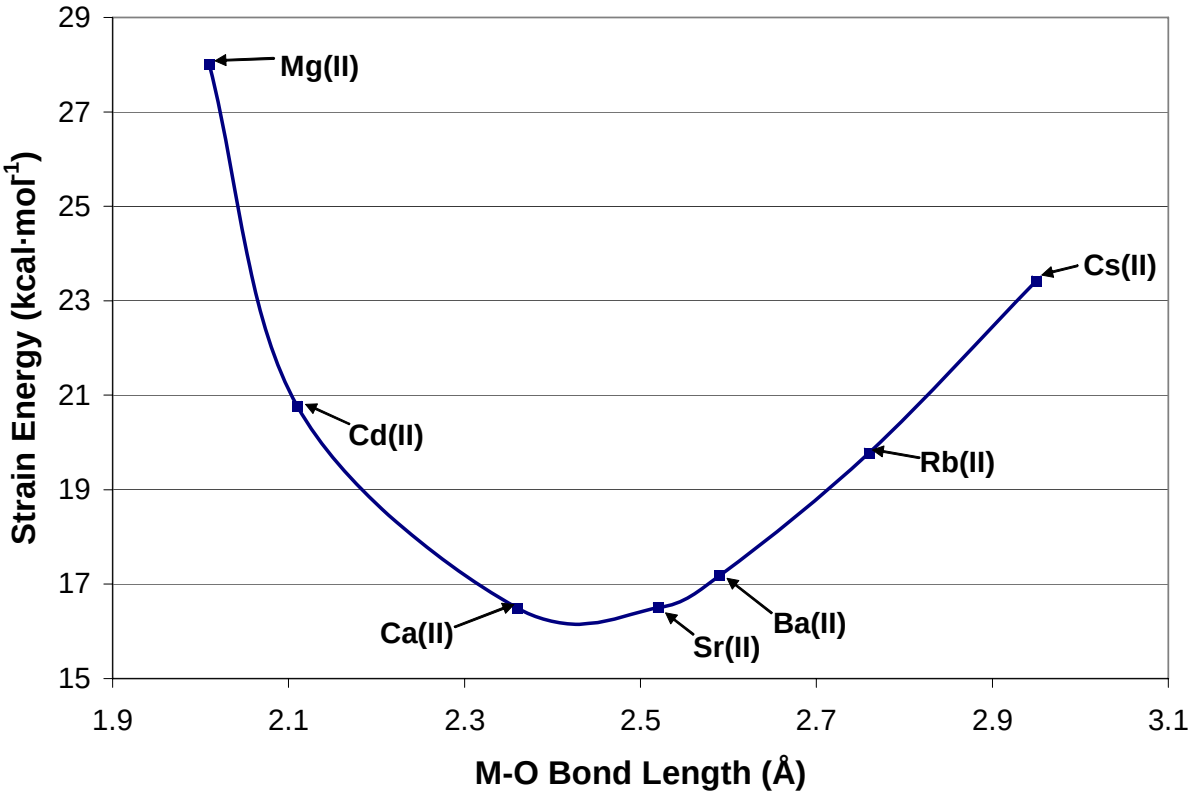

Figure 11: The calculated strain energy (kcal·mol^{-1}) versus metal-oxygen bond length (Å) for M^{n+}-PDA complexes using Hyperchem embedded MM+ calculations.

Table 1: The comparison of log K_1 data for metal ions with PDA and EDDA

Metal Ion	Ionic Radius (Å)	log K_1 (PDA)	log K_1 (EDDA)[10]	Δ log K
Mg^{2+}	0.74	3.30	4.0	-0.70
Ca^{2+}	1.00	7.72	4.0	3.72
Sr^{2+}	1.18	5.60	3.6	2.00
Ba^{2+}	1.36	5.50	3.3	2.20
Pb^{2+}	1.19	12.62	10.6	2.02
La^{3+}	1.03	13.40	7.0	6.40
Gd^{3+}	0.93	14.84	8.1	6.74
Cd^{2+}	0.95	12.87	9.1	3.77
Zn^{2+}	0.74	11.63	11.1	0.53
Ni^{2+}	0.69	12.73	13.6	-0.87
Cu^{2+}	0.57	13.70	16.2	-2.50

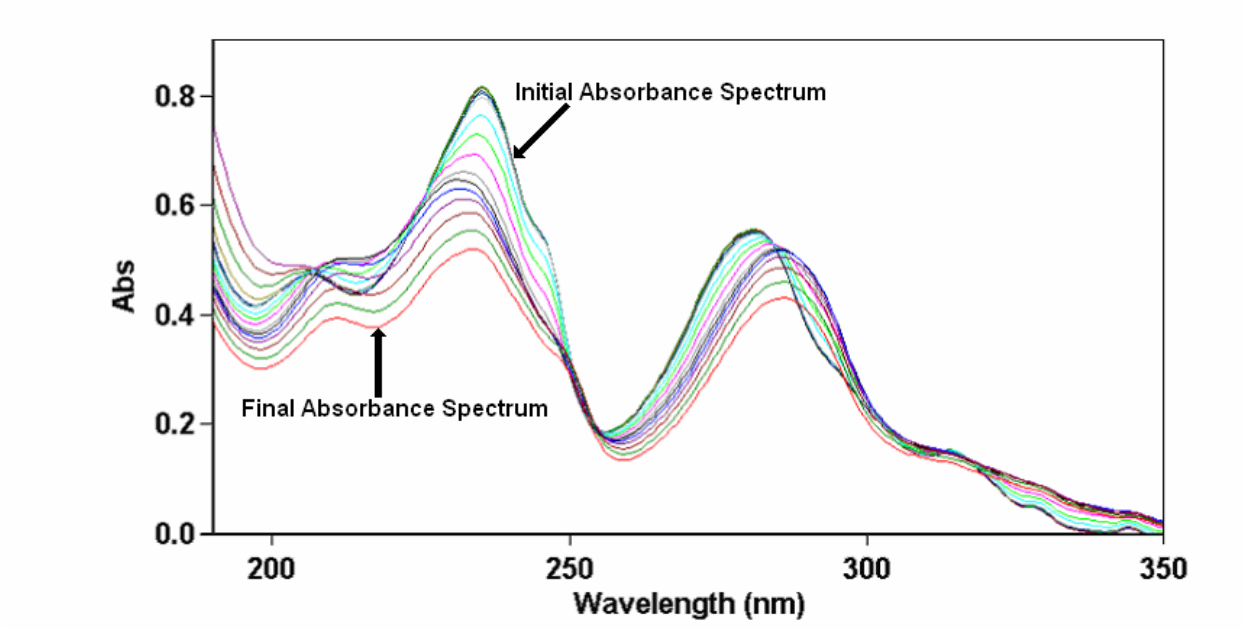

a.)

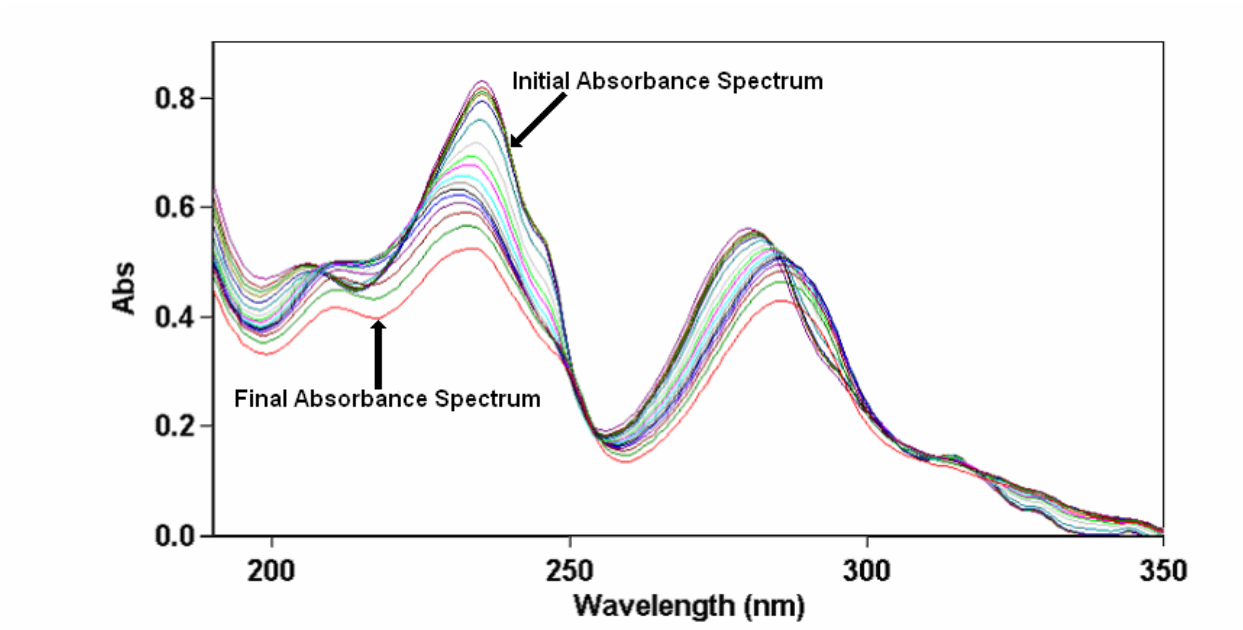

b.)

Figure 12: The UV absorbance spectra for the titration of (a) 1:1 Ba(II) and PDA and (b) 1:1:1 Ba(II), PDA, and EDTA

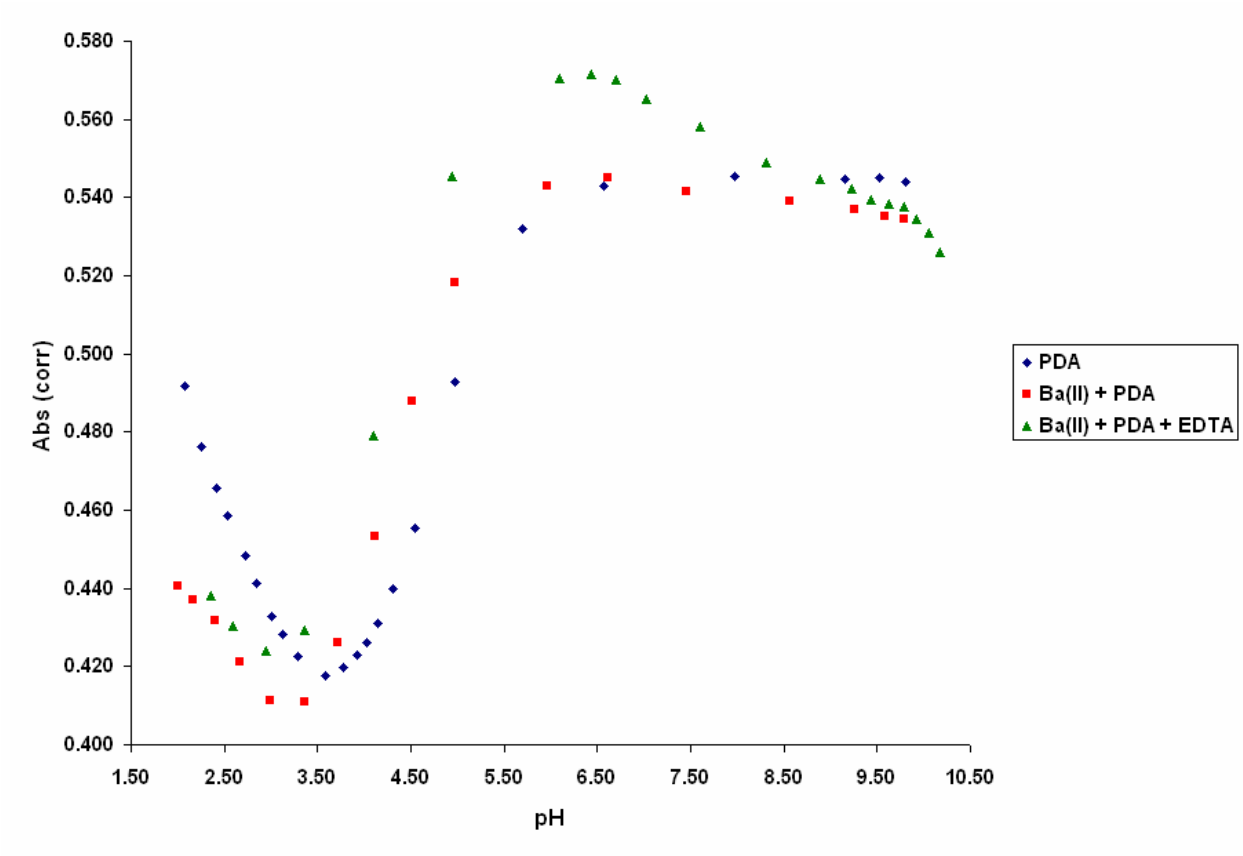

Figure 13: The combined 246 nm corrected absorbance data versus pH from titration experiments involving Ba(II). The titration of PDA at this wavelength is also shown for reference.

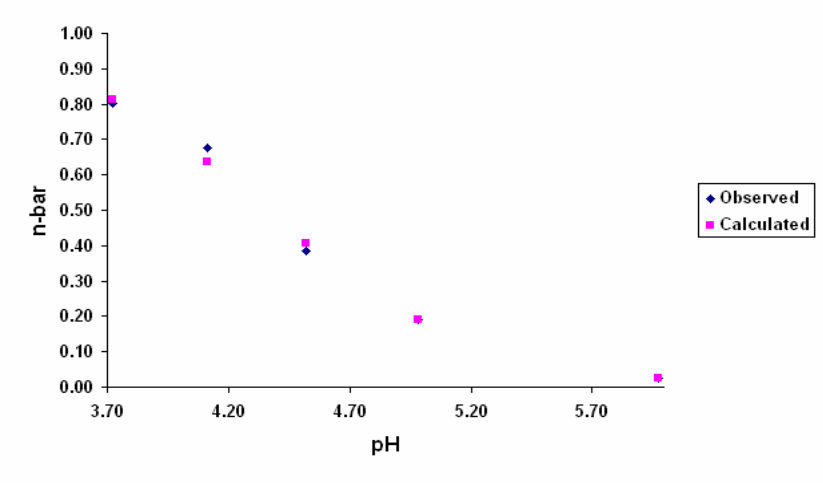

a.)

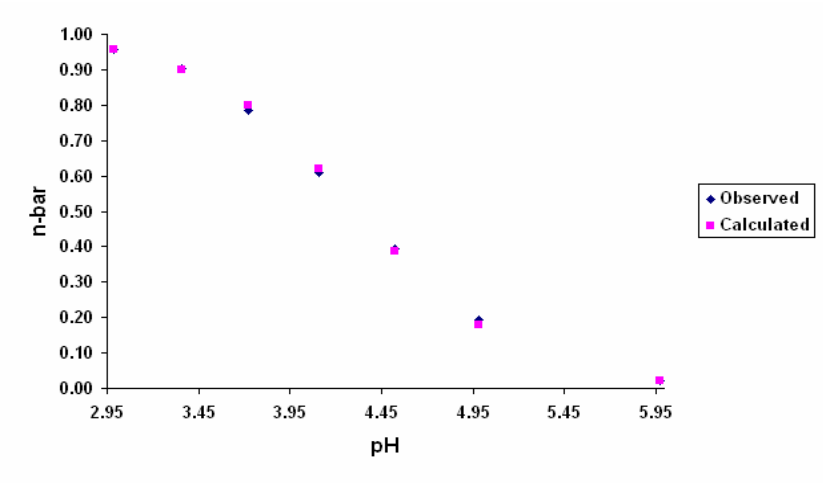

b.)

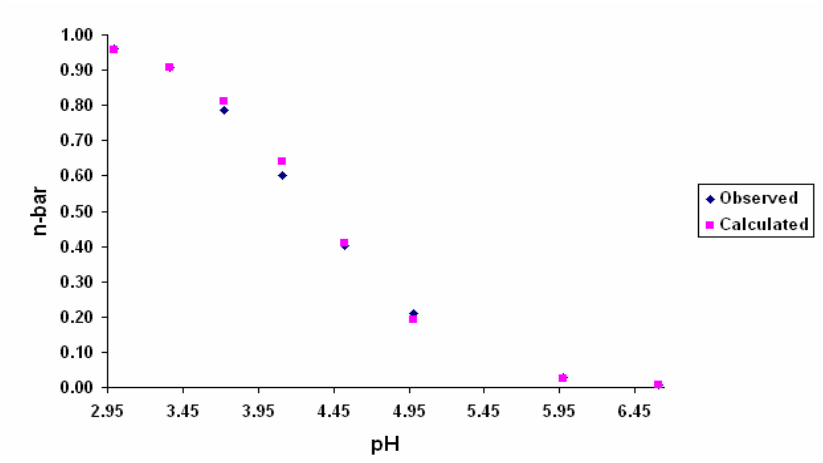

c.)

Figure 14: The comparison of $\bar{n}$ observed versus $\bar{n}$ calculated with respect to pH at wavelengths of a.) 226 nm, b.) 235 nm, and c.) 280 nm for the competition of PDA and EDTA for Ba(II).

stability of the PDA complex of Ba(II) relative to the EDDA complex of Ba(II).

Cadmium(II)-PDA results

Cd(II) has an ionic radius of 0.95, which is almost ideal to span the region between the carboxylate groups of PDA. The UV absorbance spectra are shown in Figure 15 for the titration of Cd(II) with PDA. A example plot of corrected absorbance versus pH for Cd(II) is shown in Figure 16. Also, the observed and calculated $\bar{n}$ versus pH plots are shown in Figure 17. From the selected wavelengths described above, a log K_1 of 12.87 was calculated for Cd(II) with PDA using Equations (1-9). When compared to the log K_1 of EDDA, which is 9.1, PDA showed an increase in complex stability. A Δ log K_1 of 3.77 quantified the difference in stability of the PDA complex versus the EDDA complex of Cd(II).

Calcium(II)-PDA results

The ionic radius of Ca(II) is 1.00 Å, which allows a suitable fit between the carboxylate groups of PDA. The UV absorbance spectra are shown in Figure 18 for the titration of Ca(II) with PDA. A example plot of corrected absorbance versus pH for Ca(II) is shown in Figure 19. Also, the observed and calculated $\bar{n}$ versus pH plots are shown in Figure 20. From the selected wavelengths described above, a log K_1 of 7.72 was calculated from the absorbance data for Ca(II) with PDA using Equations (1-9). This showed an enhanced complex stability when compared to EDDA. The reported formation constant for EDDA is 4.0 for Ca(II) and the Δ log K_1 for the PDA complex versus the EDDA complex of Ca(II) is 3.72.

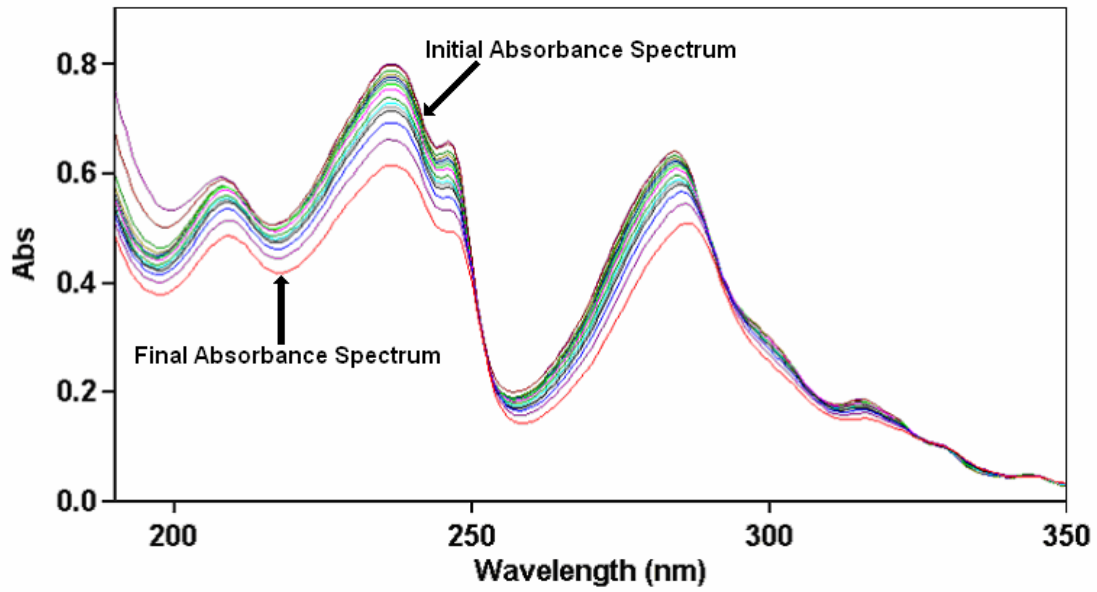

a.)

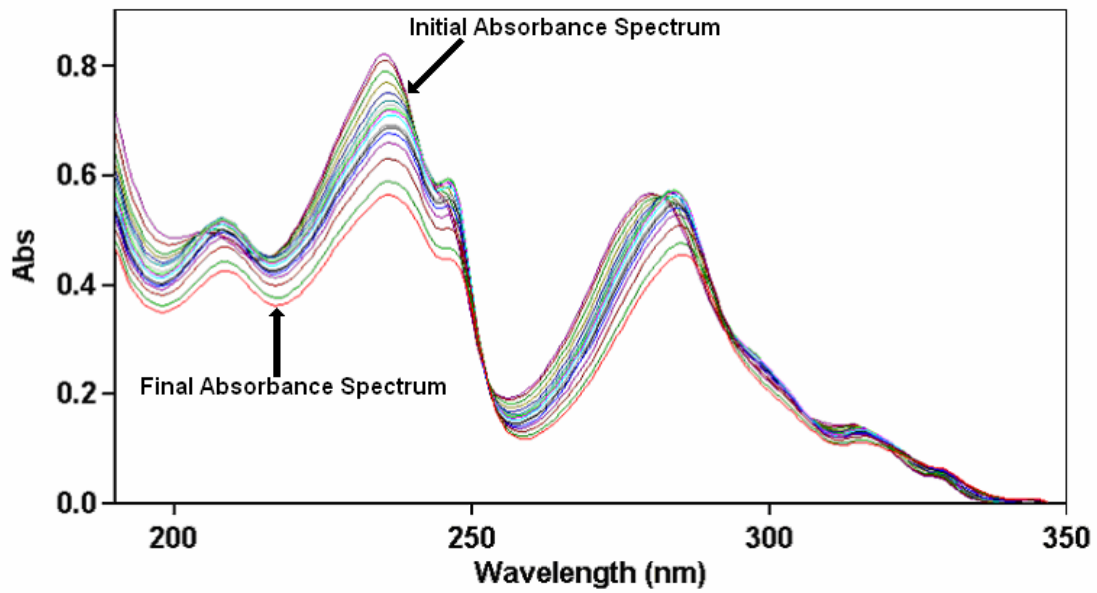

b.)

Figure 15: The UV absorbance spectra for the titration of (a) 1:1 Cd(II) and PDA and (b) 1:1:1 Cd(II), PDA, and EDTA

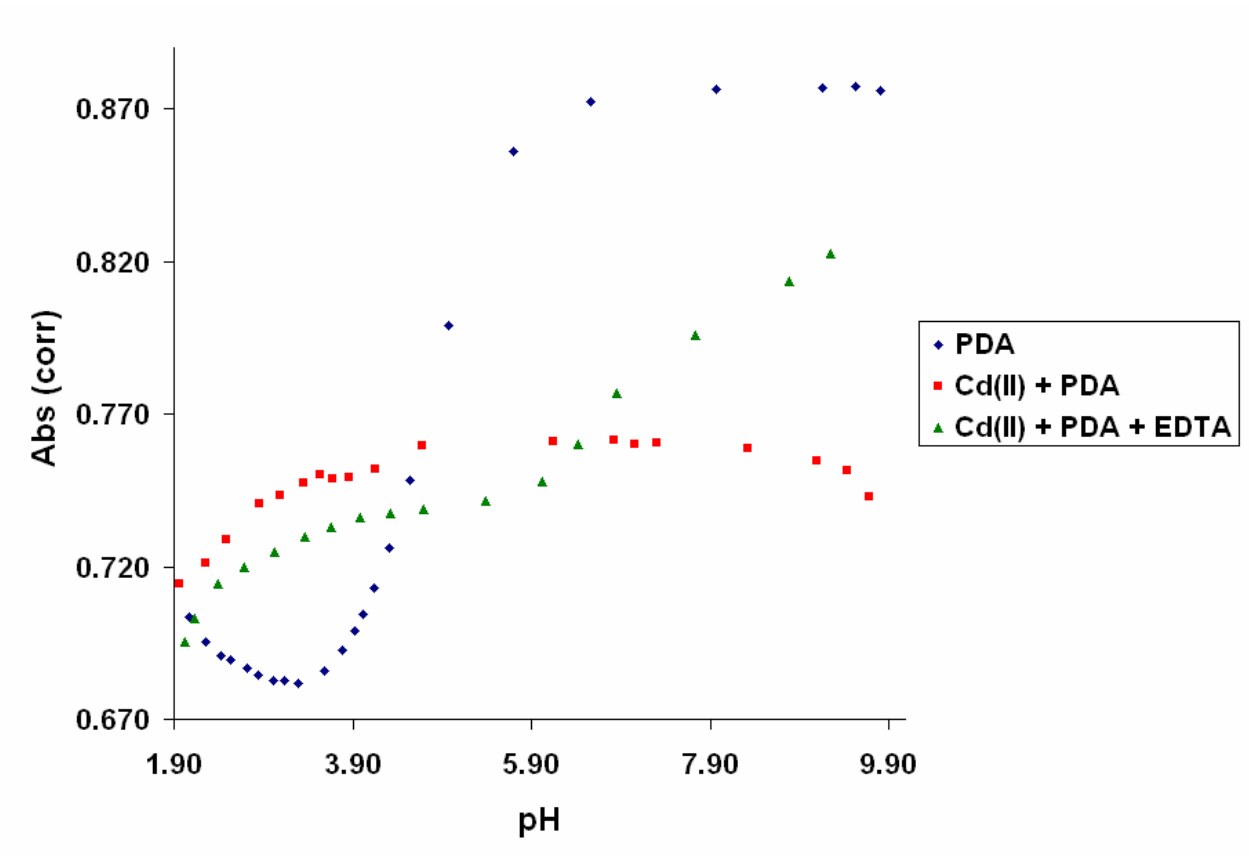

Figure 16: The combined 235 nm corrected absorbance data versus pH from titration experiments involving Cd(II). The titration of PDA at this wavelength is also shown for reference.

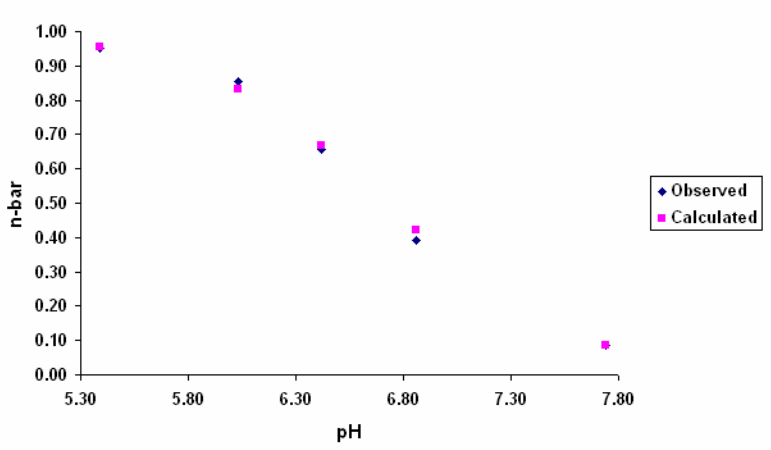

a.)

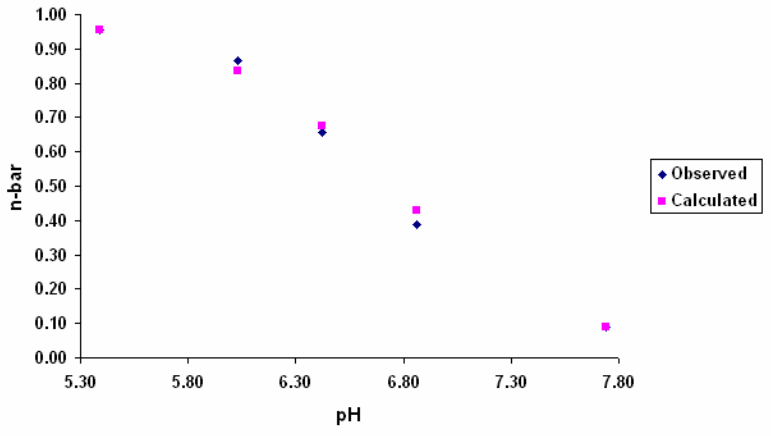

b.)

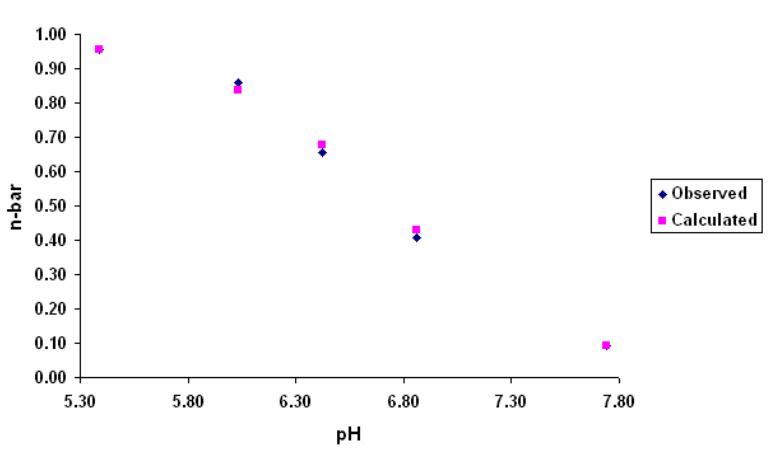

c.)

Figure 17: The comparison of $\bar{n}$ observed versus $\bar{n}$ calculated with respect to pH at wavelengths of a.) 235 nm, b.) 246 nm, and c.) 286 nm for the competition of PDA and EDTA for Cd(II).

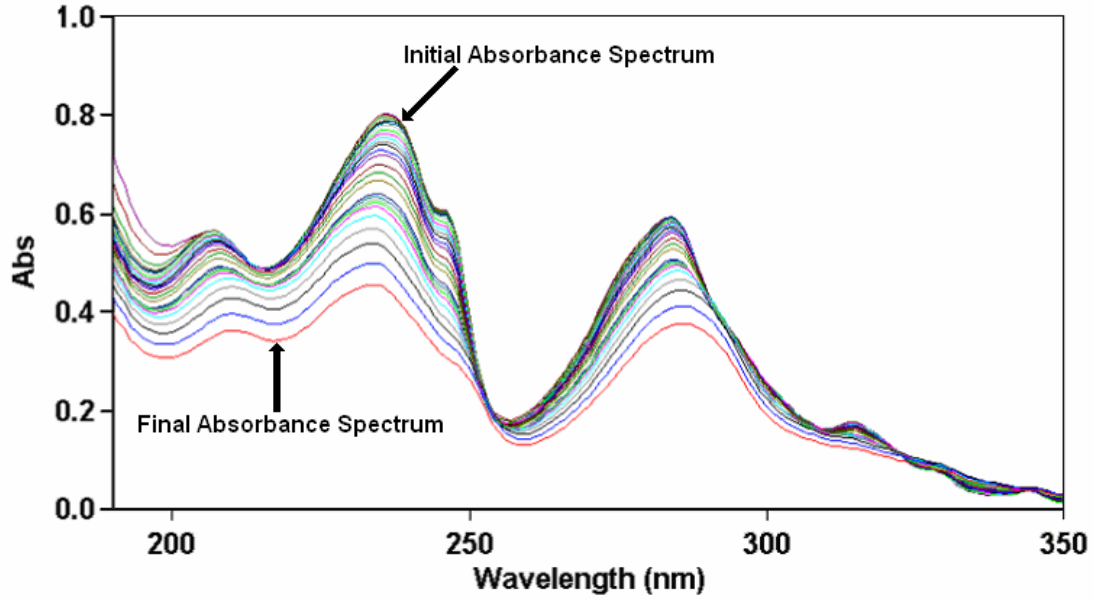

a.)

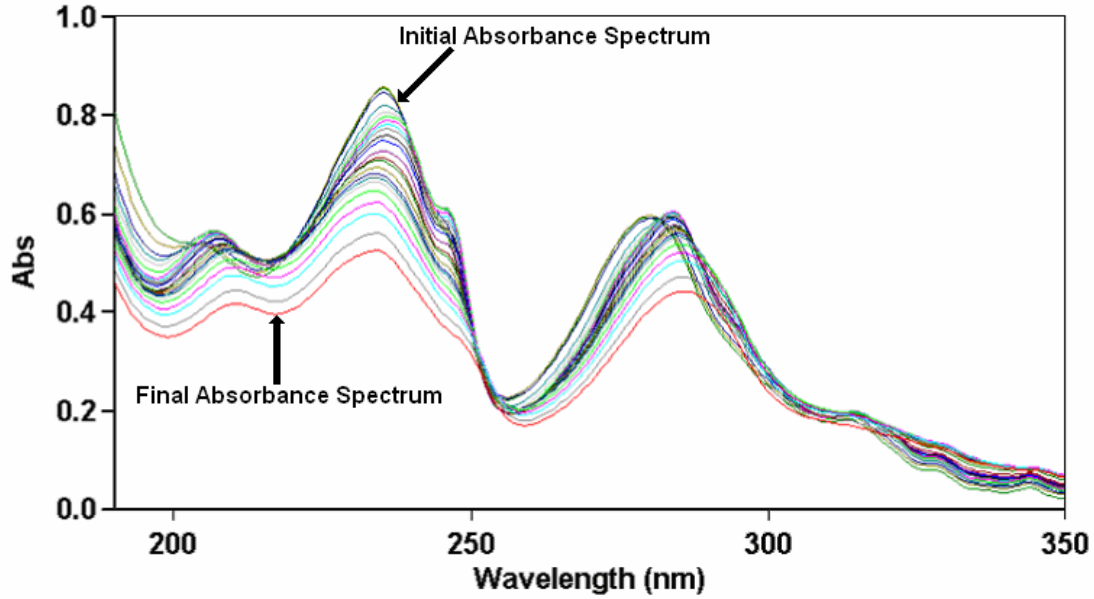

b.)

Figure 18: The UV absorbance spectra for the titration of (a) 1:1 Ca(II) and PDA and (b) 1:1:1 Ca(II), PDA, and EDTA

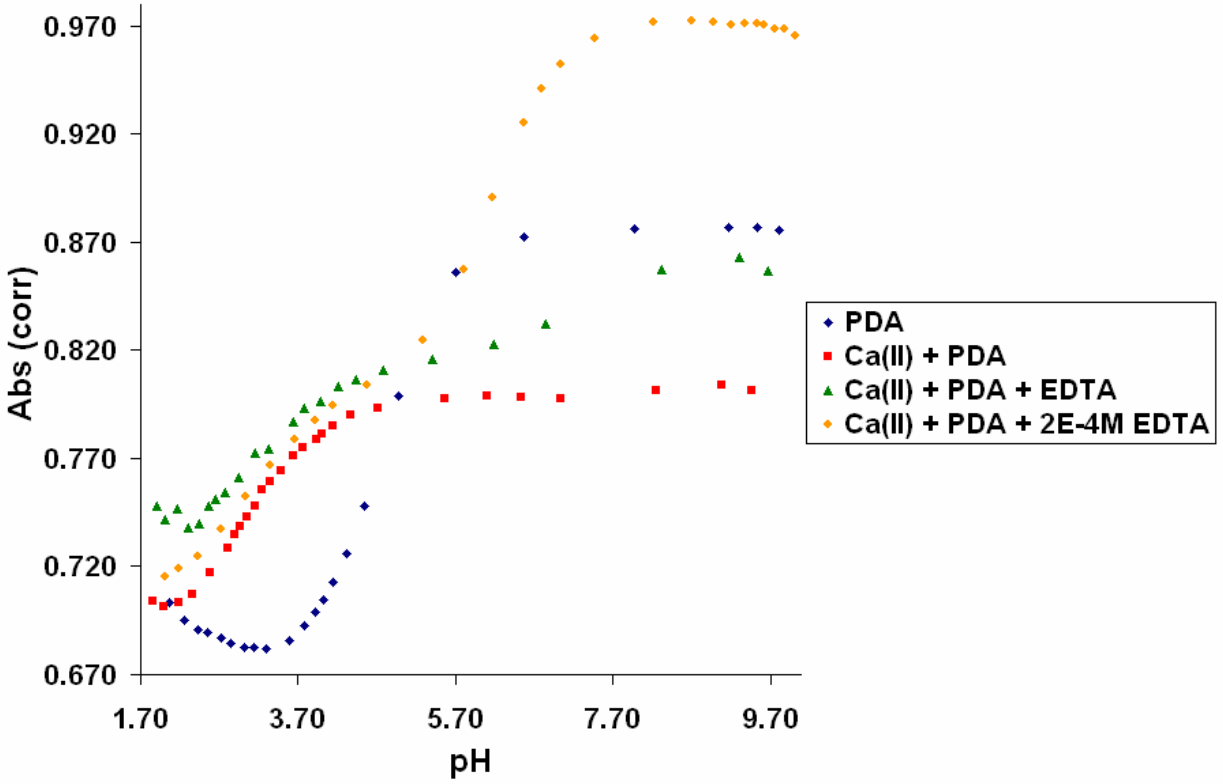

Figure 19: The combined 235 nm corrected absorbance data versus pH from titration experiments involving Ca(II). The titration of PDA at this wavelength is also shown for reference.

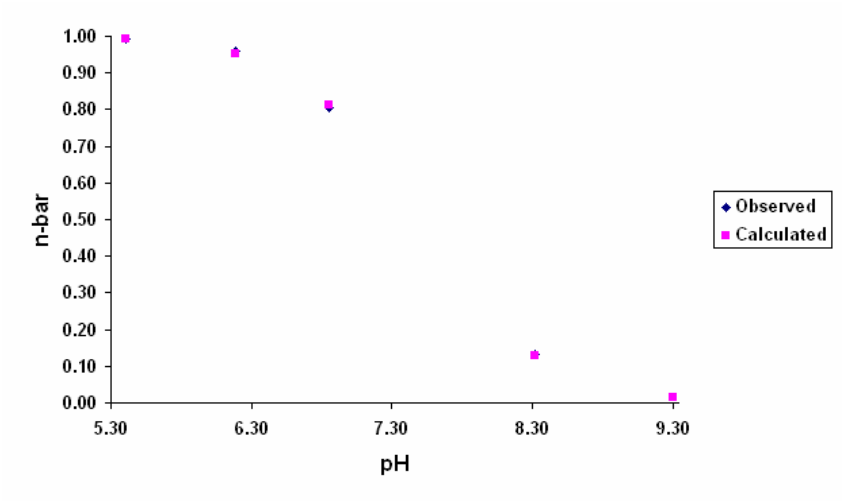

a.)

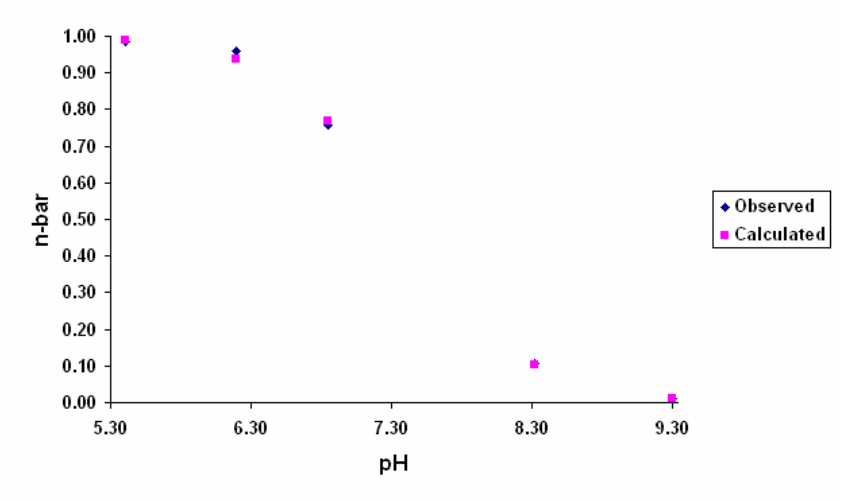

b.)

Figure 20: The comparison of $\bar{n}$ observed versus $\bar{n}$ calculated with respect to pH at wavelengths of a.) 246 nm and b.) 280 nm for the competition of PDA and EDTA for Ca(II).

Copper(II)-PDA results

The ionic radius of Cu(II) is 0.57 Å, which is far below the target ionic radius of 1.0 Å for PDA. The UV absorbance spectra are shown in Figure 21 for the titration of Cu(II) with PDA. A example plot of corrected absorbance versus pH for Ba(II) is shown in Figure 22. Also, the observed and calculated $\bar{n}$ versus pH plots are shown in Figure 23. From the selected wavelengths described above, a log K_1 of 13.70 for Cu(II) with PDA was calculated from the absorbance data using Equations (1-9). The reported formation constant for EDDA with Cu(II) is 16.2, which is stronger when compared to the log K_1 for that of PDA with Cu(II). A Δ log K_1 of –2.50 between the log K_1 values of PDA and EDDA with Cu(II) was calculated and showed the lack of stability of the PDA complex of Cu(II) relative to the EDDA complex of Cu(II).

Gadolinium(III)-PDA results

The ionic radius of Gd(III) is 0.93 Å, which is relatively close to the ideal ionic radius of 1.0 Å for PDA. The UV absorbance spectra are shown in Figure 24 for the titration of Gd(III) with PDA. A example plot of corrected absorbance versus pH for Gd(III) is shown in Figure 25. Also, the observed and calculated $\bar{n}$ versus pH plots are shown in Figure 26. From the selected wavelengths described above, a log K_1 of 14.84 was calculated from the absorbance data for Gd(III) with PDA using Equations (1-9). The reported formation constant for EDDA is 8.1 with Gd(III), which yields a Δ log K_1 of 6.74 when compared with the log K_1 for PDA with Gd(III). The benefits of preorganization may be seen from this overwhelming difference in log K_1 between PDA and EDDA for Gd(III).

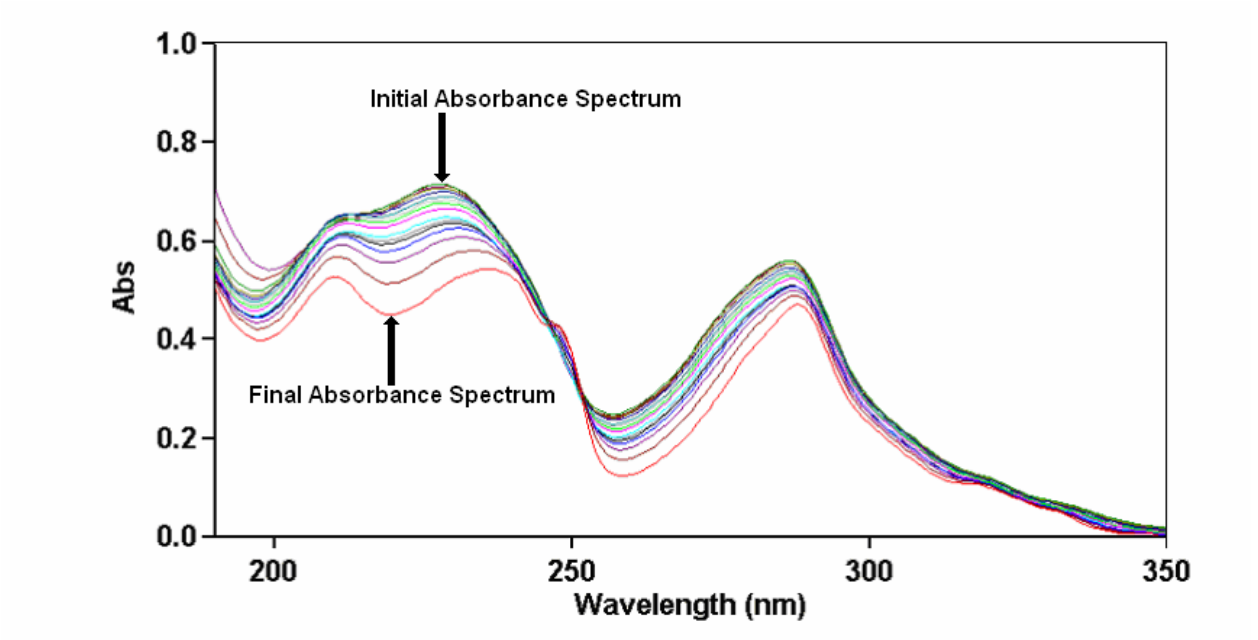

a.)

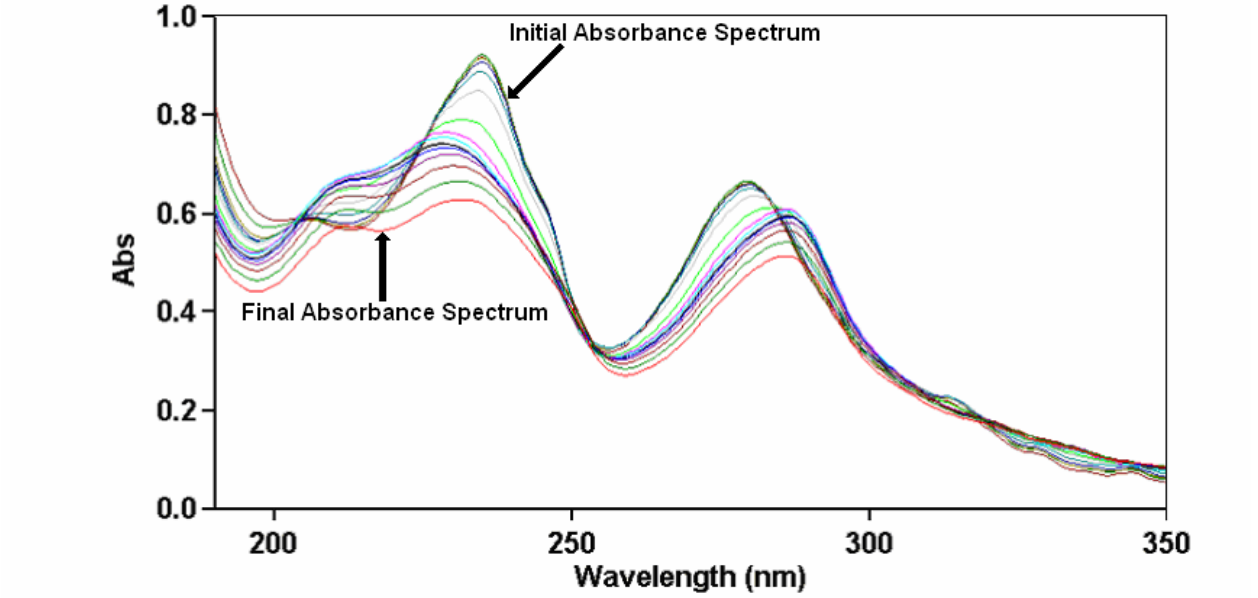

b.)

Figure 21: The UV absorbance spectra for the titration of (a) 1:1 Cu(II) and PDA and (b) 1:1:1 Cu(II), PDA, and EDTA

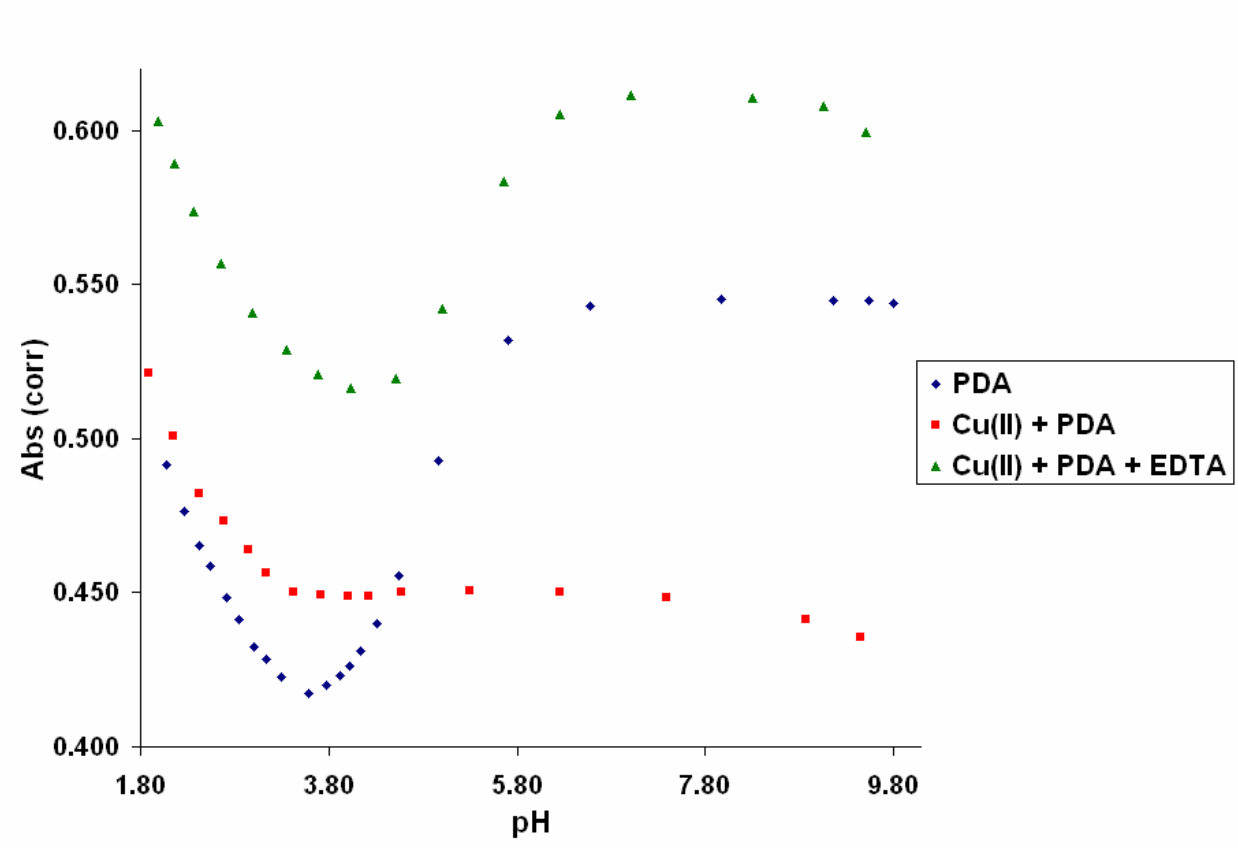

Figure 22: The combined 246 nm corrected absorbance data versus pH from titration experiments involving Cu(II). The titration of PDA at this wavelength is also shown for reference.

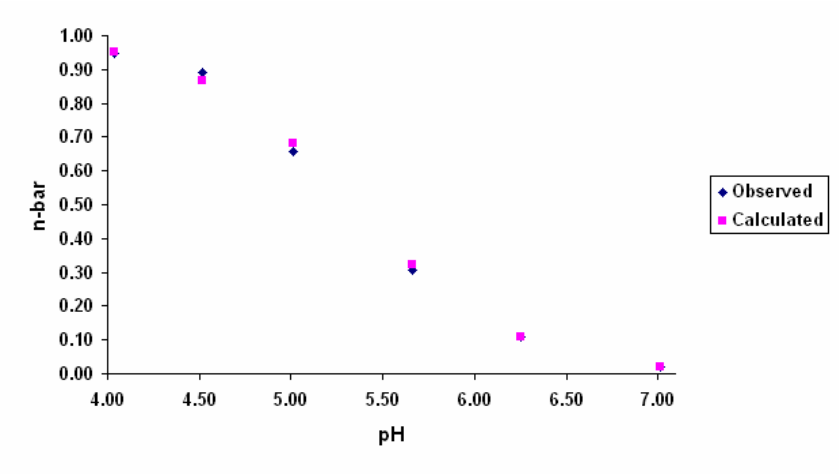

a.)

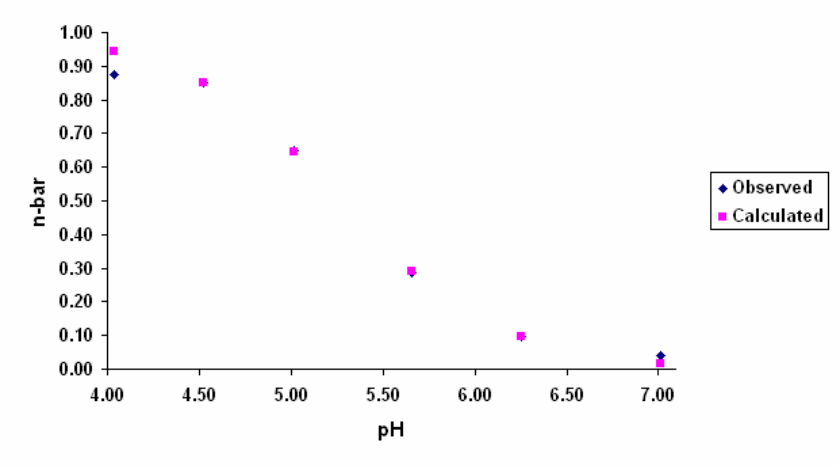

b.)

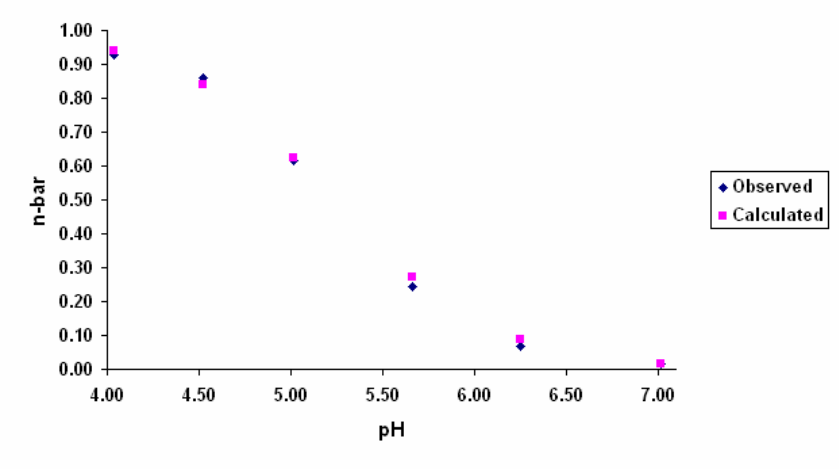

c.)

Figure 23: The comparison of $\bar{n}$ observed versus $\bar{n}$ calculated with respect to pH at wavelengths of a.) 235 nm, b.) 246 nm, and c.) 280 nm for the competition of PDA and EDTA for Cu(II).

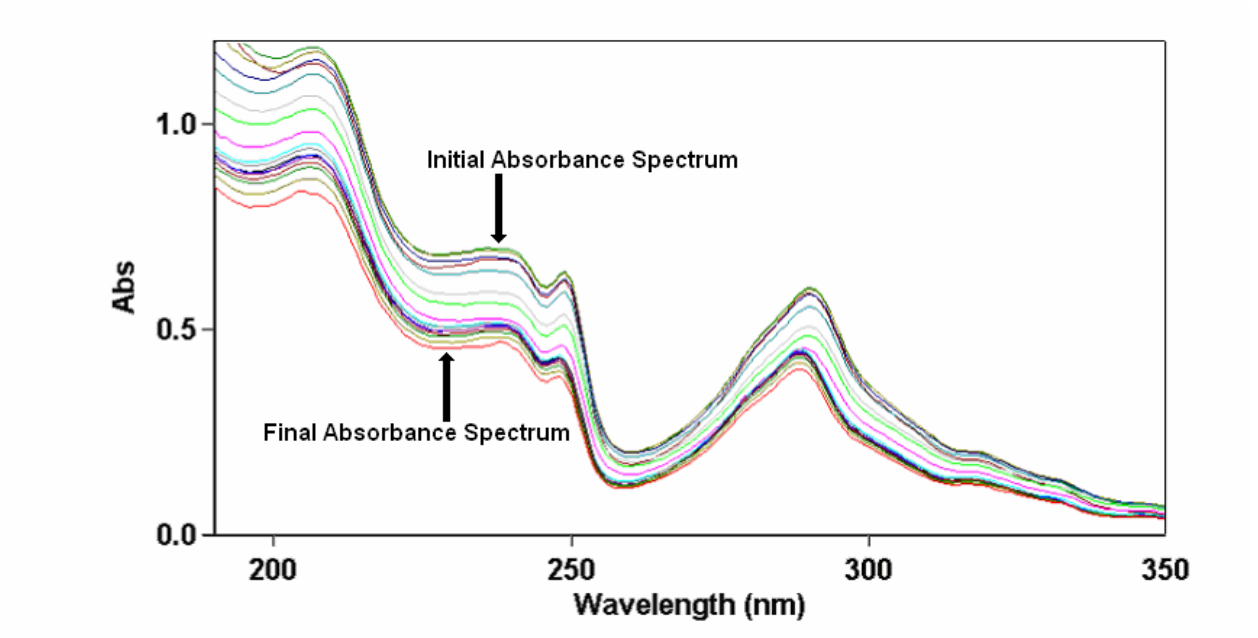

a.)

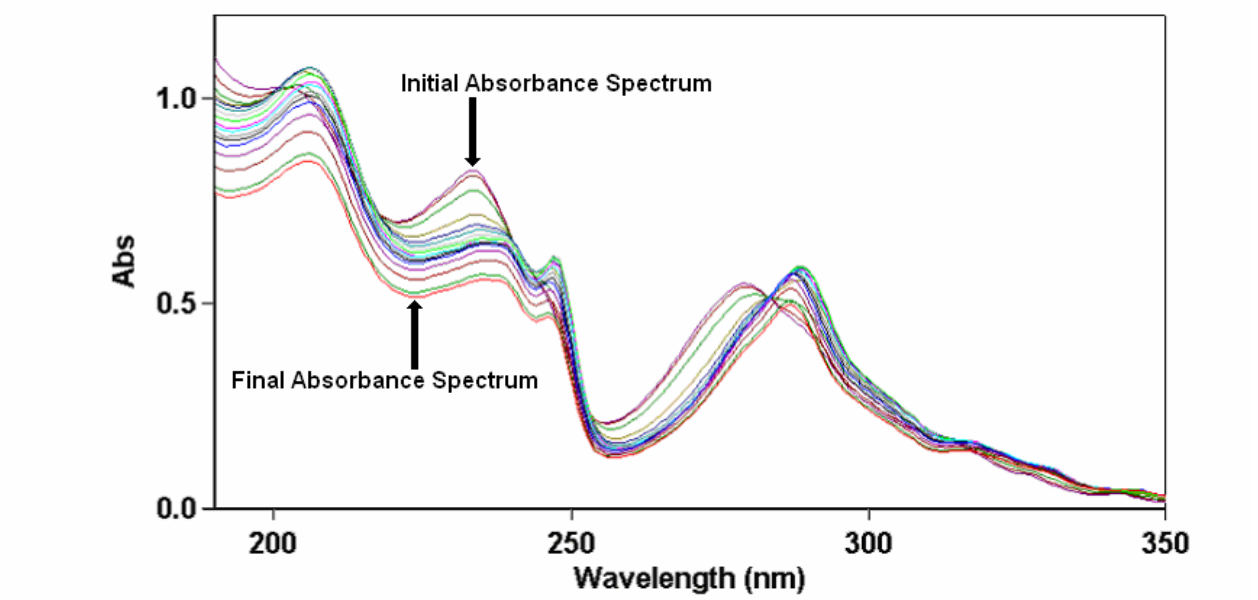

b.)

Figure 24: The UV absorbance spectra for the titration of (a) 1:1 Gd(III) and PDA and (b) 1:1:1 Gd(III), PDA, and EDTA

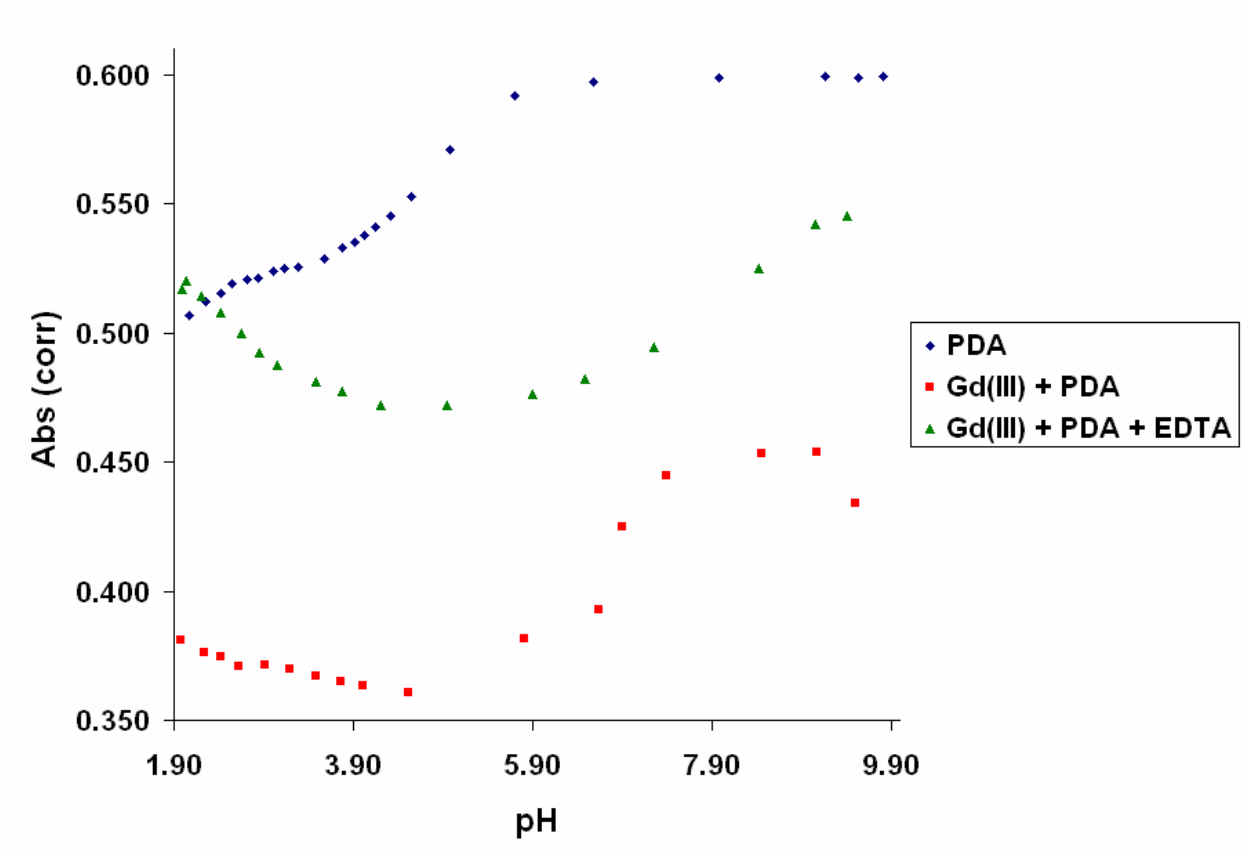

Figure 25: The combined 280 nm corrected absorbance data versus pH from titration experiments involving Gd(III). The titration of PDA at this wavelength is also shown for reference.

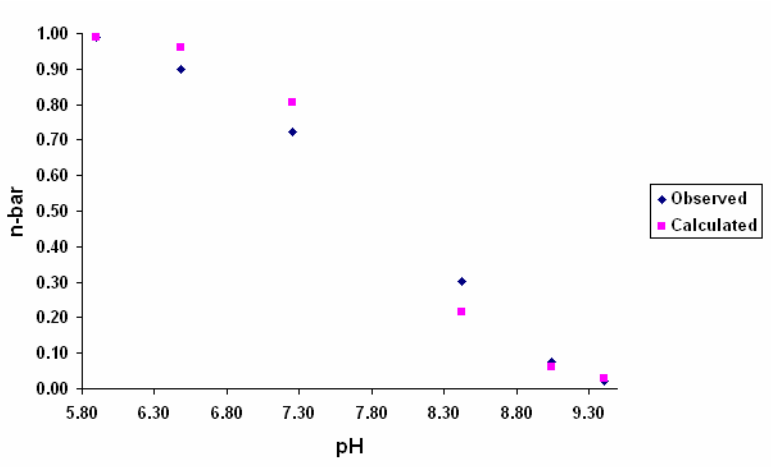

a.)

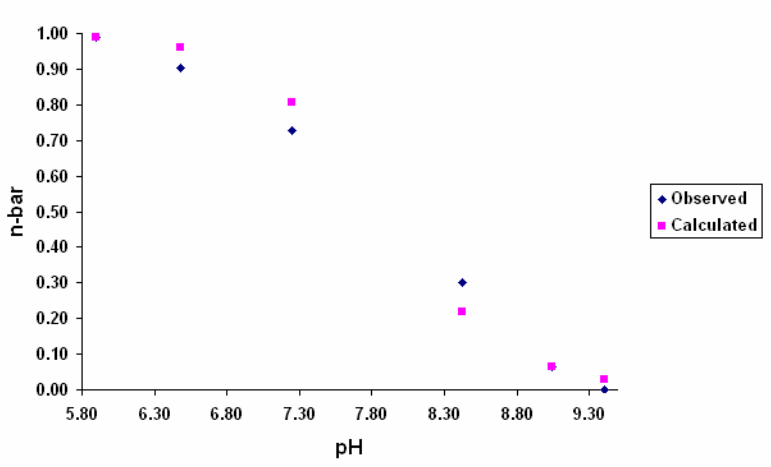

b.)

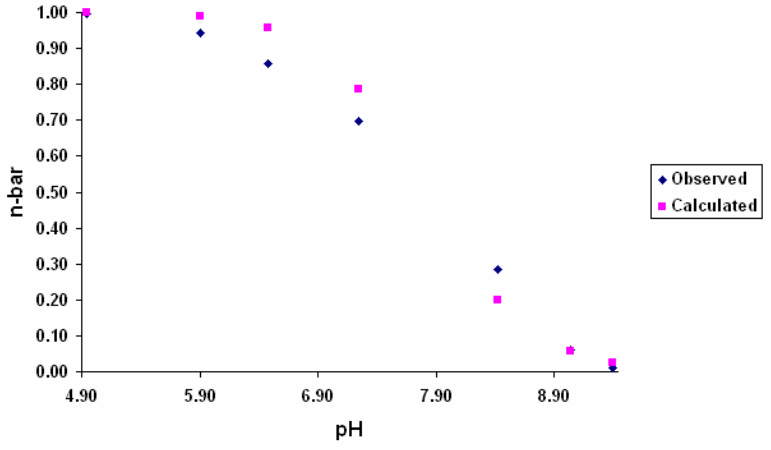

c.)

Figure 26: The comparison of $\bar{n}$ observed versus $\bar{n}$ calculated with respect to pH at wavelengths of a.) 226 nm, b.) 235 nm, and c.) 280 nm for the competition of PDA and EDTA for Gd(III).

Lanthanum(III)-PDA results

The ionic radius of La(III) is 1.03 Å, which is only slightly higher than the preferred 1.0 Å for PDA. PDA had a much higher affinity for La(III) than did EDTA, so DTPA was substituted as the competing ligand for the titration experiment. The ability of the tetradentate ligand, PDA, to compete effectively with the octadentate ligand, DTPA, is due to the preorganized structure of PDA. The UV absorbance spectra are shown in Figure 27 for the titration of La(III) with PDA. A example plot of corrected absorbance versus pH for La(III) is shown in Figure 28. Also, the observed and calculated $\bar{n}$ versus pH plots are shown in Figure 29. From the selected wavelengths described above, a log K_1 of 13.40 was calculated for La(III) with PDA using Equations (1-9). Comparitively, the log K_1 for La(III) with EDDA is 7.0, which gives a Δ log K_1 of 6.40 when compared with the log K_1 for PDA with La(III). The difference in log K_1 values of PDA versus EDDA for La(III) showed a remarkable increase in stability for the preorganized structure of PDA with La(III).

Lead(II)-PDA results

The ionic radius of Pb(II) is 1.19 Å, which is slightly above the preferred 1.0 Å for PDA. The UV absorbance spectra is shown in Figure 30 for the titration of Pb(II) with PDA. A example plot of corrected absorbance versus pH for Pb(II) is shown in Figure 31. Also, the observed and calculated $\bar{n}$ versus pH plots are shown in Figure 32. A charge transfer band for Pb(II) was seen in the UV absorbance spectra at approximately 230 nm. This may have interfered with the absorbance data taken at 226 nm. A log K_1 of 12.62 was calculated using Equations (1-9) for Pb(II) with PDA from the absorbance data at the wavelengths mentioned above, excluding the absorbance data taken at 226 nm. An increase in complex stability is seen

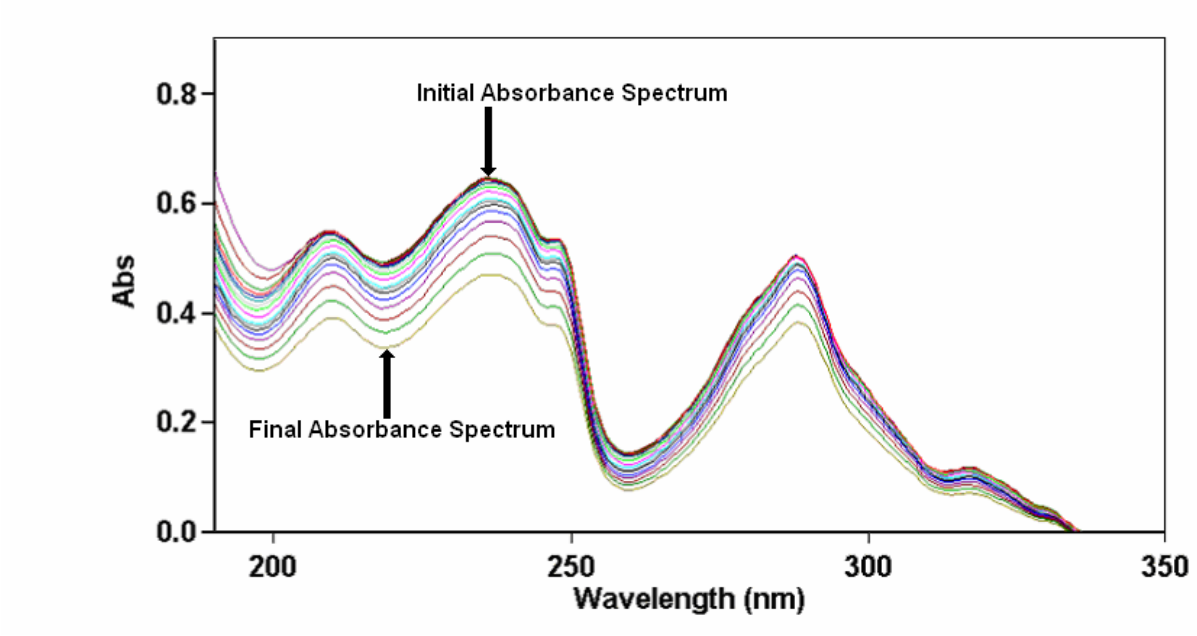

a.)

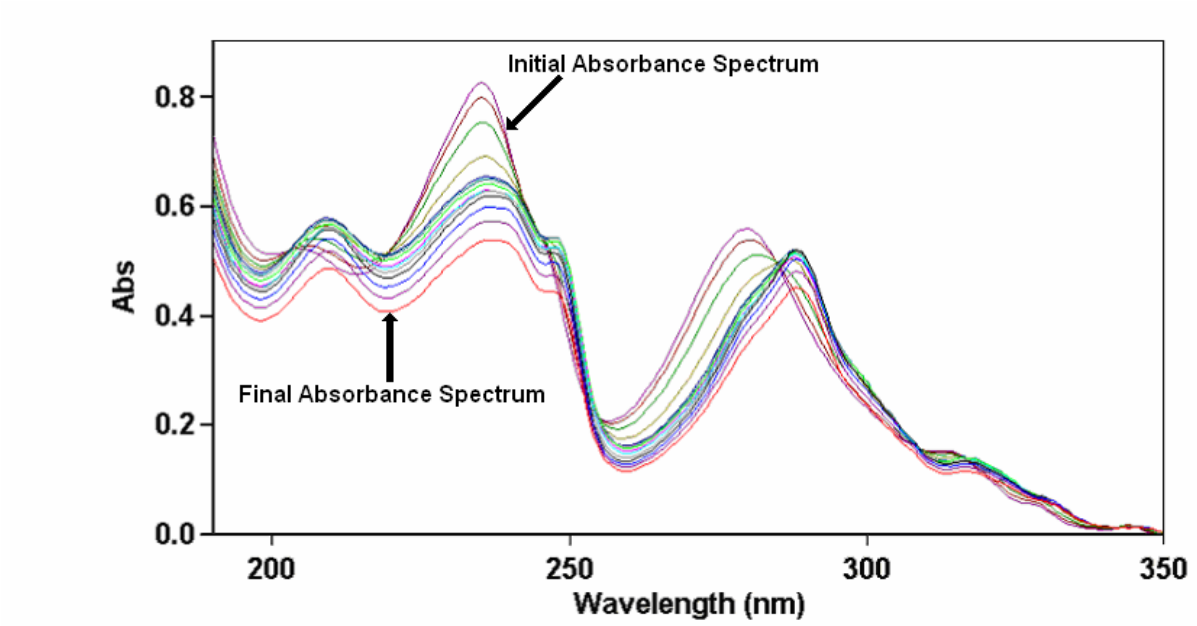

b.)

Figure 27: The UV absorbance spectra for the titration of (a) 1:1 La(III) and PDA and (b) 1:1:1 La(III), PDA, and DTPA

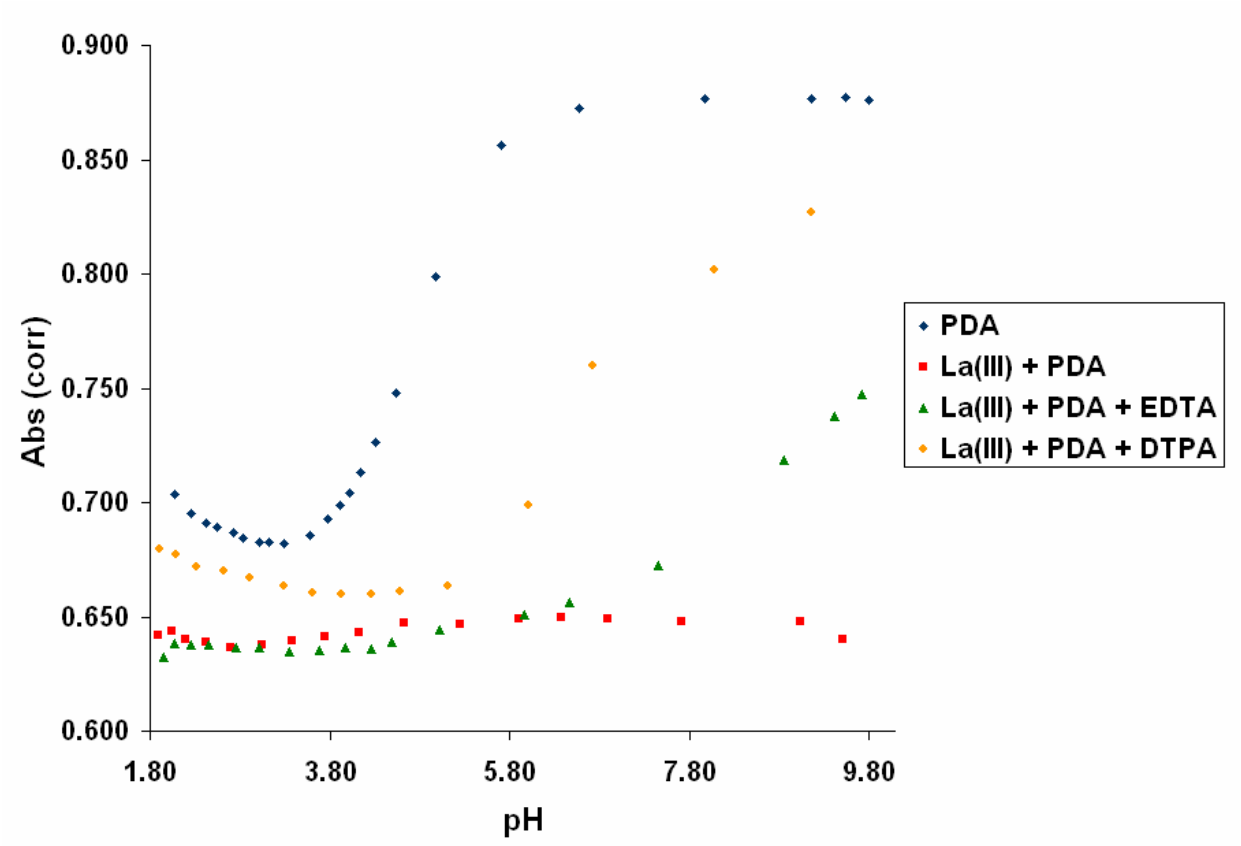

Figure 28: The combined 235 nm corrected absorbance data versus pH from titration experiments involving La(III). The titration of PDA at this wavelength is also shown for reference.

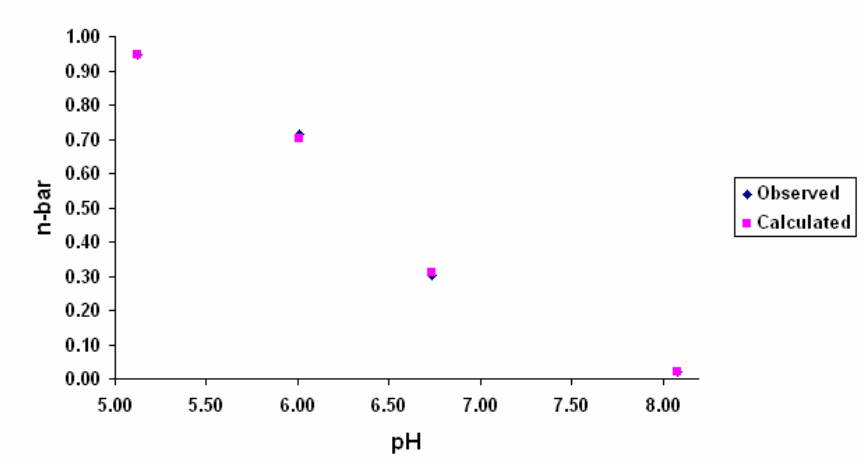

a.)

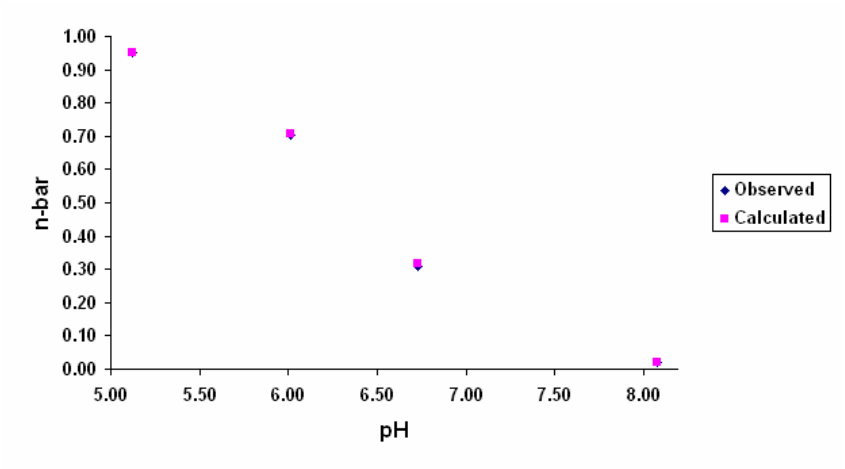

b.)

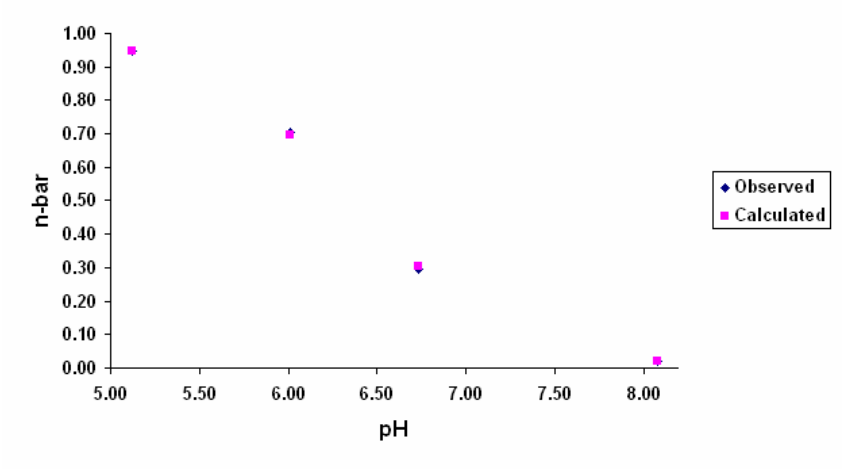

c.)

Figure 29: The comparison of $\bar{n}$ observed versus $\bar{n}$ calculated with respect to pH at wavelengths of a.) 235 nm, b.) 246 nm, and c.) 280 nm for the competition of PDA and DTPA for La(III).

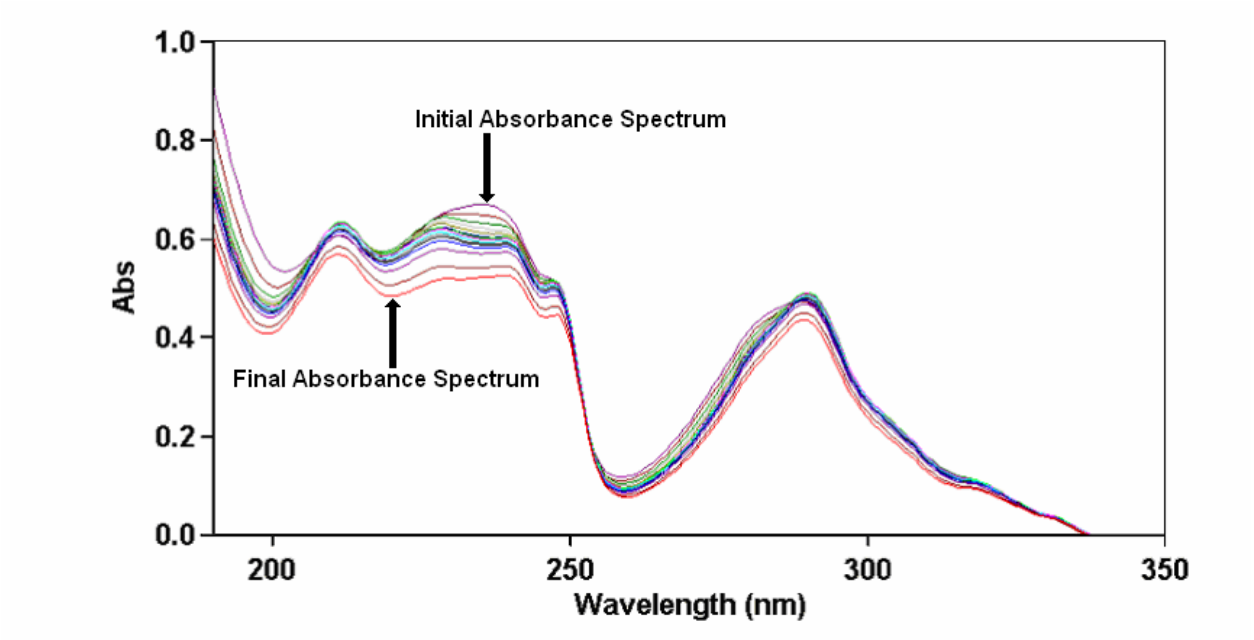

a.)

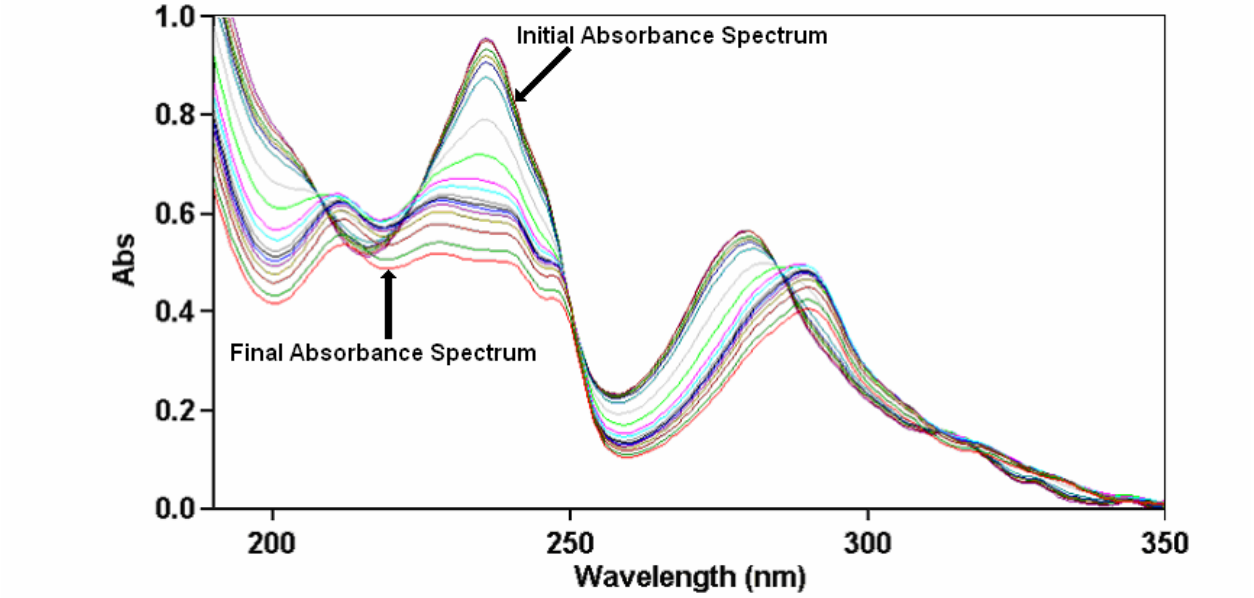

b.)

Figure 30: The UV absorbance spectra for the titration of (a) 1:1 Pb(II) and PDA and (b) 1:1:1 Pb(II), PDA, and EDTA

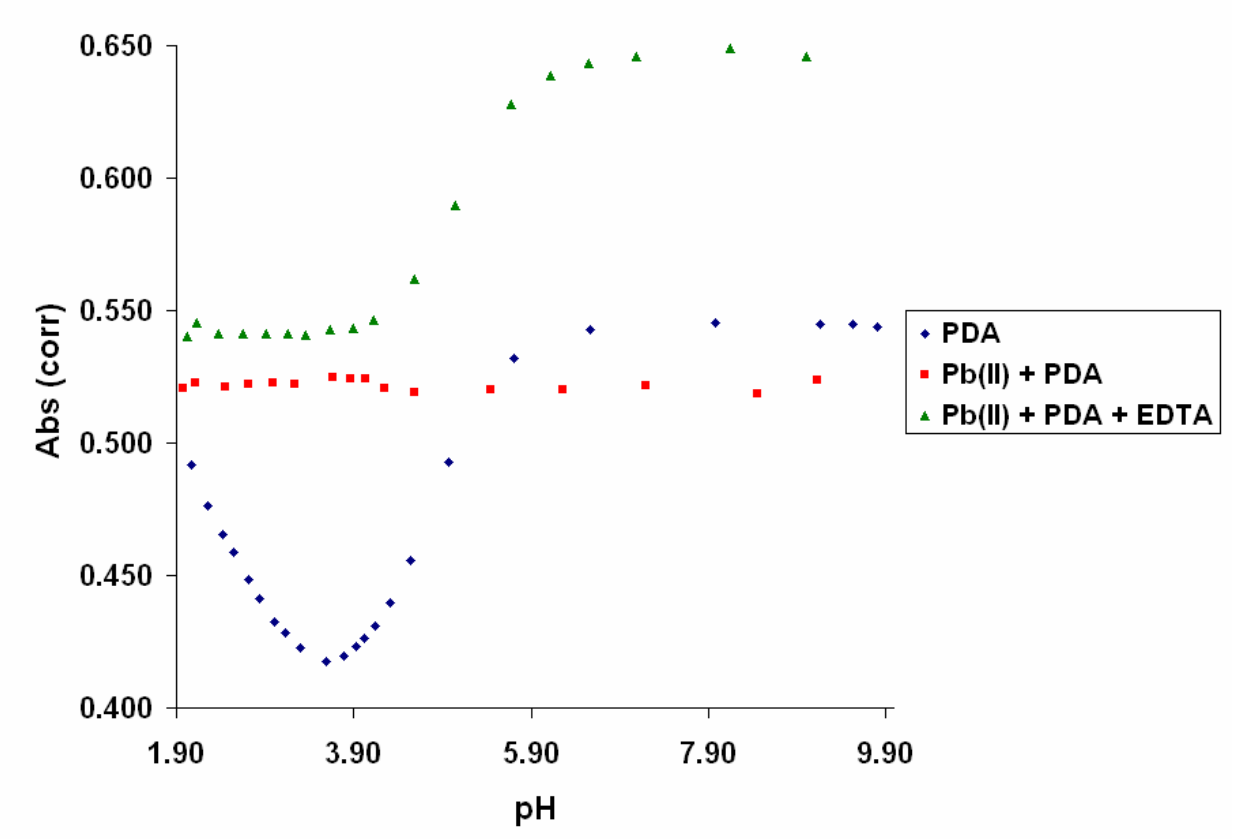

Figure 31: The combined 246 nm corrected absorbance data versus pH from titration experiments involving Pb(II). The titration of PDA at this wavelength is also shown for reference.

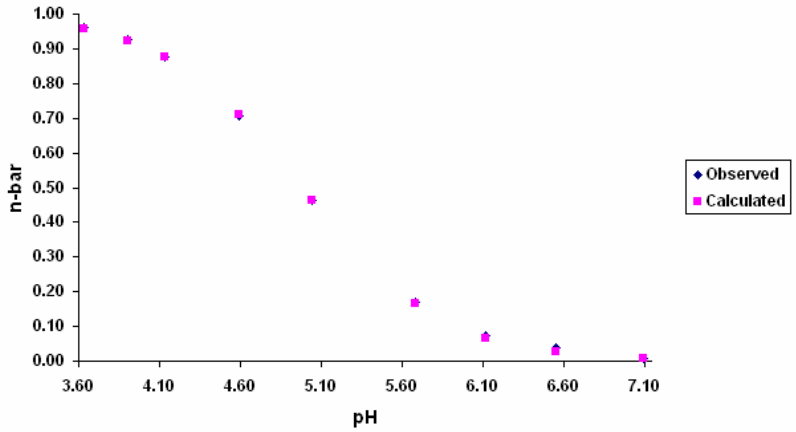

a.)

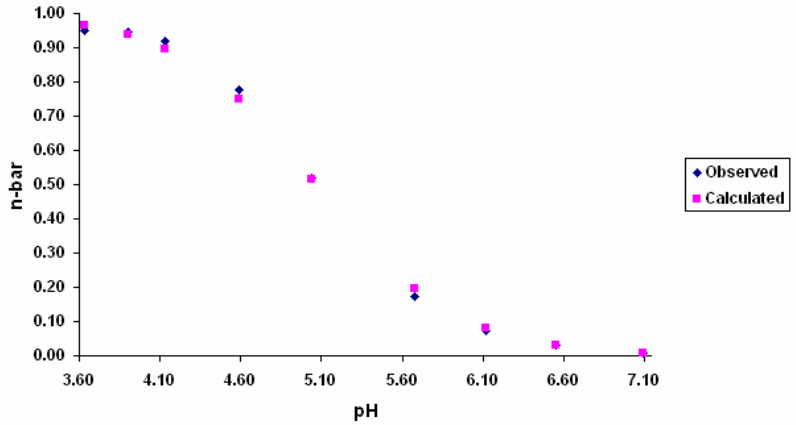

b.)

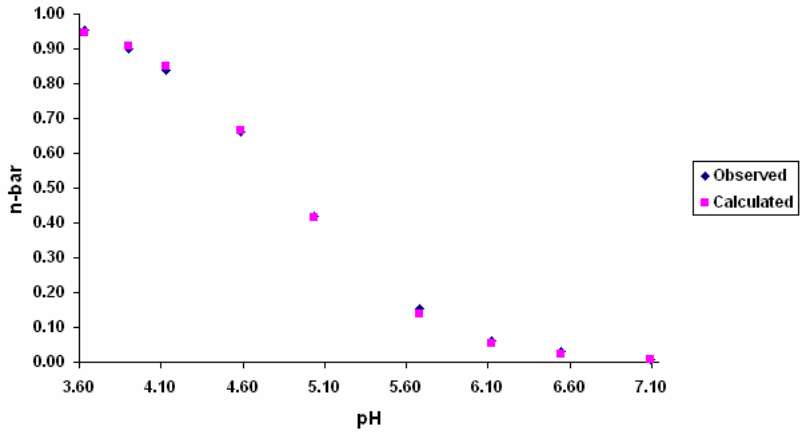

c.)

Figure 32: The comparison of $\bar{n}$ observed versus $\bar{n}$ calculated with respect to pH at wavelengths of a.) 235 nm, b.) 246 nm, and c.) 280 nm for the competition of PDA and EDTA for Pb(II).

for Pb(II) and PDA with respect to EDDA. A log K_1 of 10.6 for Pb(II) with EDDA was reported and the Δ log K_1 between PDA and EDDA for Pb(II) was determined to be 2.02. Due to the larger ionic radius of Pb(II), the difference in stability constants for the PDA complex versus the EDDA complex was not as pronounced.

Magnesium(II)-PDA results

The ionic radius of Mg(II) is 0.74 Å, which is far below the target ionic radius of a metal ion for a PDA complex. Due to the large cavity size of PDA, the smaller Mg(II) metal ion struggles to bridge the gap between the carboxylate groups. Therefore, an enhanced complex stability was not seen for the Mg(II) metal ion with PDA relative to the EDDA complex with Mg(II). The competition experiment between PDA and EDTA for Mg(II) reveals that the Mg(II) never formed a complex with PDA in the presence of EDTA. The UV absorbance spectra are shown in Figure 33 for the titration of Mg(II) with PDA. A example plot of corrected absorbance versus pH for Mg(II) is shown in Figure 34. From the selected wavelengths described above, a log K_1 for Mg(II) with PDA was 3.30. The reported value of EDDA with Mg(II) was 4.0. The similarities between the log K_1 values for PDA and EDDA with Mg(II) suggested that the increase in strain energy for PDA to complex Mg(II) resulted in an overall decrease for log K_1.

Nickel(II)-PDA results

The ionic radius of Ni(II) is 0.69, which is below the preferred ionic radius of 1.0 Å for PDA. The Ni(II)PDA complex is destabilized because Ni(II) cannot adequately span the gap between the carboxylate groups of PDA. Therefore, PDA compensates for this lack of ionic

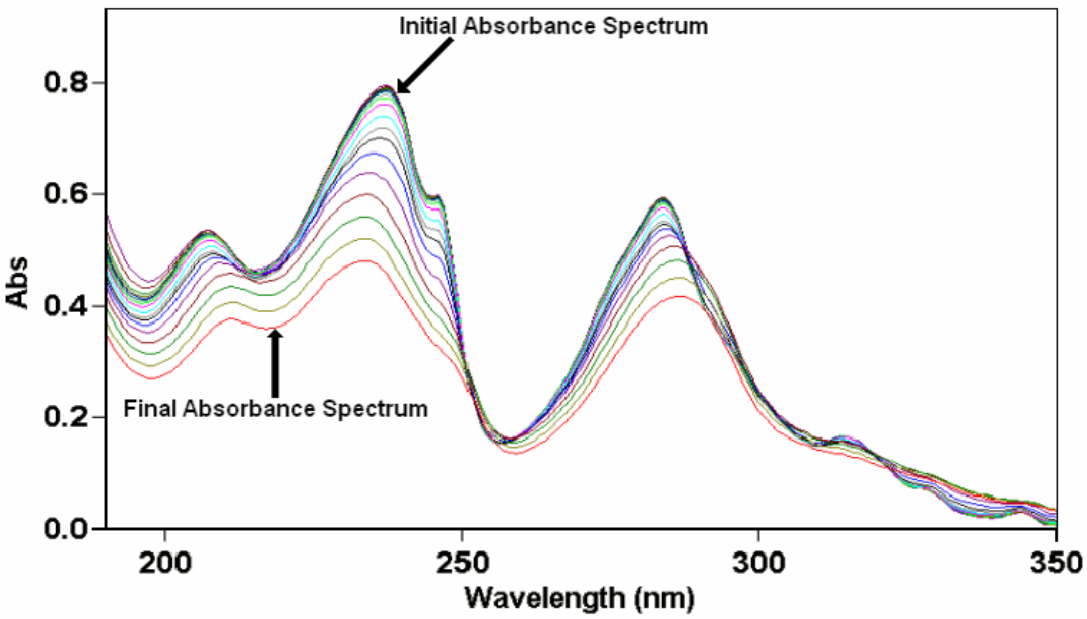

a.)

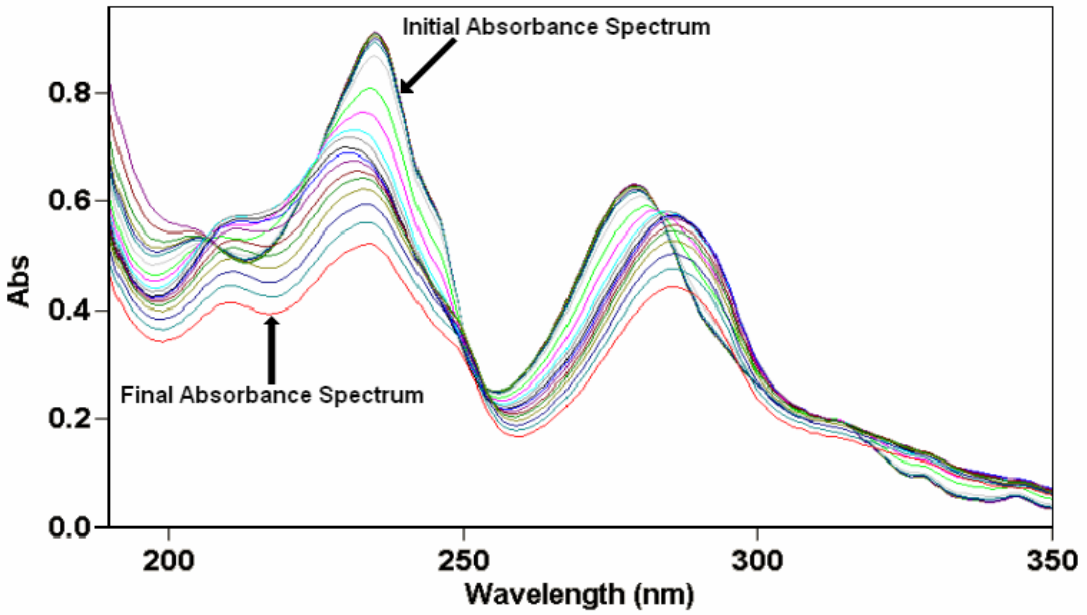

b.)

Figure 33: The UV absorbance spectra for the titration of (a) 1:1 Mg(II) and PDA and (b) 1:1:1 Mg(II), PDA, and EDTA

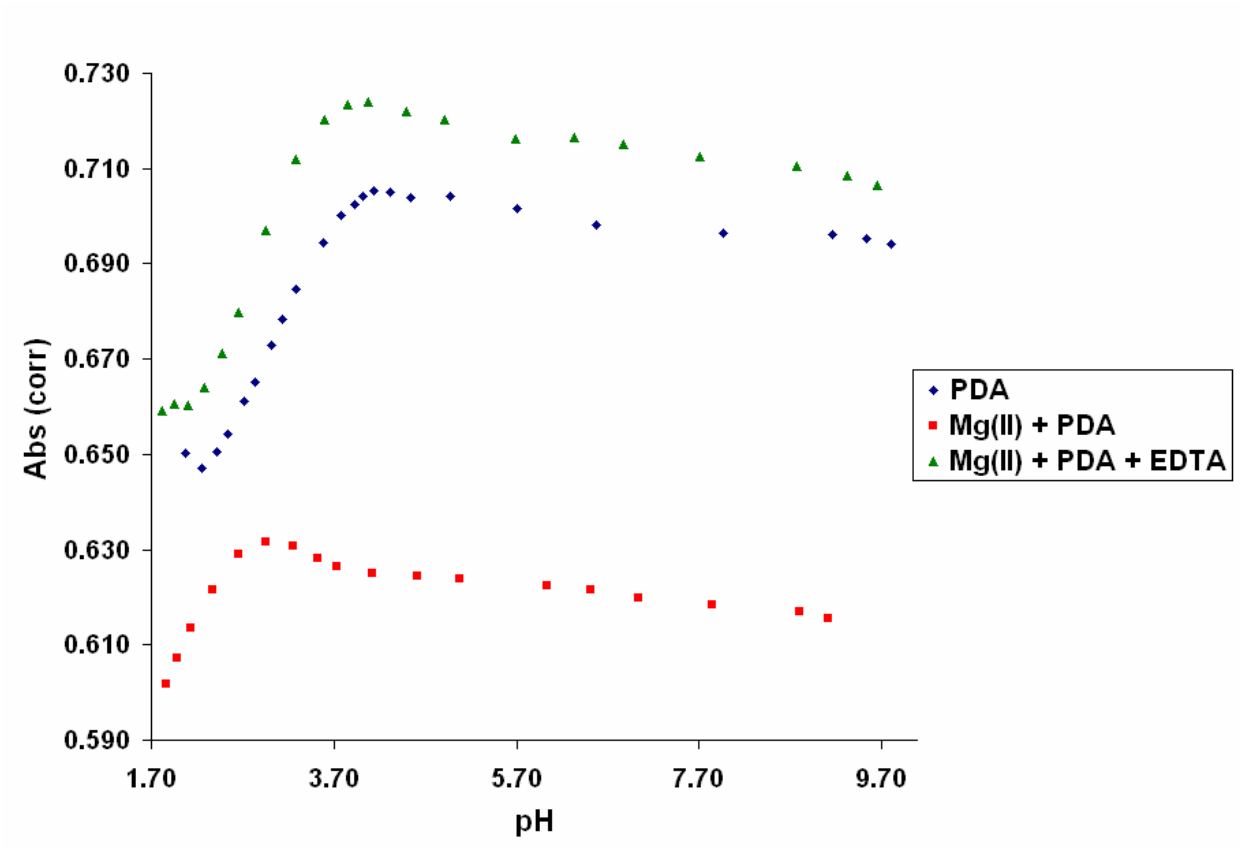

Figure 34: The combined 226 nm corrected absorbance data versus pH from titration experiments involving Mg(II). The sample solution used for the titration of Mg(II) and PDA contained 0.0333 *M* Mg(II). The titration of PDA at this wavelength is also shown for reference.

radius by adjusting its rigid structure to accommodate the Ni(II) metal ion. The UV absorbance spectra are shown in Figure 35 for the titration of Ni(II) with PDA. An example plot of corrected absorbance versus pH for Ni(II) is shown in Figure 36. Also, the observed and calculated $\bar{n}$ versus pH plots are shown in Figure 37. From the selected wavelengths described above, a log K_1 of 12.73 was calculated for PDA with Ni(II), which was slightly lower than the log K_1 reported formation constant of 13.6 for EDDA with Ni(II). A Δ log K_1 between PDA and EDDA with Ni(II) was –0.87, which suggested that there is an increase in the overall strain energy for the PDA complex of Ni(II).

Strontium(II)-PDA results

The ionic radius of Sr(II) is 1.18 Å, which is slightly higher than the target ionic radius of 1.0 Å for PDA. The UV absorbance spectra are shown in Figure 38 for the titration of Sr(II) with PDA. A example plot of corrected absorbance versus pH for Sr(II) is shown in Figure 39. Also, the observed and calculated $\bar{n}$ versus pH plots are shown in Figure 40. From the selected wavelengths described above, a log K_1 of 5.60 was calculated from the absorbance data for PDA with Sr(II) using Equations (1-9) and compared with the reported value of 3.6 for EDDA with Sr(II). The Δ log K_1 between the PDA and EDDA for Sr(II) was 2.0, which shows an increase in the complex stability for PDA with Sr(II) relative to the EDDA complex with Sr(II). Due to the larger ionic radius of Sr(II), the difference in stability constants for the PDA complex versus the EDDA complex was not as pronounced.

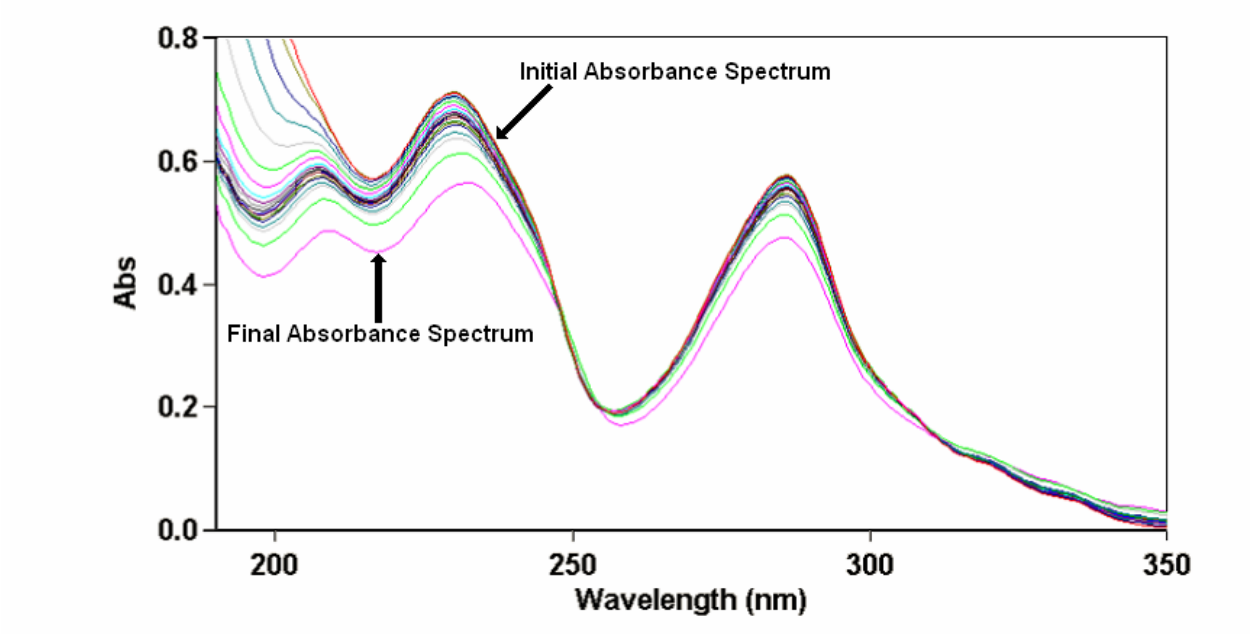

a.)

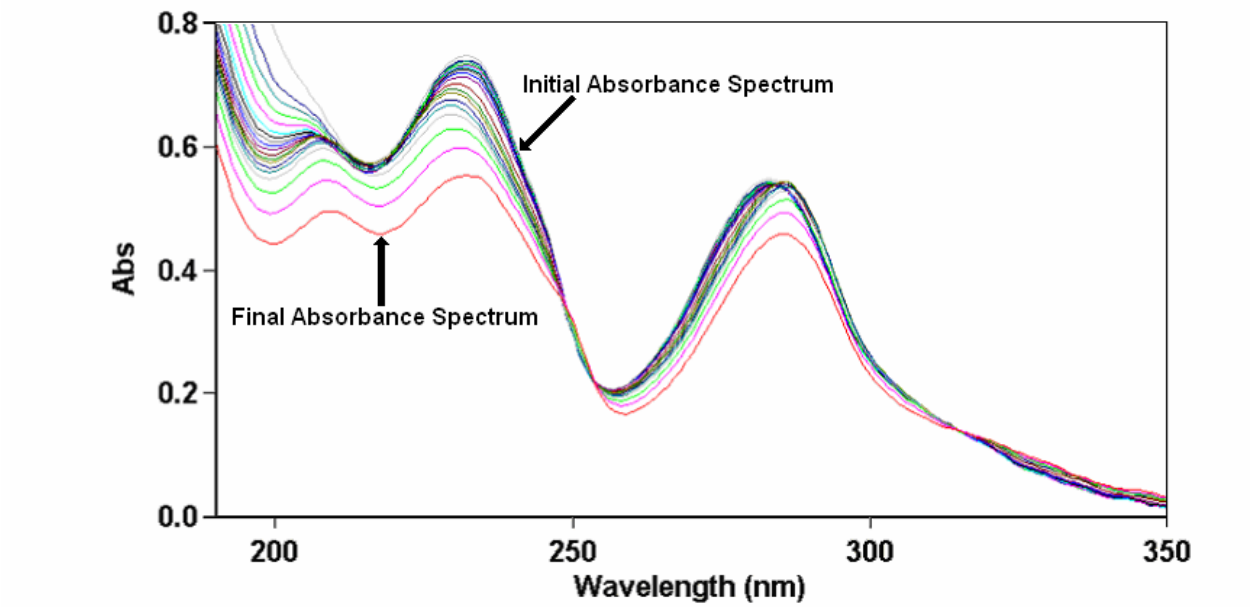

b.)

Figure 35: The UV absorbance spectra for the titration of (a) 1:1 Ni(II) and PDA and (b) 1:1:1 Ni(II), PDA, and EDTA

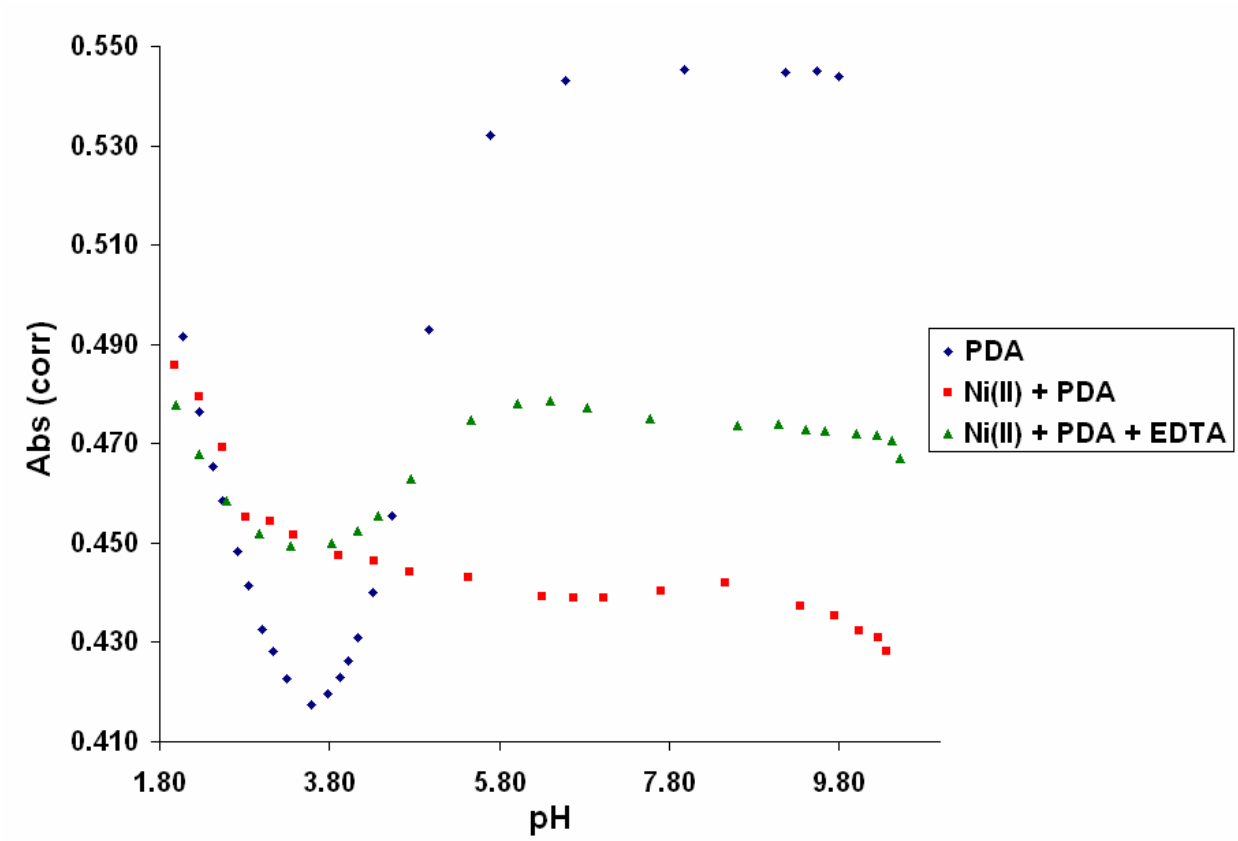

Figure 36: The combined 246 nm corrected absorbance data versus pH from titration experiments involving Ni(II). The titration of PDA at this wavelength is also shown for reference.

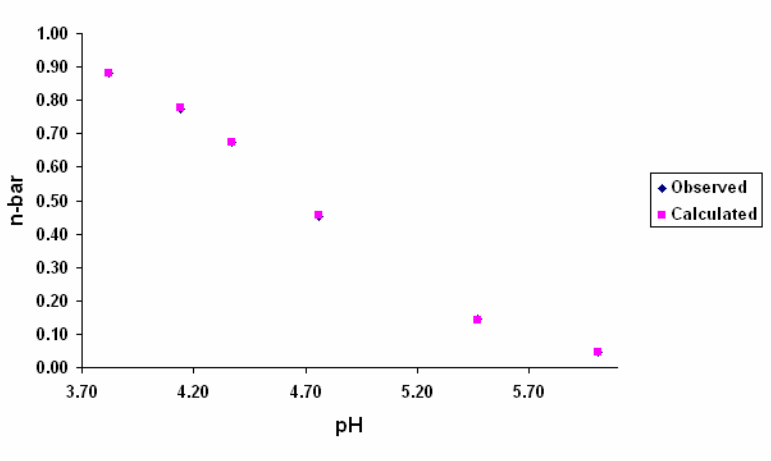

a.)

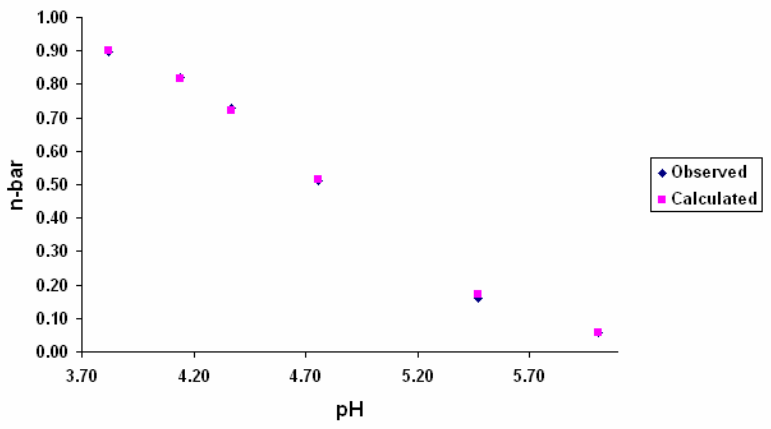

b.)

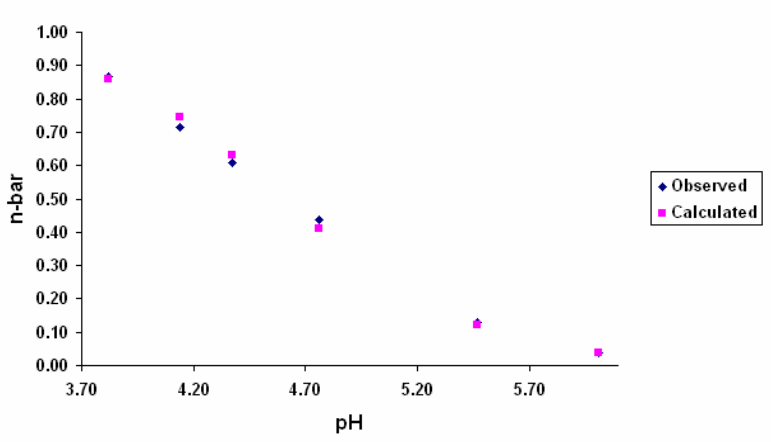

c.)

Figure 37: The comparison of $\bar{n}$ observed versus $\bar{n}$ calculated with respect to pH at wavelengths of a.) 235 nm, b.) 246 nm, and c.) 280 nm for the competition of PDA and EDTA for Ni(II).

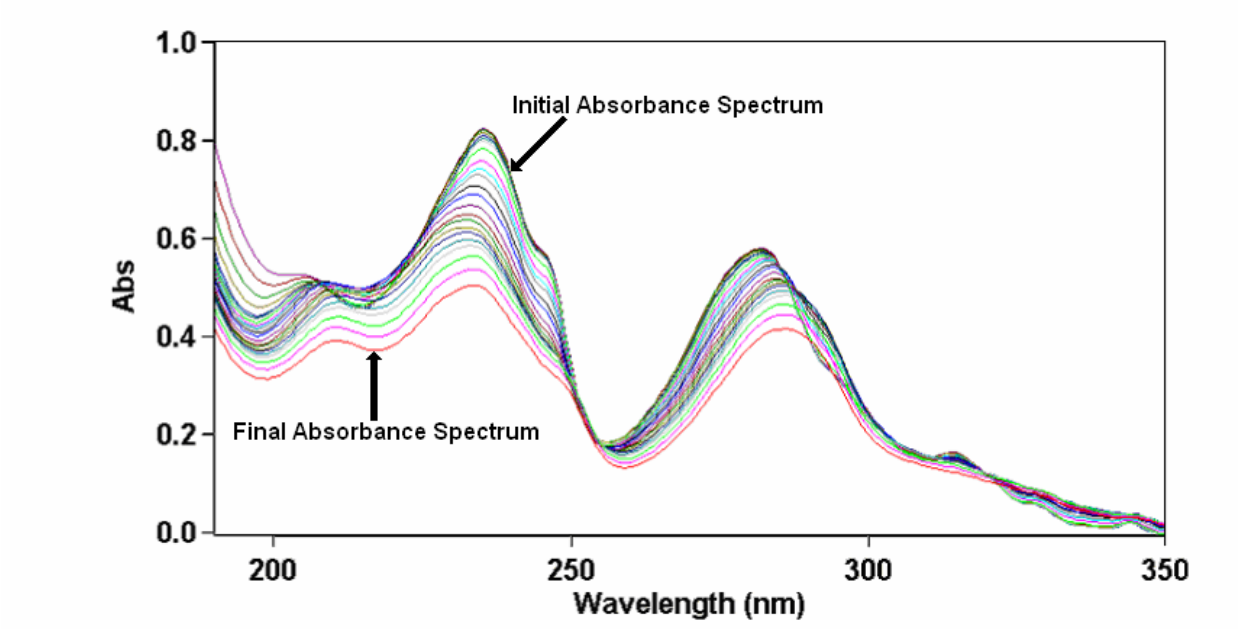

a.)

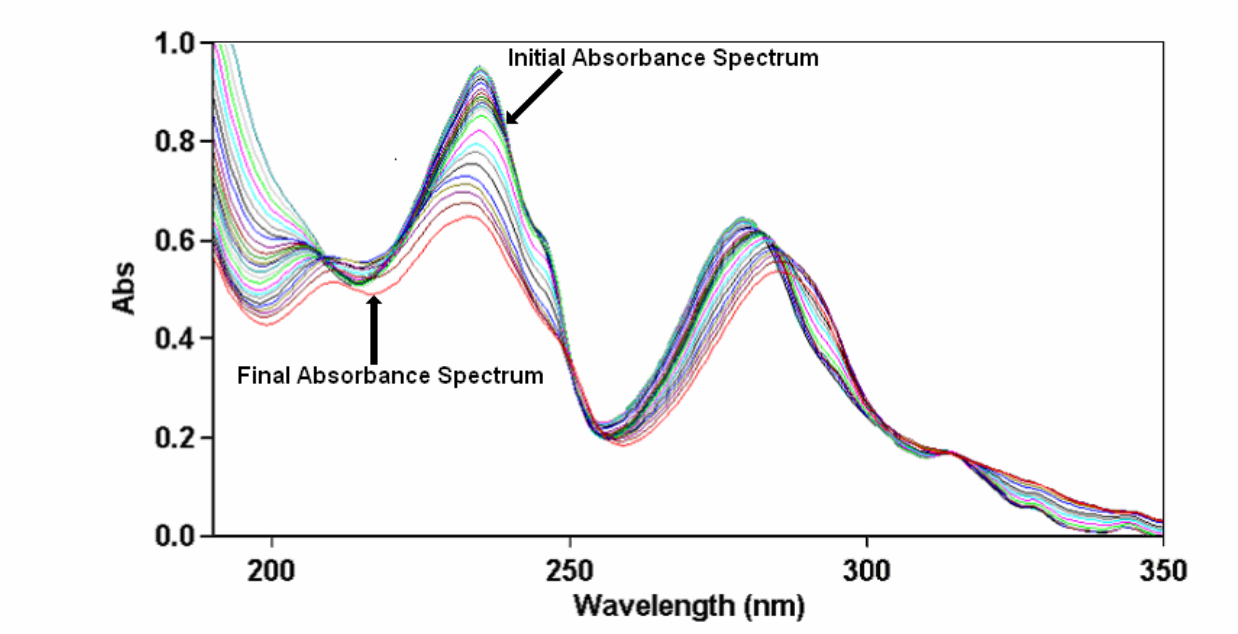

b.)

Figure 38: The UV absorbance spectra for the titration of (a) 1:1 Sr(II) and PDA and (b) 1:1:1 Sr(II), PDA, and EDTA

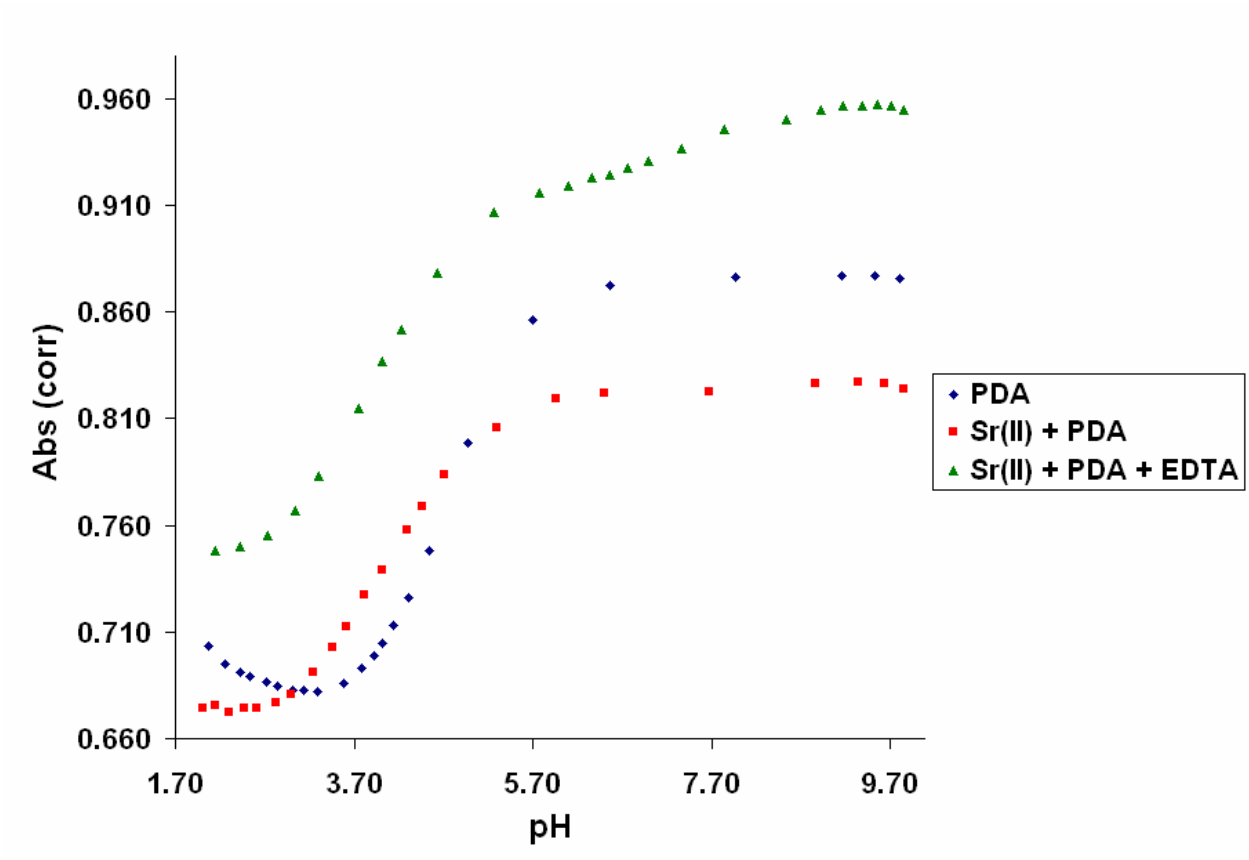

Figure 39: The combined 235 nm corrected absorbance data versus pH from titration experiments involving Sr(II). The titration of PDA at this wavelength is also shown for reference.

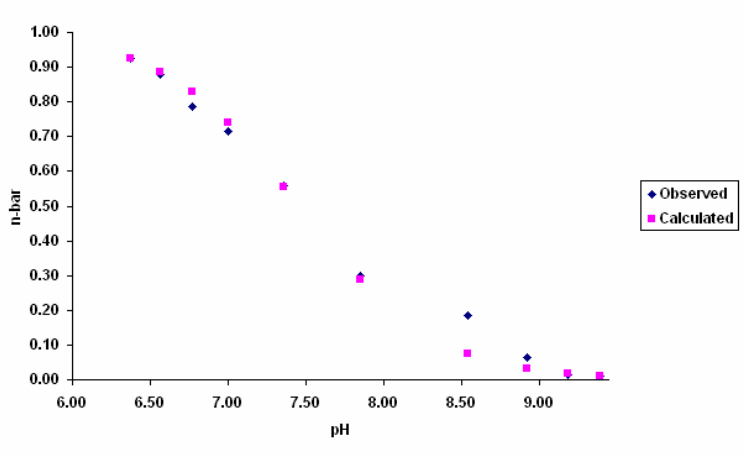

a.)

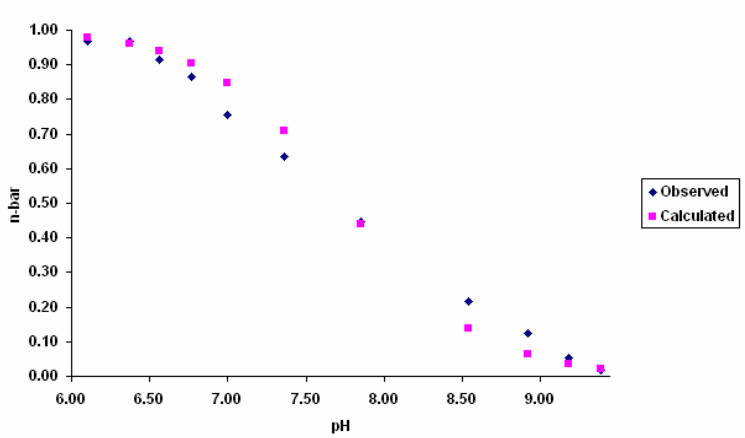

b.)

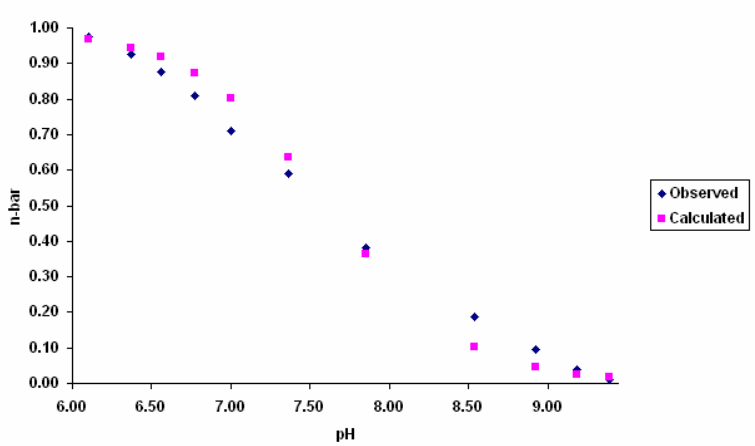

c.)

Figure 40: The comparison of $\bar{n}$ observed versus $\bar{n}$ calculated with respect to pH at wavelengths of a.) 235 nm, b.) 246 nm, and c.) 286 nm for the competition of PDA and EDTA for Sr(II).

Zinc(II)-PDA results

The ionic radius of Zn(II) is 0.74, which is below the preferred ionic radius of 1.0 Å for a PDA complex. The UV absorbance spectra are shown in Figure 41 for the titration of Zn(II) with PDA. A example plot of corrected absorbance versus pH for Zn(II) is shown in Figure 42. Also, the observed and calculated $\bar{n}$ versus pH plots are shown in Figure 43. From the selected wavelengths described above, a log K_1 of 11.63 was calculated from the absorbance data for PDA with Zn(II) using Equations (1-9) and compared with the reported value of 11.1 for EDDA with Zn(II). The Δ log K_1 between the PDA and EDDA complexes of Zn(II) was 0.53, which shows a slight increase in the overall stability of the PDA complex relative to the EDDA complex with Zn(II).

Crystal Structure Results

Crystal structures of Co(II)[12], Mg(II)[13], and Ni(II)[14] have been reported for PDA. The crystal structures of $[Co(PDA)_2]^{2-}$, $[Mg(PDA)(H_2O)_3]$, and $[Ni(PDA)(H_2O)_3]$ are shown in Figures 44, 45, and 46, respectively. The PDA crystal structure Mg(II) shows a slightly better fit for the metal ion into PDA, whereas Co(II) must coordinate between a neutral nitrogen and a negative oxygen donor of two separate PDA molecules. This shows the effect that ionic radius and coordination number of a metal ion has when a complex of PDA is formed. Smaller metal ions, like Ni(II), have difficulty filling the space between the carboxylate groups of PDA. Even though a small metal ion may complex PDA, a greater strain is placed on the PDA complex in order to accommodate the metal ion's ionic radius. Therefore, optimal stabilization may be obtained by selecting a metal ion with an ionic radius of approximately 1.0 Å for PDA.

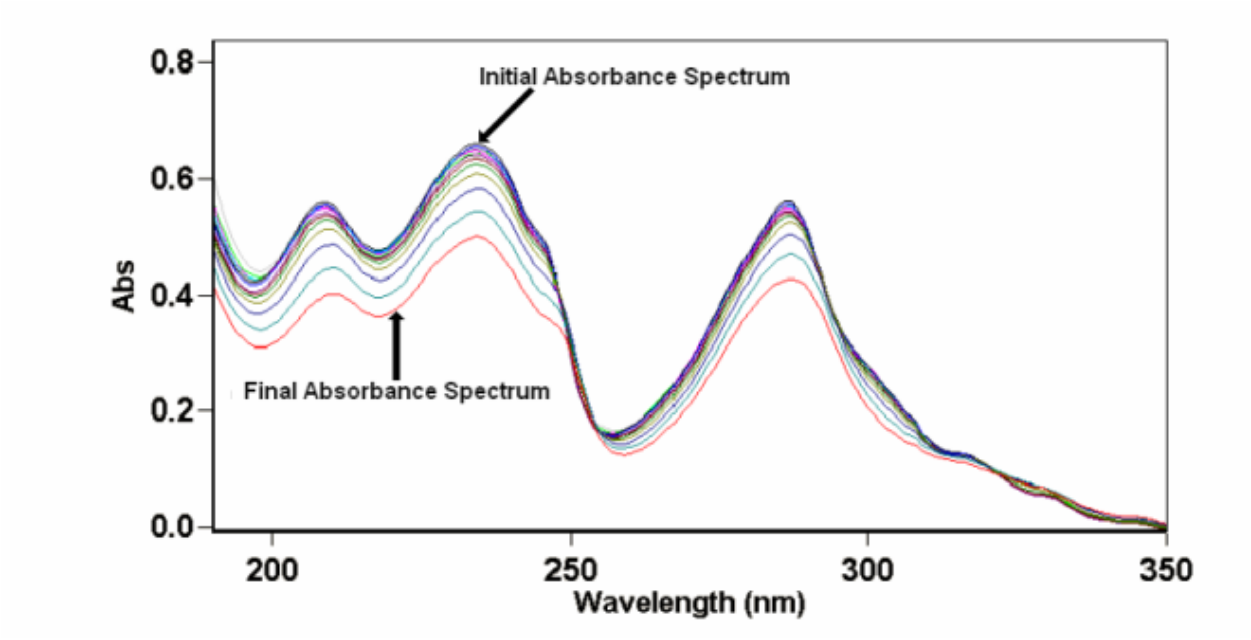

a.)

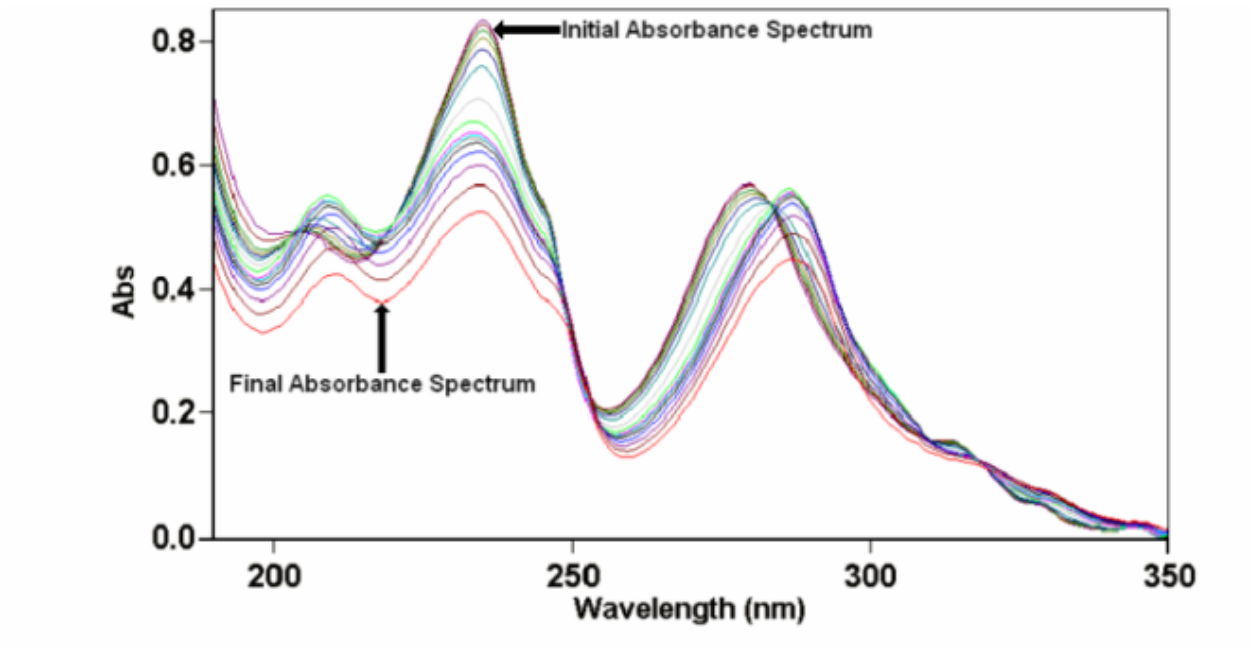

b.)

Figure 41: The UV absorbance spectra for the titration of (a) 1:1 Zn(II) and PDA and (b) 1:1:1 Zn(II), PDA, and EDTA

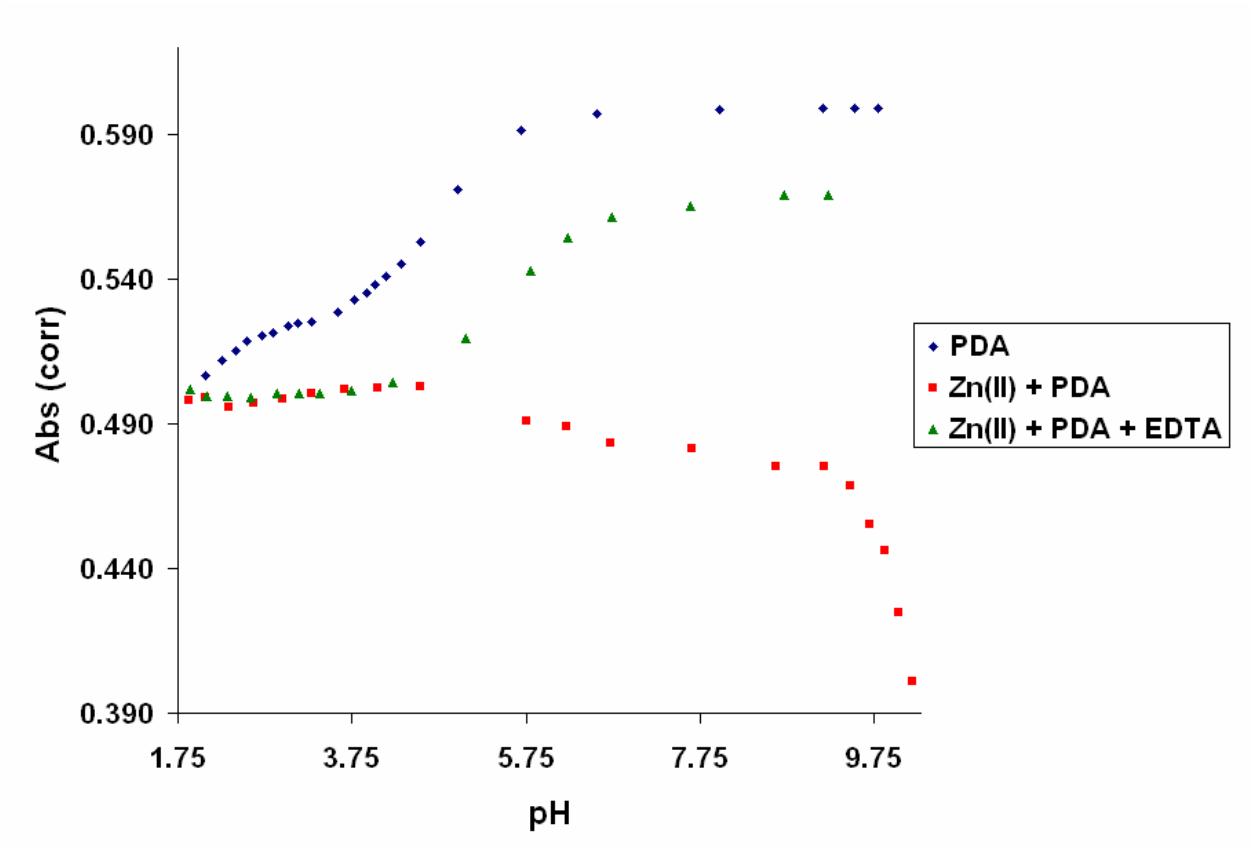

Figure 42: The combined 280 nm corrected absorbance data versus pH from titration experiments involving Zn(II). The titration of PDA at this wavelength is also shown for reference.

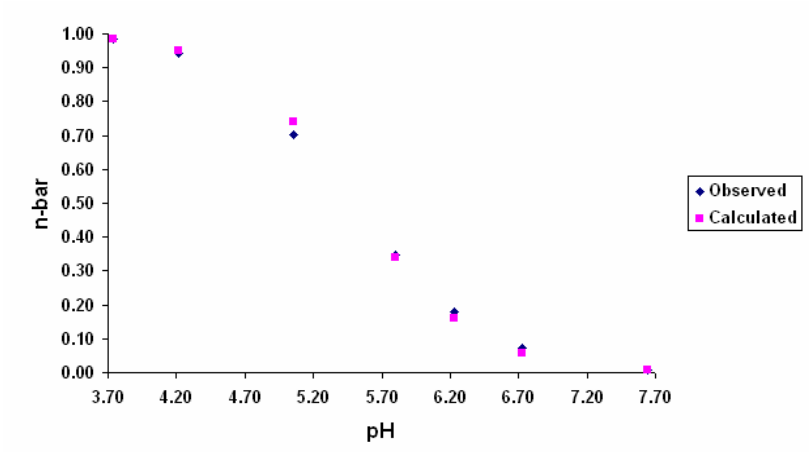

a.)

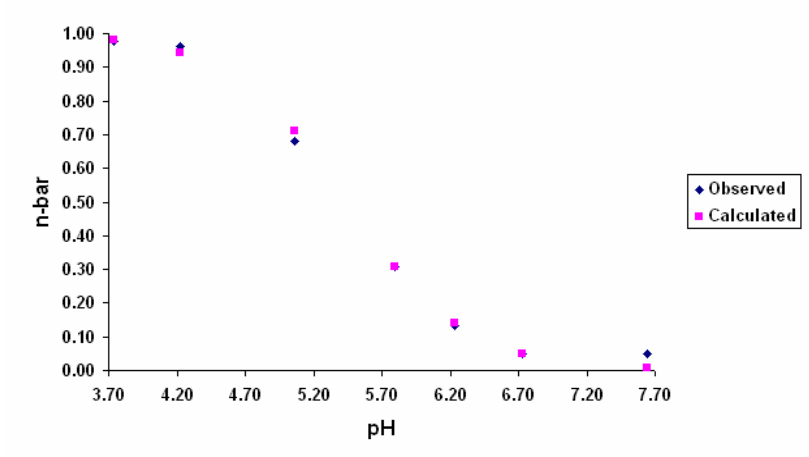

b.)

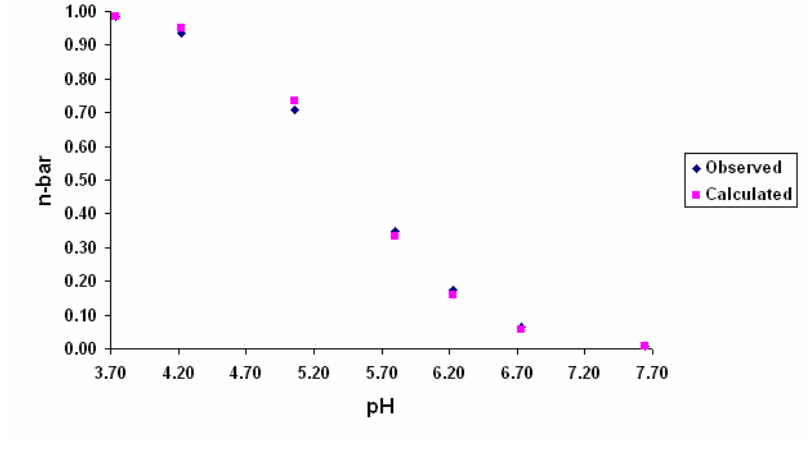

c.)

Figure 43: The comparison of $\bar{n}$ observed versus $\bar{n}$ calculated with respect to pH at wavelengths of a.) 235 nm, b.) 246 nm, and c.) 280 nm for the competition of PDA and EDTA for Zn(II).

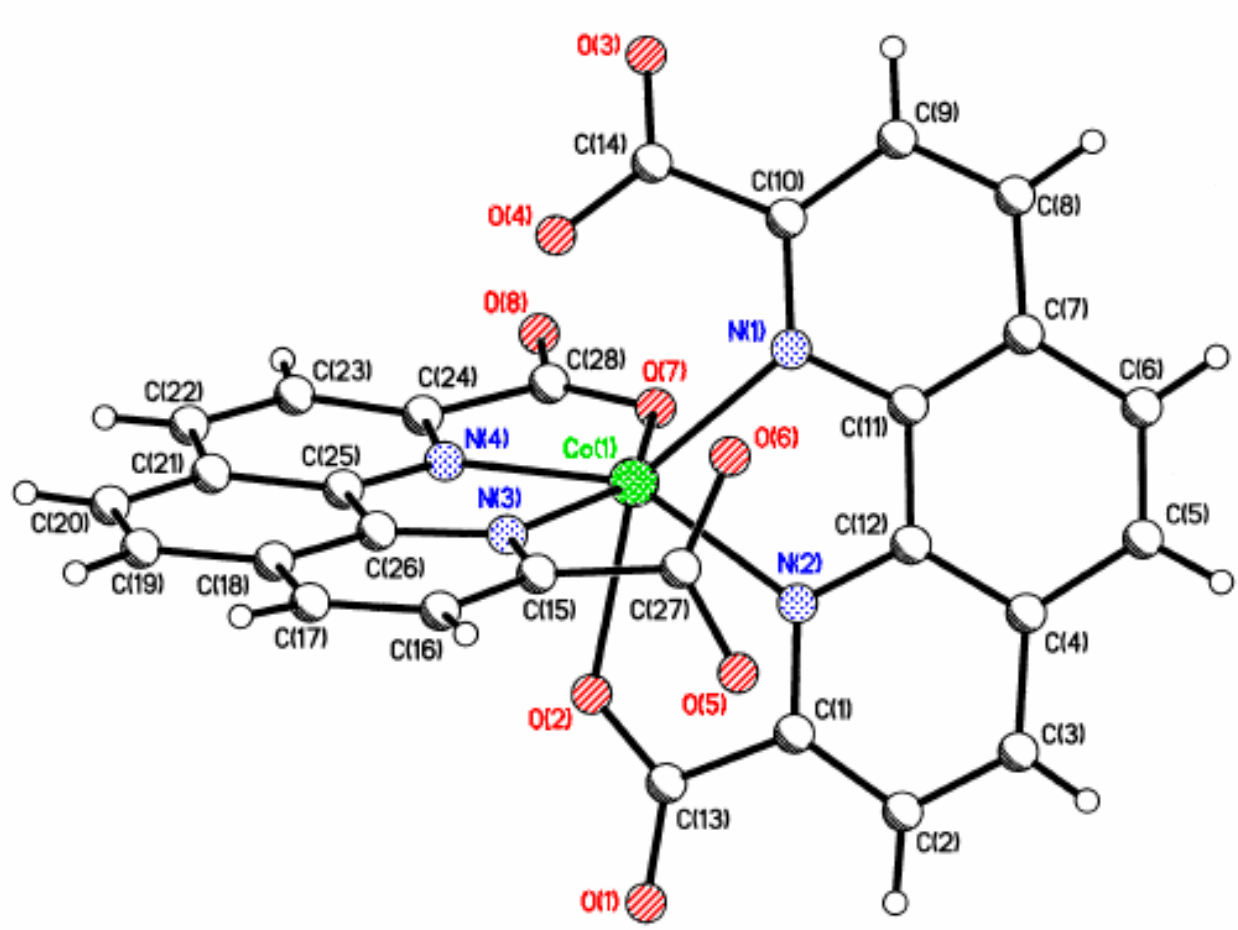

Figure 44: The crystal structure of the $[Co(PDA)_2]^{2-}$ complex.[12]

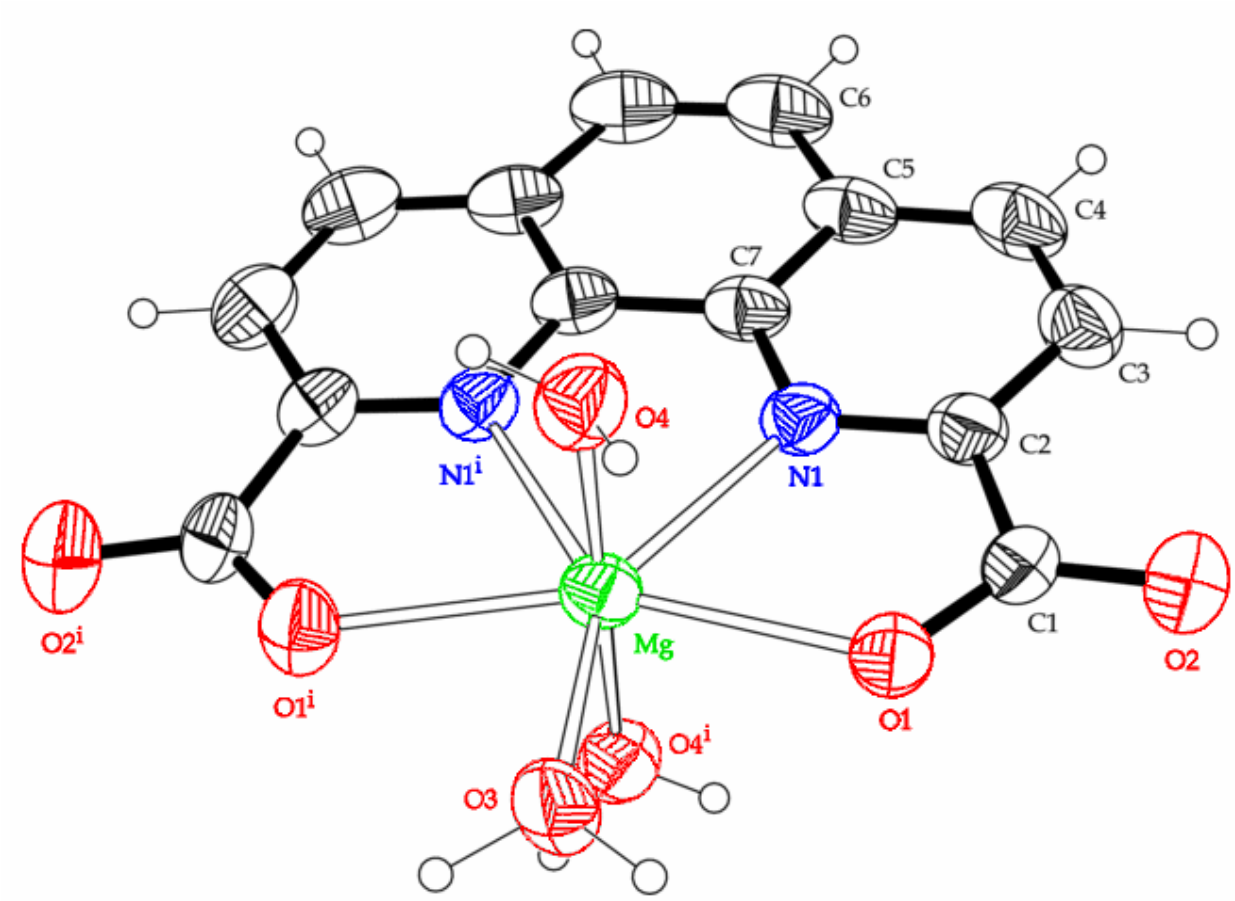

Figure 45: The crystal structure of the $[Mg(PDA)(H_2O)_3]$ complex.[13]

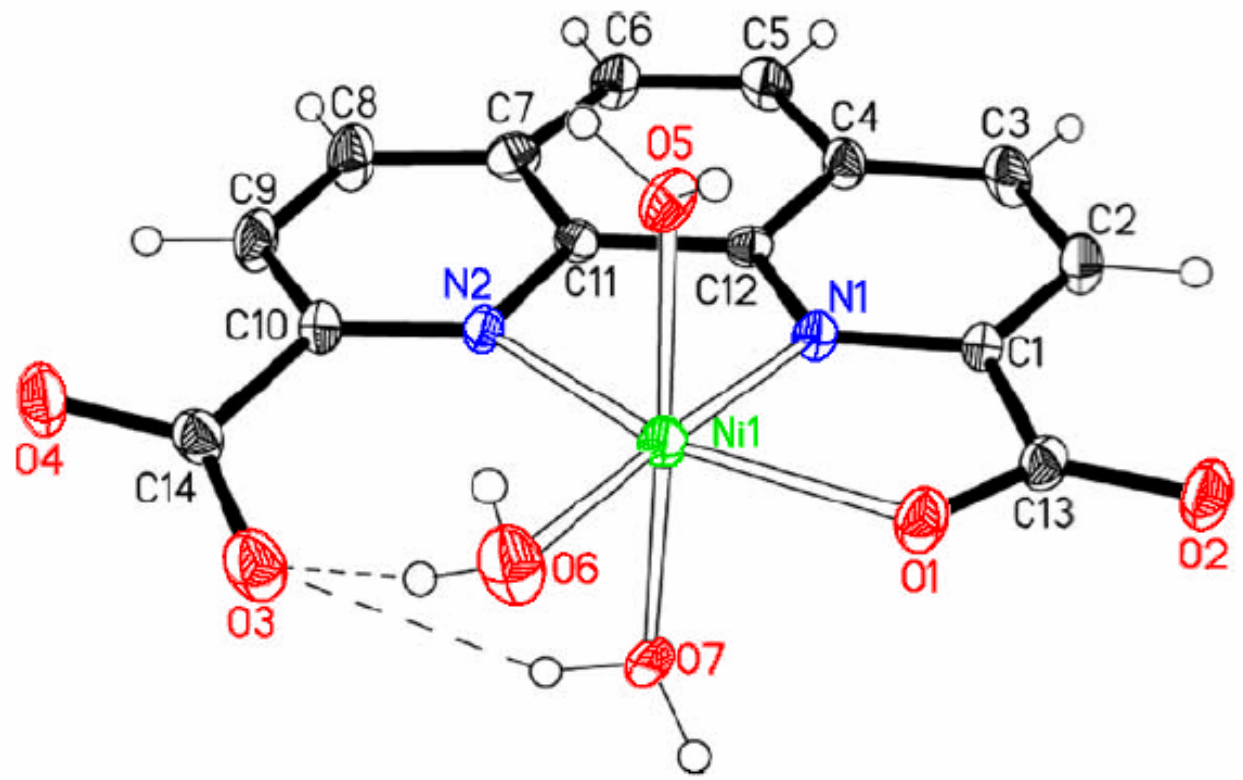

Figure 46: The crystal structure of the $[Ni(PDA)(H_2O)_3]$ complex.[14]

[Ca(PDA)(H_2O)$_2$] crystal structure

The crystal synthesis of [Ca(PDA)(H_2O)$_2$] yielded fine, yellow crystals on the interface of the *n*-butanol/H_2O layers. An IR analysis, illustrated in Figure 47, was performed on the crystals and referenced to PDA to show the differences in IR spectra. The crystal structure of [Ca(PDA)(H_2O)$_2$] consisted of a Ca(II) metal ion coordinated to the two negative oxygen donors of the carboxylate groups, two neutral nitrogen donors of the phenanthroline moiety, two waters, and both oxygens of a neighboring carboxylate group of PDA, as shown in Figure 48. Therefore, Ca(II) was eight-coordinate and the [Ca(PDA)(H_2O)$_2$] complex was of a polymeric formation, since there was a bridge between a carboxylate group of a neighboring unit cell. The crystal data and structural refinement parameters for the [Ca(PDA)(H_2O)$_2$] complex are listed in Table 2. Also, the spatial coordinates of the atoms for the [Ca(PDA)(H_2O)$_2$] complex are given in Tables 3 and 4.

The bond distances for the [Ca(PDA)(H_2O)$_2$] complex are displayed in Table 5. Each unit cell of the crystal contained a Ca(II) ion positioned among the four donor atoms of PDA. The bond distance between the Ca(II) and nitrogens of PDA were 2.550 and 2.555 Å, which were longer bonds than that for the carboxylate groups of the PDA. The Ca(II) and carboxylate oxygen bond distances from PDA were 2.468 and 2.462 Å. Both oxygens of the neighboring carboxylate group of another [Ca(PDA)(H_2O)$_2$] unit cell was also coordinated to the Ca(II). These Ca(II) and oxygen bond distances were much longer at 2.638 and 2.524 Å. Two H_2O molecules were also coordinated to the Ca(II) metal ion, which had Ca(II) and oxygen bond distances of 2.410 and 2.387 Å.

A list of bond angles for the [Ca(PDA)(H_2O)$_2$] complex are given in Table 6. The bond angles of N(2)-C(11)-C(14) and O(3)-C(14)-C(11) for the carboxylate groups were 113.0° and

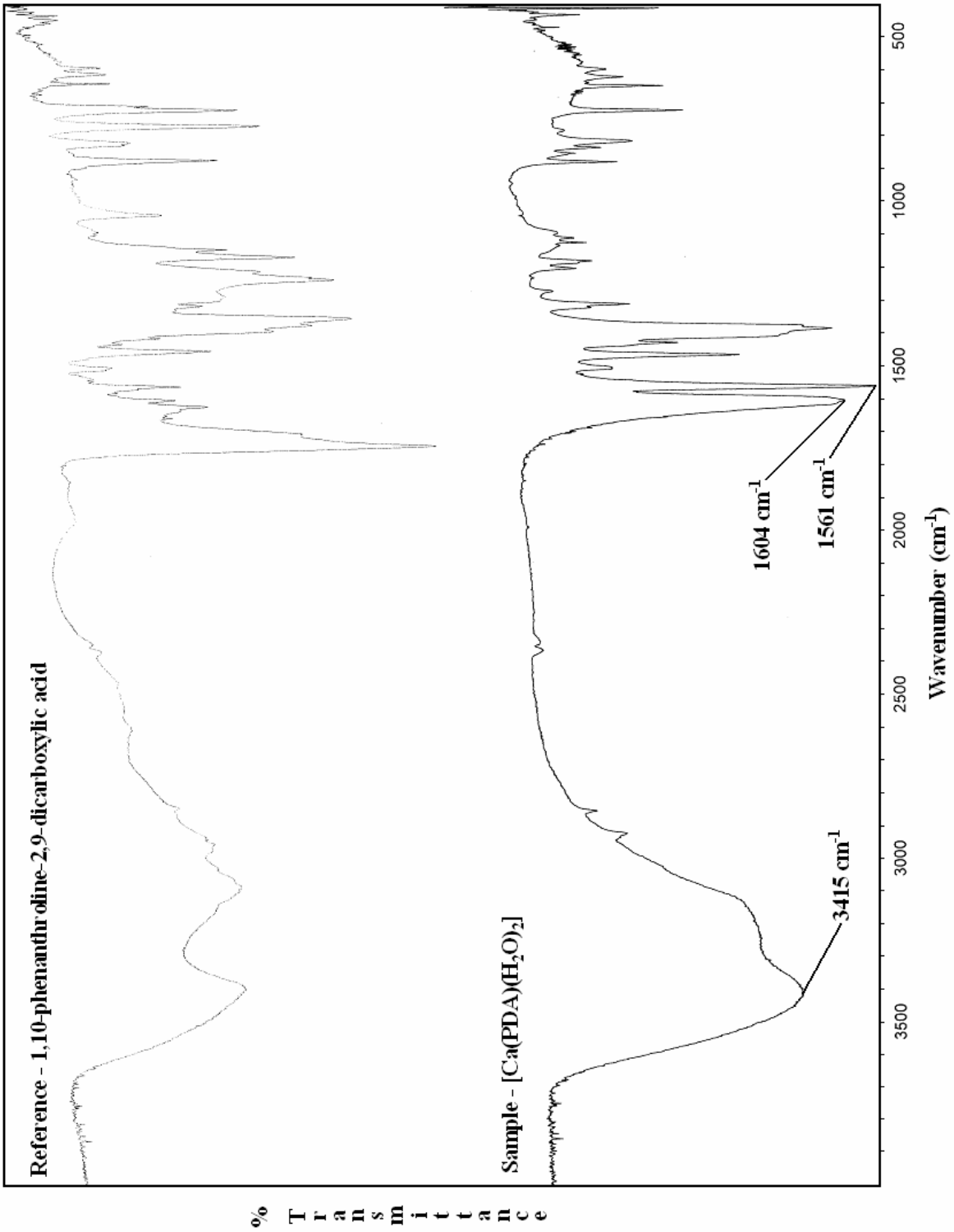

Figure 47: The IR spectrum of $[Ca(PDA)(H_2O)_2]$ crystals with the IR spectrum of PDA as a reference.

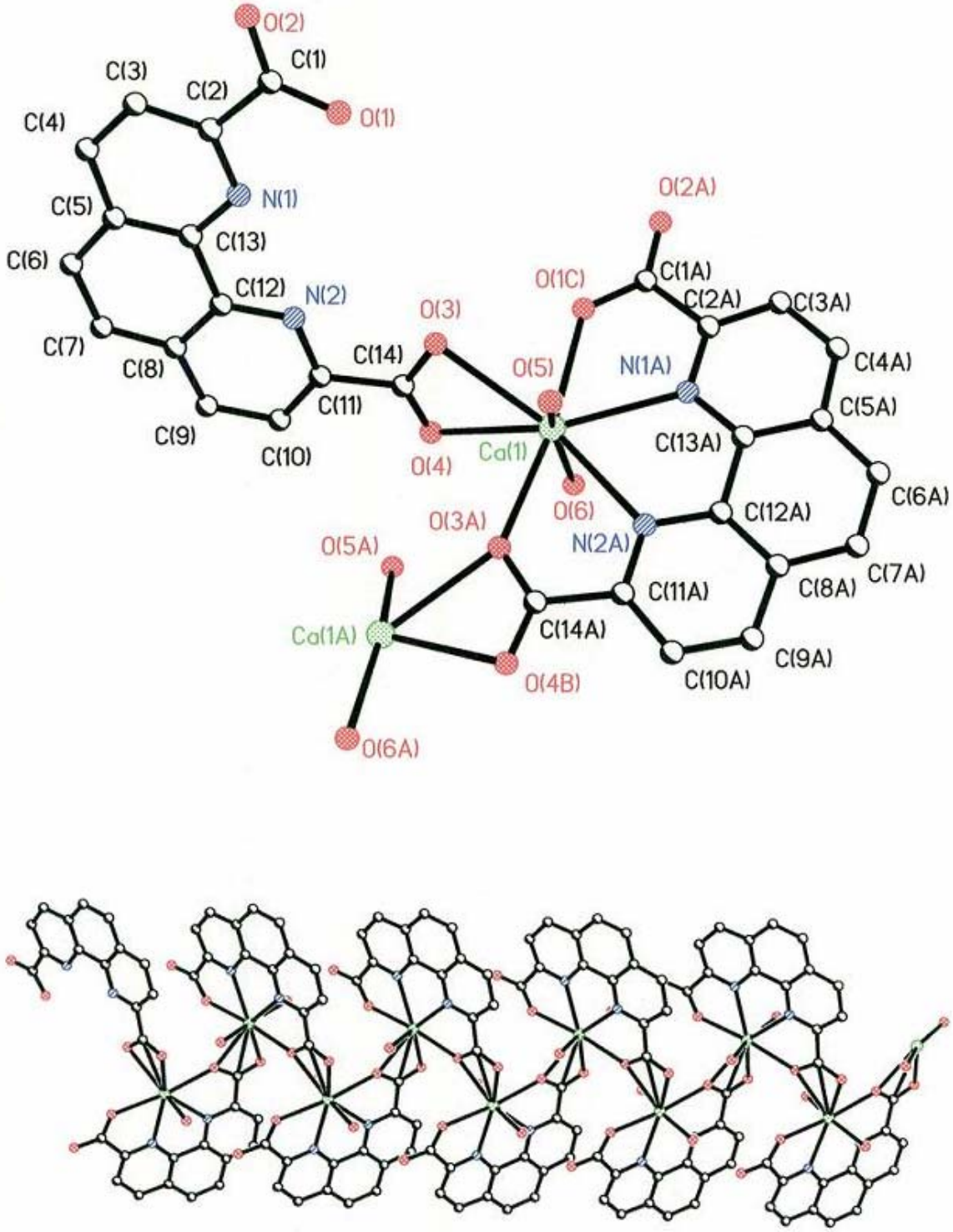

Figure 48: The crystal structure and atom assignments for the [Ca(PDA)(H_2O)$_2$)] complex.

Table 2: The crystal data and structure refinement for the [Ca(PDA)(H_2O)$_2$] complex.

Identification code	ca_pda
Empirical formula	CaC14H6N2O8
Formula weight	370.29 g/mol
Temperature	183(2) K
Wavelength	0.71073 Å
Crystal system, space group	Orthorhombic, Fdd2
Unit cell dimensions	a = 44.007(9)Å alpha = 90° b = 18.945(4)Å beta = 90° c = 7.2446(14)Å gamma = 90°
Volume	6040(2) Å3
Z, Calculated density	16, 1.629 Mg/m3
Absorption coefficient	0.465 mm-1
F(000)	3008
Crystal size	0.20×0.03×0.03 mm
Theta range for data collection	2.34 to 25.00°
Limiting indices	-51≤h≤52, -22≤k≤21, -8≤l≤8
Reflections collected / unique	7199 / 2629 [R(int) = 0.1532]
Completeness to theta = 25.00	99.70%
Absoption correction	REQAB (multi-scan)
Max. and min. transmission	0.9862 and 0.9128
Refinement method	Full-matrix least-squares on F2
Data / restraints / parameters	2629 / 1 / 235
Goodness-of-fit on F2	0.999
Final R indices [I>2sigma(I)]	R1 = 0.0882, wR2 = 0.1937
R indices (all data)	R1 = 0.1367, wR2 = 0.2193
Absolute structure parameter	0.56(12)
Largest diff. peak and hole	0.570 and -0.409 e.A-3

Table 3: The atomic coordinates ($\times 10^4$) and equivalent isotropic displacement parameters ($Å^2 \times 10^3$) for [Ca(PDA)]. U(eq) is defined as one third of the trace of the orthoganalized Uij tensor.

	x	y	z	U(eq)
Ca(1)	-320(1)	2941(1)	8104(3)	33(1)
O(1)	406(2)	1408(4)	201(9)	43(2)
O(8A)	37(3)	4259(9)	3170(20)	43(4)
O(8B)	86(3)	4365(8)	4520(20)	50(4)
O(2)	709(2)	996(4)	-2017(10)	44(2)
O(3)	146(1)	2651(3)	5940(12)	45(2)
O(7)	136(3)	4757(8)	8310(20)	55(4)
O(5)	-396(2)	1748(5)	7047(12)	59(2)
O(6)	-344(1)	3969(3)	10000(9)	36(2)
O(4)	230(1)	3303(3)	8440(10)	38(2)
N(1)	871(2)	1849(4)	2169(10)	31(2)
N(2)	731(1)	2498(4)	5310(9)	24(2)
C(1)	662(2)	1277(5)	-524(14)	34(2)
C(2)	939(2)	1525(4)	583(12)	30(2)
C(3)	1230(2)	1424(6)	-35(14)	38(2)
C(4)	1471(2)	1648(5)	1047(13)	35(2)
C(5)	1418(2)	1975(5)	2754(11)	25(2)
C(6)	1649(2)	2220(5)	3951(14)	36(2)
C(7)	1575(2)	2526(4)	5617(12)	29(2)
C(8)	1267(2)	2635(5)	6131(12)	28(2)
C(9)	1181(2)	2964(5)	7758(13)	34(2)
C(10)	873(2)	3076(5)	8123(15)	29(2)
C(11)	661(2)	2827(5)	6872(13)	32(2)
C(12)	1032(2)	2409(5)	4971(13)	31(2)
C(13)	1107(2)	2062(5)	3194(15)	32(2)
C(14)	316(2)	2948(6)	7109(15)	42(3)

Table 4: The hydrogen coordinates ($\times 10^4$) and isotropic displacement parameters ($Å^2 \times 10^3$) for the $[Ca(PDA)(H_2O)_2]$ complex.

	x	y	z	U(eq)
H(3)	1266	1201	-1205	45
H(4)	1676	1579	625	42
H(6)	1859	2174	3601	44
H(7)	1733	2668	6445	34
H(9)	1332	3114	8630	41
H(10)	810	3320	9218	35

Table 5: The bond lengths (Å) for the [Ca(PDA)(H_2O)$_2$] complex.

Bond	Bond Length (Å)	Bond	Bond Length (Å)
Ca(1)-O(6)	2.387(7)	N(1)-Ca(1)#2	2.550(8)
Ca(1)-O(5)	2.410(8)	N(2)-C(11)	1.328(11)
Ca(1)-O(3)#1	2.462(8)	N(2)-C(12)	1.357(11)
Ca(1)-O(1)#1	2.468(7)	N(2)-Ca(1)#2	2.555(7)
Ca(1)-O(4)	2.524(7)	C(1)-C(2)	1.534(12)
Ca(1)-N(1)#1	2.550(8)	C(2)-C(3)	1.370(13)
Ca(1)-N(2)#1	2.555(7)	C(3)-C(4)	1.386(13)
Ca(1)-O(3)	2.638(7)	C(4)-C(5)	1.402(12)
Ca(1)-C(14)	2.890(10)	C(5)-C(13)	1.415(12)
O(1)-C(1)	1.265(12)	C(5)-C(6)	1.417(13)
O(1)-Ca(1)#2	2.468(7)	C(6)-C(7)	1.379(13)
O(8A)-O(8B)	1.025(19)	C(7)-C(8)	1.417(12)
O(2)-C(1)	1.223(12)	C(8)-C(9)	1.387(13)
O(3)-C(14)	1.263(13)	C(8)-C(12)	1.400(13)
O(3)-Ca(1)#2	2.462(8)	C(9)-C(10)	1.398(12)
O(7)-O(7)#3	1.51(3)	C(10)-C(11)	1.382(13)
O(4)-C(14)	1.236(13)	C(11)-C(14)	1.545(13)
N(1)-C(2)	1.337(12)	C(12)-C(13)	1.482(14)
N(1)-C(13)	1.340(12)		

Table 6: The bond angles (deg) for the $[Ca(PDA)(H_2O)_2]$ complex.

Angle	Bond Angle (deg)	Angle	Bond Angle (deg)
O(6)-Ca(1)-O(5)	160.4(3)	C(14)-O(4)-Ca(1)	94.2(6)
O(6)-Ca(1)-O(3)#1	84.6(2)	C(2)-N(1)-C(13)	116.2(8)
O(5)-Ca(1)-O(3)#1	83.2(3)	C(2)-N(1)-Ca(1)#2	120.9(6)
O(6)-Ca(1)-O(1)#1	94.3(2)	C(13)-N(1)-Ca(1)#2	122.9(6)
O(5)-Ca(1)-O(1)#1	100.2(3)	C(11)-N(2)-C(12)	116.0(8)
O(3)#1-Ca(1)-O(1)#1	170.7(2)	C(11)-N(2)-Ca(1)#2	121.4(6)
O(6)-Ca(1)-O(4)	76.5(2)	C(12)-N(2)-Ca(1)#2	122.6(6)
O(5)-Ca(1)-O(4)	114.8(2)	O(2)-C(1)-O(1)	127.1(9)
O(3)#1-Ca(1)-O(4)	75.3(2)	O(2)-C(1)-C(2)	117.4(9)
O(1)#1-Ca(1)-O(4)	95.4(2)	O(1)-C(1)-C(2)	115.4(8)
O(6)-Ca(1)-N(1)#1	89.0(2)	N(1)-C(2)-C(3)	123.7(9)
O(5)-Ca(1)-N(1)#1	85.9(3)	N(1)-C(2)-C(1)	114.3(8)
O(3)#1-Ca(1)-N(1)#1	126.0(2)	C(3)-C(2)-C(1)	122.0(9)
O(1)#1-Ca(1)-N(1)#1	63.1(2)	C(2)-C(3)-C(4)	119.2(9)
O(4)-Ca(1)-N(1)#1	153.4(2)	C(3)-C(4)-C(5)	120.4(9)
O(6)-Ca(1)-N(2)#1	82.7(2)	C(4)-C(5)-C(13)	114.3(8)
O(5)-Ca(1)-N(2)#1	78.1(3)	C(4)-C(5)-C(6)	124.4(8)
O(3)#1-Ca(1)-N(2)#1	63.2(2)	C(13)-C(5)-C(6)	121.3(8)
O(1)#1-Ca(1)-N(2)#1	125.9(2)	C(7)-C(6)-C(5)	120.2(8)
O(4)-Ca(1)-N(2)#1	135.0(2)	C(6)-C(7)-C(8)	121.2(8)
N(1)#1-Ca(1)-N(2)#1	62.8(2)	C(9)-C(8)-C(12)	116.4(8)
O(6)-Ca(1)-O(3)	123.2(2)	C(9)-C(8)-C(7)	123.3(8)
O(5)-Ca(1)-O(3)	74.1(2)	C(12)-C(8)-C(7)	120.2(8)
O(3)#1-Ca(1)-O(3)	99.25(10)	C(8)-C(9)-C(10)	119.6(9)
O(1)#1-Ca(1)-O(3)	73.6(2)	C(11)-C(10)-C(9)	118.6(9)
O(4)-Ca(1)-O(3)	50.9(2)	N(2)-C(11)-C(10)	124.3(9)
N(1)#1-Ca(1)-O(3)	127.8(3)	N(2)-C(11)-C(14)	113.0(9)
N(2)#1-Ca(1)-O(3)	148.8(2)	C(10)-C(11)-C(14)	122.6(9)
O(6)-Ca(1)-C(14)	100.6(3)	N(2)-C(12)-C(8)	125.1(8)
O(5)-Ca(1)-C(14)	93.5(3)	N(2)-C(12)-C(13)	115.4(8)
O(3)#1-Ca(1)-C(14)	84.9(3)	C(8)-C(12)-C(13)	119.5(8)
O(1)#1-Ca(1)-C(14)	86.2(3)	N(1)-C(13)-C(5)	126.1(9)
O(4)-Ca(1)-C(14)	25.2(3)	N(1)-C(13)-C(12)	116.3(8)
N(1)#1-Ca(1)-C(14)	148.7(3)	C(5)-C(13)-C(12)	117.5(8)
N(2)#1-Ca(1)-C(14)	147.6(3)	O(4)-C(14)-O(3)	125.6(10)
O(3)-Ca(1)-C(14)	25.9(3)	O(4)-C(14)-C(11)	118.1(10)
C(1)-O(1)-Ca(1)#2	126.1(6)	O(3)-C(14)-C(11)	116.3(10)
C(14)-O(3)-Ca(1)#2	125.3(6)	O(4)-C(14)-Ca(1)	60.6(5)
C(14)-O(3)-Ca(1)	88.3(7)	O(3)-C(14)-Ca(1)	65.8(5)
Ca(1)#2-O(3)-Ca(1)	146.2(3)	C(11)-C(14)-Ca(1)	168.1(7)

Symmetry transformations used to generate equivalent atoms:

1: -x, -y+½, z+½ **2**: -x, -y+½, z-½ **3**: -x, -y+1, z

Table 7: The anisotropic displacement parameters ($Å^2 \times 10^3$) for the $[Ca(PDA)(H_2O)_2]$ complex. The anisotropic displacement factor exponent takes the form: $-2\pi^2 [h^2a^{*2}U11 + ... + 2hka^*b^*U12]$.

	U11	U22	U33	U23	U13	U12
Ca(1)	33(1)	27(1)	39(1)	-4(1)	5(1)	-2(1)
O(1)	39(4)	47(5)	42(4)	2(3)	-11(3)	2(3)
O(8A)	45(8)	49(10)	35(7)	13(8)	9(8)	-9(6)
O(8B)	50(9)	38(10)	63(11)	17(9)	8(9)	-1(7)
O(2)	54(4)	40(4)	38(4)	-11(4)	-10(4)	7(3)
O(3)	23(3)	22(3)	89(6)	-11(4)	4(4)	-2(3)
O(7)	66(10)	58(11)	41(7)	-4(8)	22(7)	-31(8)
O(5)	44(4)	50(5)	82(6)	-26(5)	22(4)	-16(4)
O(6)	37(3)	31(4)	40(4)	1(3)	-3(3)	3(3)
O(4)	41(4)	22(4)	50(4)	-10(3)	22(3)	1(3)
N(1)	44(4)	13(4)	36(4)	-3(3)	-5(4)	-2(3)
N(2)	32(4)	13(4)	27(4)	7(3)	9(3)	1(3)
C(1)	47(6)	9(5)	45(6)	6(4)	-11(5)	-2(4)
C(2)	43(5)	23(5)	23(4)	9(4)	-12(4)	-4(4)
C(3)	38(5)	42(7)	33(5)	1(5)	-6(4)	8(4)
C(4)	41(5)	29(6)	34(5)	9(4)	1(4)	12(4)
C(5)	33(4)	18(4)	24(5)	3(4)	3(4)	5(4)
C(6)	30(5)	30(6)	49(6)	1(4)	-2(4)	-2(4)
C(7)	41(5)	17(5)	27(4)	-3(4)	-1(5)	3(4)
C(8)	36(5)	22(5)	25(4)	-1(4)	-6(4)	-1(4)
C(9)	44(5)	22(5)	36(6)	10(4)	-7(4)	-1(4)
C(10)	25(4)	27(5)	35(4)	2(5)	-4(5)	-5(4)
C(11)	34(5)	29(5)	33(5)	16(4)	8(4)	0(4)
C(12)	40(5)	16(5)	37(5)	0(4)	6(4)	5(4)
C(13)	38(4)	23(4)	34(5)	8(4)	-5(5)	1(4)
C(14)	34(5)	36(6)	55(7)	14(6)	3(5)	-8(5)

116.3°, respectively. These bond angles were compared to the bond angles around theoretical, non-complexed PDA. A Hyperchem MM+ geometry optimized calculation was performed for the non-complexed PDA ligand. These corresponding bond angles, determined from Hyperchem, were 119.1° and 116.3° and compared to the experimental bond angles of N(2)-C(11)-C(14) and O(3)-C(14)-C(11) for the [Ca(PDA)(H_2O)$_2$] complex. This comparison showed a minimal deviation from the theoretical bond angles of the non-complexed PDA when compared to the [Ca(PDA)(H_2O)$_2$] complex. Therefore, the strain energy is minimized for PDA when complexed with Ca(II).

DMOPA crystal structure

Crystals of 2,9-bis(carbomethoxy)-1,10-phenanthroline monohydrate, DMOPA, were determined to be an impurity of PDA after recrystallization from methanol. The IR analysis of DMOPA is shown in Figure 49 and has a C=O stretch at 1724 cm^{-1}, which is much lower than that for PDA. These crystals were found as white platelets that bared no resemblance to the yellow, needle-like crystals of PDA. The planar crystal structure of DMOPA is illustrated in Figure 50, which shows a molecule of H_2O placed equidistant from the two oxygen atoms of the carbomethoxy groups. This crystal structure shows the affect that preorganization has, since DMOPA has the ability to integrate a H_2O molecule into its structure. The more flexible analog of DMOPA, N,N´-bis(carbomethoxy)-ethylenediamine, does not have the structural rigidity needed to incorporate a water molecule into its crystal structure.

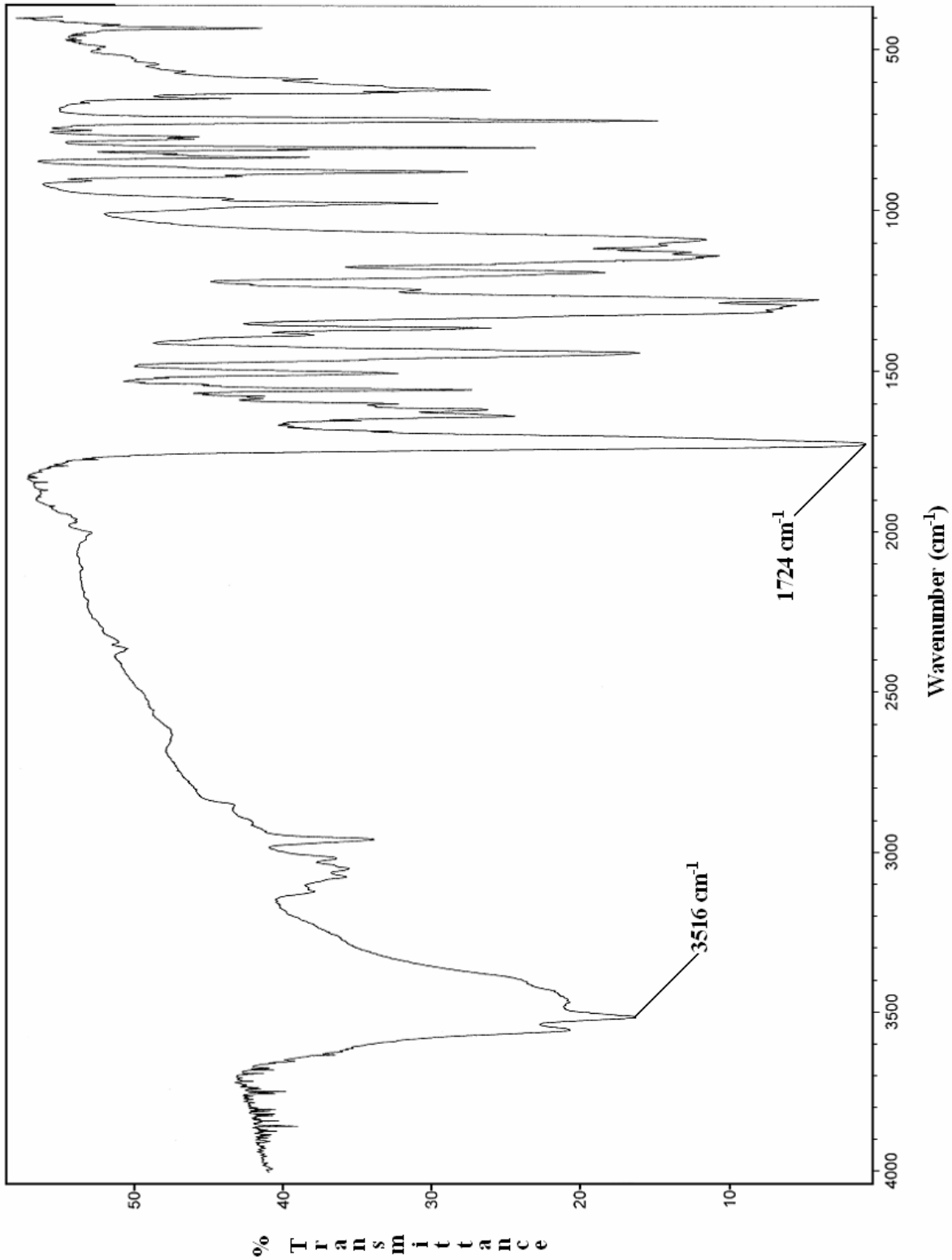

Figure 49: The IR spectrum of 2,9-bis(carbomethoxy)-1,10-phenanthroline.

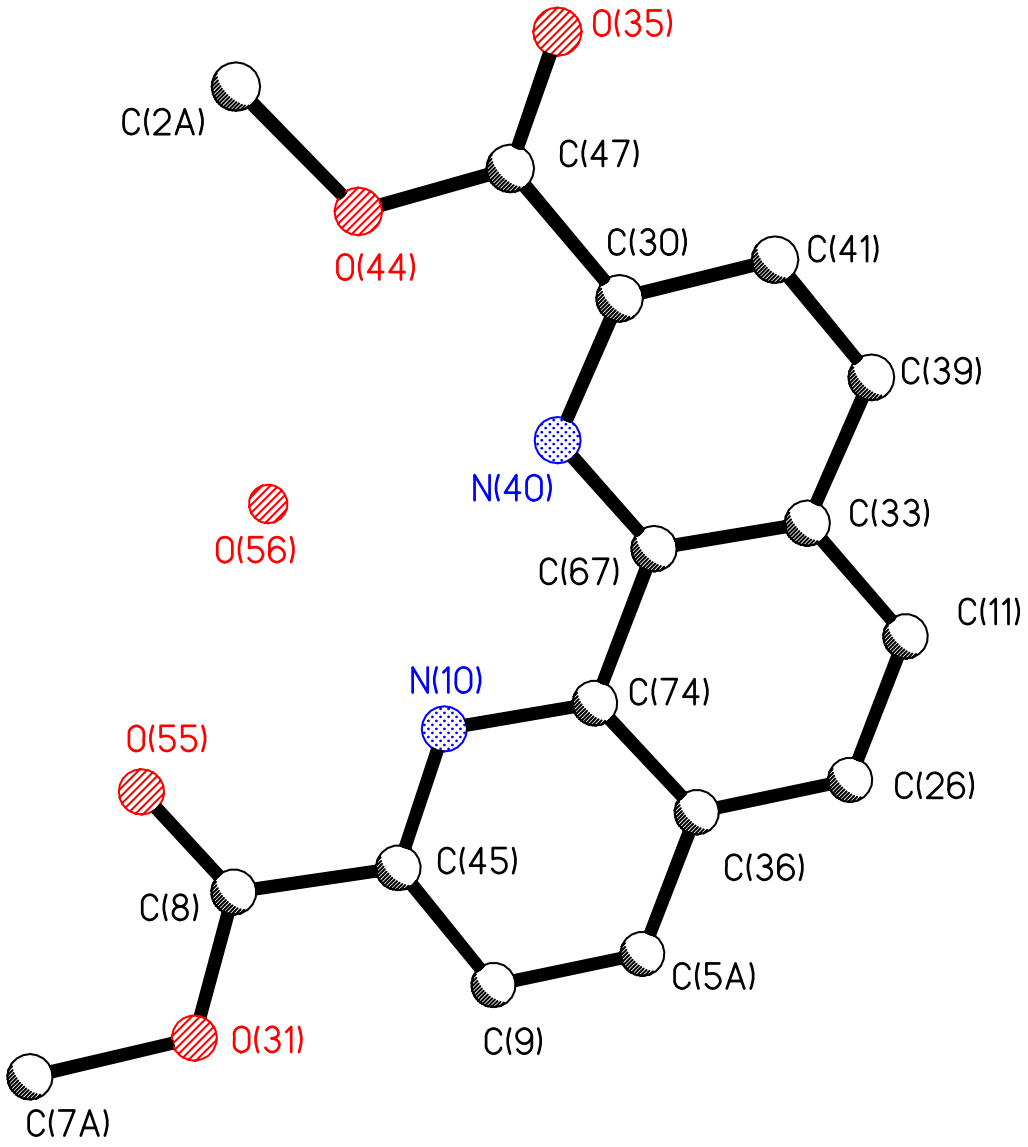

Figure 50: The crystal structure and atom assignments for 2,9-bis(carbomethoxy)-1,10-phenanthroline monohydrate (DMOPA·H_2O).

^{153}Gd(III) Radiolabeling of PDA

Three separate ^{153}Gd(III) radiolabeling experiments were performed for PDA to determine the stability of the ^{153}Gd(III)-PDA complex and its possible biomedical application as a contrast agent for MRI. The first of the ^{153}Gd(III) radiolabeling experiments confirmed what was found for the titration experiments for PDA with Gd(III). A radio-TLC experiment was performed and verified that PDA formed a complex with ^{153}Gd(III). The conditions for the radio-TLC yielded R_f values of 0.3 for the ^{153}Gd(III)-PDA complex and 0.0 for ^{153}Gd(III) with ethanol as the mobile phase. The radio-TLC diagram of ^{153}Gd(III)-PDA and ^{153}Gd(III) is shown in Figure 51.

The second experiment showed that the ^{153}Gd(III)-PDA displayed a remarkable stability when exposed to a competing ligand, DTPA, in equimolar amounts. This was unexpected, since DTPA is an unpreorganized octadentate ligand that would normally overcome a tetradentate ligand, such as PDA. The affect of preorganization can be seen by this competition experiment. A radio-TLC experiment was conducted to determine how much of the ^{153}Gd(III) was in PDA versus DTPA. The conditions for the radio-TLC experiment yielded R_f values of 0.0 for ^{153}Gd-PDA and 0.6 for ^{153}Gd-DTPA with 1:1 methanol/10% ammonium acetate. The radio-TLC diagram, illustrated in Figure 52, showed that 50% of the ^{153}Gd(III) was complexed with PDA and 50% of the ^{153}Gd(III) was complexed with DTPA. Therefore, the ability for PDA to complex ^{153}Gd(III) competitively with DTPA was verified by radio-TLC analysis.

The third experiment was performed to determine the stability of the ^{153}Gd(III)-PDA complex in a biological medium, rat serum. Radio-TLC analysis was performed after 5 minutes of incubating a solution of ^{153}Gd(III)-PDA complex in rat serum. The results gave two possible scenarios for the fate of the ^{153}Gd(III)-PDA complex. The ^{153}Gd(III)-PDA peak had disappeared

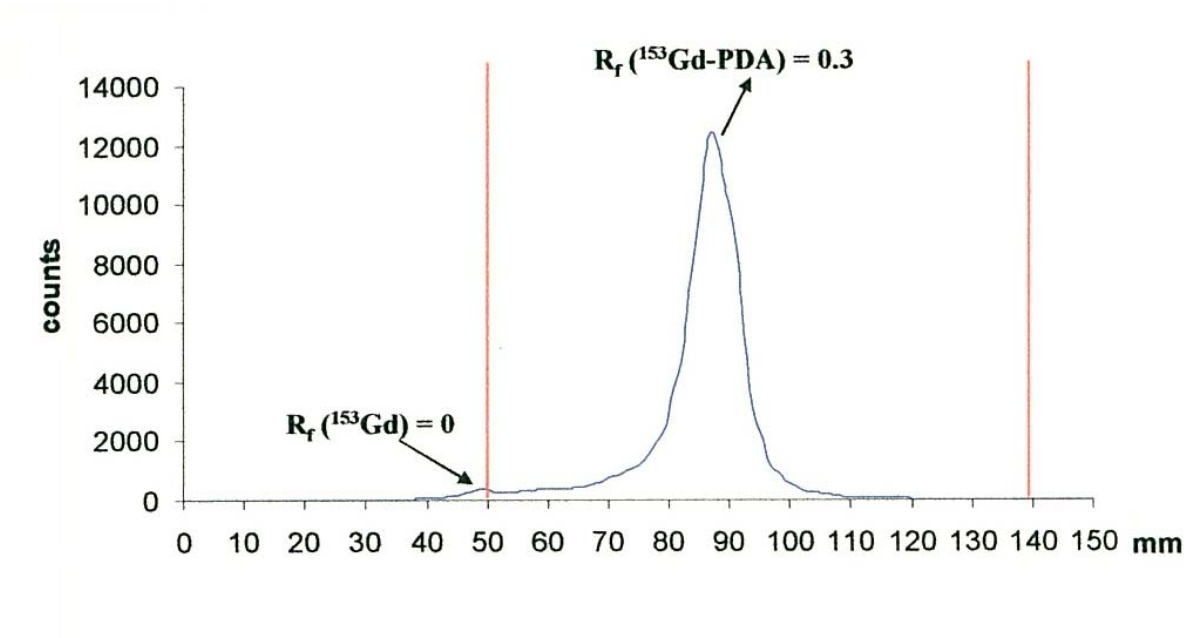

Figure 51: The radio-TLC diagram of the ^{153}Gd(III)-PDA complex.

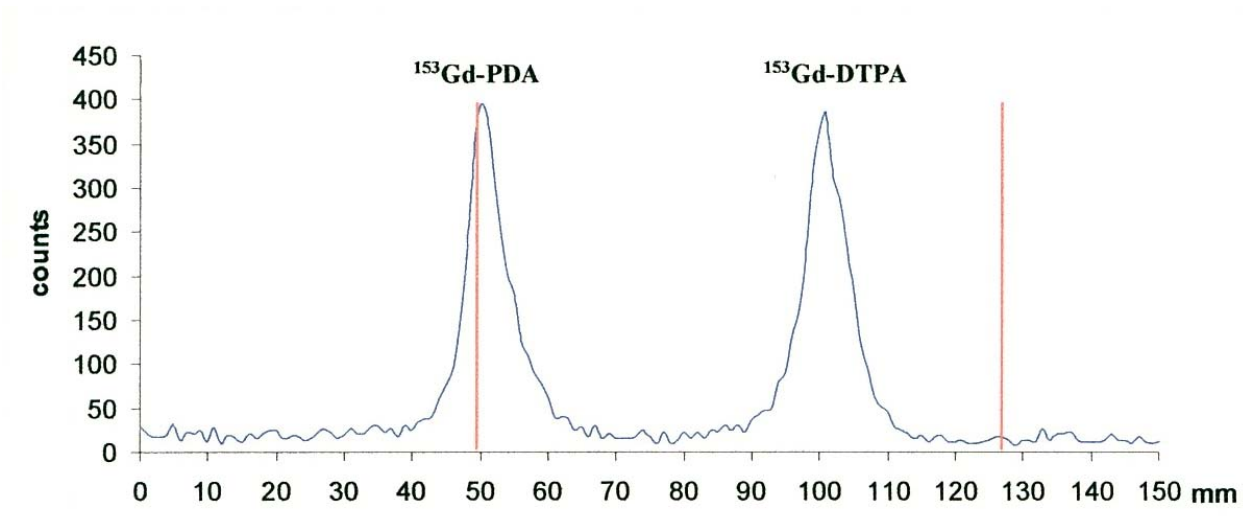

Figure 52: The radio-TLC diagram for the competition experiment of PDA and DTPA for ^{153}Gd(III).

and a new peak was shown in Figure 53. This suggested that either the ^{153}Gd(III) was displaced from the ^{153}Gd(III)-PDA complex into the proteins of the rat serum or the ^{153}Gd(III)-PDA complex was bound to the proteins.

CONCLUSIONS

For years, macrocycles have been used to enhance the thermodynamic stability, as well as the metal ion selectivity, of a metal-ligand complex. The ability to selectively chelate a metal ion is of particular importance to inorganic chemistry. This is typically done using ligand donor atoms with higher affinities for the desired metal ion to be chelated, matching the number of ligand donor atoms closely with coordination number for the metal ion, or by introducing a size-selective framework for the donor atoms of the ligand. 1,10-phenanthroline-2,9-dicarboxylate (PDA) exhibits selectivity for larger metal ions using these principles of ligand design.

Characterization of PDA by IR and ^{1}H-NMR spectroscopy showed that pure PDA was synthesized by following synthetic techniques from Chandler, et. al., although some inconsistencies were shown. Methanol may not be the most suitable recrystallization solvent since 2,9-bis(carbomethoxy)-1,10-phenanthroline (DMOPA) was determined to be a byproduct from the recrystallization.

UV/Vis absorption spectrophotometry proved to be an effective and valuable technique for the detection of metal-PDA complexes in aqueous solutions as a function of pH. Absorption bands for PDA in the UV region facilitated the detection metallation and demetallation of PDA. Formation constants, log K_1 values, for larger metal ions (approximately 1.00Å) were shown to be substantially higher for the preorganized structure of PDA, compared to the unpreorganized

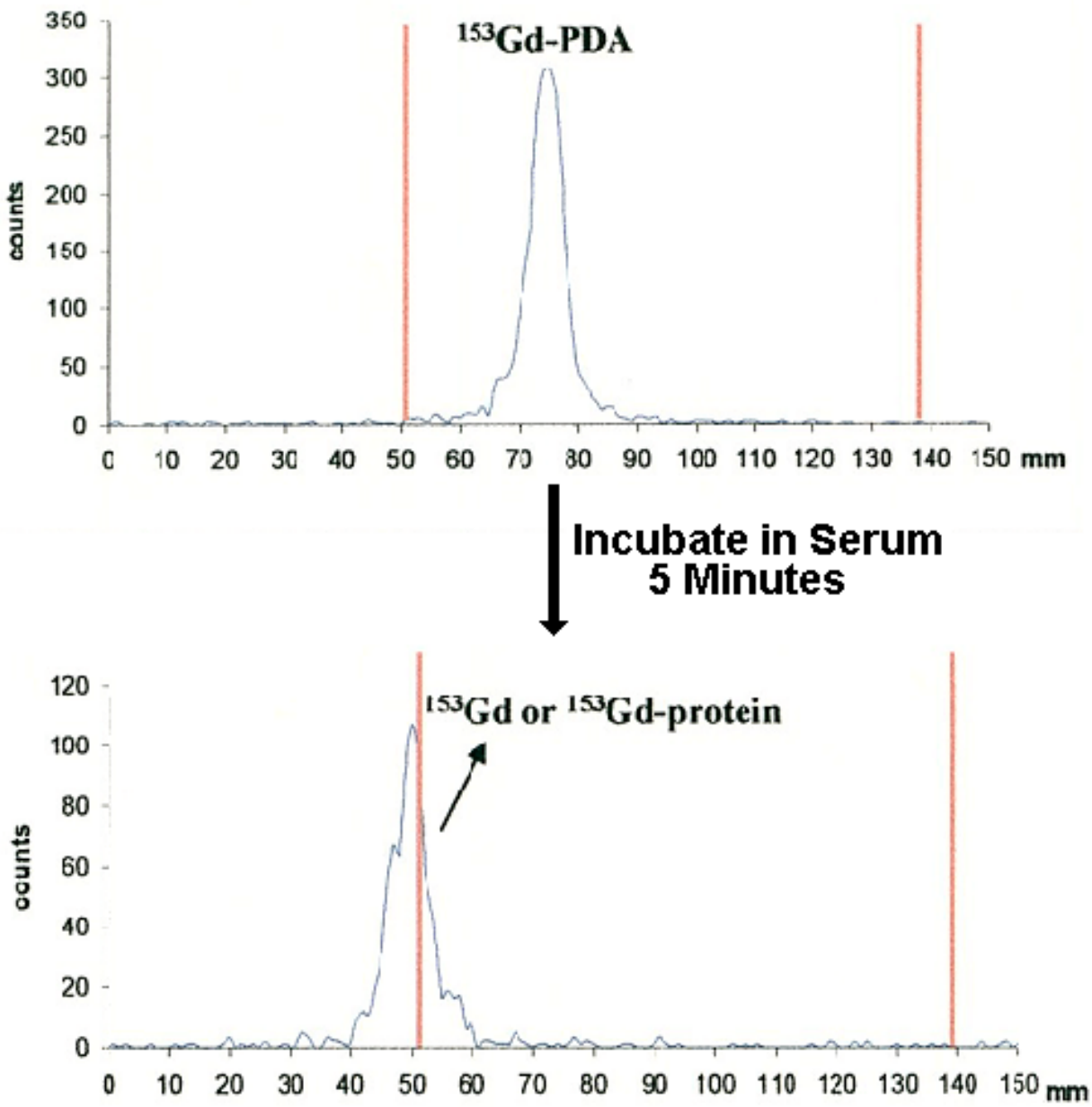

Figure 53: The radio-TLC diagrams of the ^{153}Gd(III)-PDA complex before and after rat serum was added to the sample.

analog of PDA, EDDA. A decrease in formation constants for smaller metal ions was also seen, relative to EDDA. PDA effectively competed with EDTA and even DTPA for metal ions at lower pH values, which allowed for the determination of formation constants for PDA with metal ions. This is remarkable, since PDA is only a tetradentate ligand, having two negative oxygen and two neutral nitrogen donor atoms. Overall, the hemicyclic effect, or the effect of having terminal donor atoms on a preorganized ligand, has yielded an enormous improvement for metal-PDA complex stability.

From the ^{153}Gd(III) radiolabeling experiment, PDA was shown to be an effective ligand for chelating the Gd(III) metal ion. The competition experiment between PDA and DTPA for ^{153}Gd(III) showed equimolar concentrations of Gd(III)-PDA and Gd(III)-DTPA complexes in solution, which suggested that PDA has an enormous affinity for Gd(III). Although PDA has proven its ability to complex Gd(III), alterations may need to be made to the structure of PDA, such as adding sulfonic acid substituents to the hydrophobic backbone of PDA to increase water solubility, in order to be placed into a biological medium. Future, water-soluble derivatives of PDA may prove to be valuable MRI contrasting agents. Judging from the formation constants, the preorganized structure of PDA selectively chelates larger metal ions, normally used in contrasting agents, over smaller metal ions, such as Zn(II), found in the body. In particular, the size selectivity of PDA was illustrated in the crystal structure of [Ca(PDA)(H_2O)$_2$], where the Ca(II) metal ion showed a proper fit between the carboxylate groups of PDA with minimal strain on the overall complex.

LITERATURE CITED

1. Guo, Zijian and Peter Sadler. *Angew. Chem. Int. Ed.*, **1999**. *38*. 1512-1531.

2. Cram, D.J., "The design of molecular hosts, guests, and their complexes." Nobel Lecture, **1987**.

3. Pedersen, C.J., *J. Am. Chem. Soc.*, **1967**. *89*, 2495-2496.

4. Pedersen, C.J., *J. Am. Chem. Soc.*, **1967**. *89*, 7017-7036.

5. Dietrich, B. and J. M. Lehn, *Tetrahedron Lett.*, **1969**. 2885-2888.

6. Dietrich, B. and J. M. Lehn, *Tetrahedron Lett.*, **1969**. 2889-2892.

7. Cabbiness, D.K., D. W. Margerum, *J. Am. Chem. Soc.*, **1969**. *91*. 6540.

8. Lehn, J.M., *Acc. Chem. Res.*, **1978**. *11*. 49.

9. Caravan, P., J. J. Ellison, T. J. McMurry, R. B. Lauffer, *Chemical Reviews*, **1999**. *99*. 2293-2352.

10. Martell, A.E., R. M. Smith, *Critical Stability Constant Database, 46.* National Institute of science and Technology (NIST): Gaithersburg, MD, USA, **2003**.

11. Chandler, C.J., Leslie W. Deady, and James A. Reiss. *J. Heterocyclic Chem.*, **1981**. *18*. 599-601.

12. Moghimi, A., R. Alizadeh, A. Shokrollahi, et. al. *J. of Inorg. Chem.*, **2003**. *42*. 1616-1624.

13. Park, K.-M., Il Yoon, Joobeom Seo, et. al. *Acta Cryst. Section E*, **2001**. *E57*. m154-m156.

14. Ya-Bo Xie, J.-R.L., and Xian-He Bu. *Journal of Molecular Structure*, **2005**. *741*. 249-253.